ADVANCED TECHNIQUES FOR COOPERATION AND PHYSICAL LAYER SECURITY IN VISIBLE LIGHT COMMUNICATIONS

by

Nuğman Su

B.S., Electrical and Electronics Engineering, Boğaziçi University, 2012

M.S., Electrical and Electronics Engineering, Boğaziçi University, 2015

Submitted to the Institute for Graduate Studies in
Science and Engineering in partial fulfillment of
the requirements for the degree of
Doctor of Philosophy

Graduate Program in Electrical and Electronics Engineering

Boğaziçi University

2022

ACKNOWLEDGEMENTS

This thesis has been supported in part by the Scientific and Technical Research Council of Turkey (TUBITAK) under the 1003-Priority Areas R&D Projects Support Program No. 218E034.

I would like to express my sincere gratitude to my patient supervisor, Prof. Mutlu Koca, who has supported me throughout my entire graduate journey. I am extremely grateful for his encouragement in my academic endeavors and also our friendly chats at the end of our meetings. I am deeply grateful to Prof. Erdal Panayırcı, whose insight and knowledge into the subject matter steered me through my research. This thesis would not be the same without his wise guidance and inspiring outlook.

I would like to extend my sincere thanks to Prof. Harald Haas and Prof. Vincent Poor for providing valuable feedback on my research. I would also like to thank my jury committee members Prof. Emin Anarım, Prof. Hakan Deliç, and Prof. Hakan Ali Çırpan for their time, stimulating questions, and comments.

I am thankful to my family, especially my sweet mother Hatice for her unconditional love and support. She is the one who taught me to count numbers, read words, and most importantly trust in myself. As a wise man once said, "The author of everything I have written is my mother." This accomplishment would not have been possible without her.

Last but never the least, I would like to thank my friends Nihan, Ezgi, Remzi, Sezi, Ömer, Alican, Öykü, Görkem, and many more for the countless hours of fun, and memorable gatherings, providing moral support throughout the writing of this thesis.

ABSTRACT

ADVANCED TECHNIQUES FOR COOPERATION AND PHYSICAL LAYER SECURITY IN VISIBLE LIGHT COMMUNICATIONS

Visible light communications (VLC), enabling high-rate data transfer over the idle visible light spectrum, can contribute to alleviating the congestion problem accumulating in the radio-frequency spectrum. This thesis deals with two important aspects of VLC: i) efficient cooperation techniques adapted to the intensity-modulated light-emitting-diode (LED) transmitters, ii) secure multi-user communication schemes based on the multiple-input-multiple-output (MIMO) framework. Firstly, 3-terminal full-duplex (FD) cooperative VLC systems are considered where both transmitters (source and relay) are subject to the LED clipping distortion effects. Transmission rate maximizing optimum power allocation (OPA) strategies are proposed for both the amplify-and-forward (AF) and decode-and-forward (DF) relaying capabilities. Next, the physical layer security (PLS) problem is considered for the multi-user MIMO-VLC systems with an eavesdropper (Eve). To ensure PLS, two transmit precoding schemes are proposed, based on generalized space shift keying and receive spatial modulation, respectively. The received signals of the legitimate users are optimized jointly, such that their bit error rates (BERs) are minimized and Eve's BER is significantly degraded. To be able to support massive amount users and further degrade Eve's reception, non-orthogonal multiple access (NOMA) and random constellation coding techniques are also utilized. For both cases, the achievable secrecy rates and bounds are derived analytically. The BER and secrecy performance results obtained by simulations confirm that the proposed frameworks ensure PLS for legitimate users.

ÖZET

GÖRÜNÜR IŞIKLA HABERLEŞMEDE İŞBİRLİĞİ VE FİZİKSEL KATMAN GÜVENLİĞİ İÇİN İLERİ TEKNİKLER

Görünür ışık spektrumu üzerinden yüksek hızlı veri aktarımı sağlayan görünür ışıkla haberleşme (VLC) teknolojisi, radyo frekansı spektrumunda biriken tıkanıklık sorununun hafifletilmesine katkıda bulunabilir. Bu tez, VLC'yi iki önemli açıdan irdelemektedir: i) yoğunluk modülasyonlu ışık yayan diyot (LED) vericilere uyarlanmış verimli işbirliği teknikleri, ii) çoklu giriş-çoklu-çıkış (MIMO) çerçevesini temel alan güvenli çok kullanıcılı iletişim şemaları. Öncelikle, her iki vericinin (kaynak ve röle) LED'nin sinyal kırpma etkilerine maruz kaldığı, 3-terminalli tam çift yönlü (FD) işbirlikli VLC sistemleri ele alınmıştır. Bunun için, hem yükselt-ilet (AF) hem de kodçöz-ilet (DF) aktarma teknikleri için, ulaşılabilir iletim hızını eniyileyen güç tahsisi (OPA) stratejileri önerilmiştir. Sonra, bir gizli dinleyici (Eve) varlığında çok kullanıcılı MIMO-VLC sistemleri için fiziksel katman güvenliği (PLS) problemi ele alınmıştır. PLS'yi sağlamak için, sırasıyla genelleştirilmiş uzay kaydırmalı anahtarlamaya ve alıcı uzaysal modülasyonuna dayanan iki önkodlama şeması önerilmiştir. Bu şemaya göre, yasal kullanıcıların alınan sinyalleri, bit hata oranları (BER) en aza indirilecek ve Eve'in BER'i de önemli ölçüde bozulacak şekilde eniyilenir. Çok sayıda kullanıcıyı destekleyebilmek ve Eve'in alınan sinyalini daha da bozabilmek için, dik olmayan çoklu erişim (NOMA) ve rastgele semboltakım kodlaması teknikleri de kullanılmaktadır. Her iki durumda da ulaşılabilir gizlilik oranları ve sınırları analitik olarak türetilmiştir. Simülasyonlarla elde edilen BER ve gizlilik performansı sonuçları, önerilen çerçevelerin yasal kullanıcılar için PLS sağladığını doğrulamaktadır.

TABLE OF CONTENTS

ACKNOWLEDGEMENTS . . . iii
ABSTRACT . . . iv
ÖZET . . . v
LIST OF FIGURES . . . ix
LIST OF TABLES . . . xiv
LIST OF SYMBOLS . . . xv
LIST OF ACRONYMS/ABBREVIATIONS . . . xviii
1. INTRODUCTION . . . 1
1.1. Related Background . . . 9
1.1.1. Cooperation via Relays . . . 9
1.1.2. Physical Layer Security . . . 12
1.2. Motivation for this Thesis . . . 14
1.3. Contributions of this Thesis . . . 16
2. FUNDAMENTALS OF VISIBLE LIGHT COMMUNICATIONS . . . 18
2.1. VLC Channel Model . . . 18
2.2. Cooperative VLC with LED Distortion . . . 21
2.3. GSSK-based VLC . . . 23
2.4. NOMA-based VLC . . . 25
2.5. Conclusion . . . 26
3. FULL DUPLEX COOPERATIVE VISIBLE LIGHT COMMUNICATIONS WITH CLIPPING NOISE EFFECTS . . . 27
3.1. Introduction . . . 27
3.2. VLC System Model . . . 31
3.2.1. Channel Model . . . 31
3.2.2. LED Clipping Model . . . 34
3.3. Benchmark Derivations: Direct Link and HD Relaying with Clipping Noise . . . 36
3.3.1. Direct Link . . . 36

3.3.2. Half Duplex Cooperation 38
3.3.2.1. AF Relaying 38
3.3.2.2. DF Relaying 40
3.4. Full Duplex Cooperative VLC with Clipping Noise 41
3.4.1. AF Relaying 43
3.4.2. DF Relaying 44
3.5. Transmission Rate Maximization 45
3.5.1. Equal Power Allocation Policies 47
3.5.2. Theoretical bit error rates 47
3.6. Simulation Results 48
3.7. Conclusion 60
4. PHYSICAL LAYER SECURITY FOR MULTI USER MIMO VISIBLE LIGHT COMMUNICATION SYSTEMS WITH GENERALIZED SPACE SHIFT KEYING 61
4.1. Introduction 61
4.2. Multi User MIMO-GSSK-VLC System Model 65
4.3. Spatial Constellation Design for Enhanced PLS 70
4.3.1. Transmit Power Normalization 74
4.4. Secrecy Rate Region of MU-GSSK-VLC System 76
4.5. Simulation Results 78
4.5.1. BER Performance of MU-GSSK-SCD with Perfect CSI 79
4.5.2. Practical System Design Considerations 88
4.5.3. BER Performance of MU-GSSK-SCD with Imperfect CSI 94
4.5.3.1. ML Estimation of ρ 95
4.5.4. Comparison of Results with Existing Ones 98
4.5.5. Secrecy Performance 100
4.5.6. Computational Complexity Analysis 104
4.6. Conclusion 104
4.7. Spatial Constellation Design Based Generalized Space Shift Keying For Physical Layer Security of Multi User MIMO Communication Systems . 105
4.7.1. Introduction 105

4.7.2. System Description 107
4.7.3. SCD-based PLS Improvement Technique 110
4.7.3.1. Precoder Design 111
4.7.3.2. Transmit Power Normalization 113
4.7.3.3. MU Receiver with an Eavesdropper 113
4.7.3.4. Achievable Secrecy Sum Rates 115
4.7.4. Simulation Results 116
4.7.5. Conclusion 122
5. TRANSMIT PRECODING FOR PHYSICAL LAYER SECURITY OF MIMO-NOMA BASED VISIBLE LIGHT COMMUNICATIONS 123
5.1. Introduction 123
5.2. MIMO-NOMA-VLC System Model 125
5.3. PLS Ensuring NOMA Precoder Design 130
5.3.1. The Design of the DC Bias and γ 131
5.4. Simulation Results 134
5.5. Conclusion 139
6. CONCLUSION 140
REFERENCES 142

LIST OF FIGURES

Figure 1.1. Visible light communication system for an indoor setting. 2

Figure 2.1. The emittance and incidence of a single ray for an LED - PD pair. 19

Figure 2.2. The source-relay-destination configuration. 21

Figure 3.1. Cooperative VLC terminal placement model. 31

Figure 3.2. a) Transmitter and b) receiver design for DCO-OFDM VLC. . . . 33

Figure 3.3. a) AF relay design and b) DF relay design for DCO-OFDM VLC. 34

Figure 3.4. Comparison of a) HD and b) FD modes in cooperative VLC. . . . 42

Figure 3.5. Transmission rate performances of OPA and EPA strategies for DF relaying along with direct communication. 53

Figure 3.6. BER performances of OPA and EPA strategies for DF relaying along with direct communication. 54

Figure 3.7. Transmission rate performances of OPA and EPA strategies for AF relaying along with direct communication. 54

Figure 3.8. BER performances of OPA and EPA strategies for AF relaying along with direct communication. 55

Figure 3.9. Transmission rate performances of rate maximizing OPA strategies for all communication settings. 56

Figure 3.10. BER performances of rate maximizing OPA strategies for all communication settings. 56

Figure 3.11. Transmission rate performances with no clipping (ideal) and with clipping (realistic) for DF relaying. 58

Figure 3.12. BER performances with no clipping (ideal) and with clipping (realistic) for DF relaying. 58

Figure 3.13. Transmission rate performances with no clipping (ideal) and with clipping (realistic) for AF relaying. 59

Figure 3.14. BER performances with no clipping (ideal) and with clipping (realistic) for AF relaying. 59

Figure 4.1. System architecture for the multi-user MIMO-GSSK-VLC with SCD. 67

Figure 4.2. Scenario 1 for the evaluated MIMO-VLC system. User 1 and 2 are represented with blue and magenta squares, respectively. 80

Figure 4.3. Scenario 2 for the evaluated MIMO-VLC system. User 1 and 2 are represented with blue and magenta squares, respectively. 81

Figure 4.4. Scenario 3 for the evaluated MIMO-VLC system. User 1 and 2 are represented with blue and magenta squares, respectively. 81

Figure 4.5. BER vs. SNR for Scenario 1. Eve is located at [-1, 1, 0.85]. 82

Figure 4.6. BER vs. SNR for Scenario 1. Eve is located at [0, 0, 0.85]. 83

Figure 4.7. BER vs. SNR for Scenario 1. Eve is located at [1, -1, 0.85]. 84

Figure 4.8. BER vs. SNR for Scenario 2. Eve is located at [-1.5, -0.375, 0.85]. 85

Figure 4.9. BER vs. SNR for Scenario 2. Eve is located at [-0.5, -0.25, 0.85]. . 85

Figure 4.10. BER vs. SNR for Scenario 2. Eve is located at [0.5, -0.125, 0.85]. . 86

Figure 4.11. BER vs. SNR for Scenario 3. Eve is located at [1.125, -1, 0.85]. . . 86

Figure 4.12. BER vs. SNR for Scenario 3. Eve is located at [1.25, -1, 0.85]. . . 87

Figure 4.13. BER vs. SNR for Scenario 3. Eve is located at [1.375, -1, 0.85]. . . 87

Figure 4.14. Secrecy rate regions obtained by MU-GSSK-SCD with $N_t = 16$, $N_a = 8$ and varying N_r. 89

Figure 4.15. BER performance of Eve as Eve moves within the indoor environment, and intercepts User 1's communication. User 1 is located at $[1, \ -1]$, and User 2 is located at $[1.9, \ -1]$. All units are in meters. 90

Figure 4.16. BER performance of Eve as Eve moves within the indoor environment, and intercepts User 2's communication. User 1 is located at $[1, \ -1]$, and User 2 is located at $[1.9, \ -1]$. All units are in meters. 91

Figure 4.17. BER performance of Eve as Eve moves within the indoor environment, and intercepts User 1's communication. User 1 is located at $[1, \ -1]$, and User 2 is located at $[1.1, \ -1]$. All units are in meters. 92

Figure 4.18. BER performance of Eve as Eve moves within the indoor environment, and intercepts User 2's communication. User 1 is located at $[1, \ -1]$, and User 2 is located at $[1.1, \ -1]$. All units are in meters. 93

Figure 4.19. Root mean square of the estimation error $||\rho - \hat{\rho}||$ for Scenario 1 with the imperfect CSI at the users. 96

Figure 4.20. BER vs. SNR plots for Scenario 1 with the imperfect CSI at the users. 97

Figure 4.21. Eve's BER vs. SNR curves for 8-PAM and GSSK with 3 bits/sec/Hz per user. 98

Figure 4.22. Bob's and Eve's BER vs. SNR curves for 8-PAM and GSSK with 3 bits/sec/Hz per user. 99

Figure 4.23. Secrecy rate regions when the users are 30 cms apart. 101

Figure 4.24. Secrecy rate regions when the users are 90 cms apart. 102

Figure 4.25. Secrecy rate regions for SNR of 0 dB while Eve moving away from User 1 to User 2. The separation values between the User 1 and Eve are indicated in the legend. 103

Figure 4.26. System architecture for GSSK-SCD for the multi-user MIMO communication system. 108

Figure 4.27. BER performance curves obtained by GSSK-SCD of 2 legitimate users and single Eve. 118

Figure 4.28. BER performance curves obtained by GSSK-SCD of 2 legitimate users and multiple Eves. 120

Figure 4.29. BER performance comparison of GSSK-SCD and GSSK with artificial noise. 121

Figure 4.30. Secrecy rate regions of the 2−user GSSK-SCD. 122

Figure 5.1. The transmitter design for the proposed PLS precoding scheme. . 127

Figure 5.2. The receiver design of User 1 for the proposed PLS precoding scheme.133

Figure 5.3. The receiver design of User 2 for the proposed PLS precoding scheme.133

Figure 5.4. BER performance results obtained by the proposed PLS precoding scheme. Users are located according to Scenario 1. 135

Figure 5.5. BER performance results obtained by the proposed PLS precoding scheme. Users are located according to Scenario 2. 136

Figure 5.6. The BER performance obtained by the proposed PLS precoding scheme for Scenario 3. 137

Figure 5.7. The BER performance obtained by the proposed PLS precoding scheme for Scenario 1, with increasing N_r. 138

LIST OF TABLES

Table 3.1. Comparison of the work in this chapter to the state of the art of the cooperative VLC literature. 30

Table 3.2. Rate maximizing $(B_{\mathrm{DC}}, \sigma)$ values and optimum rates for FD cooperative VLC with DF relaying. Transmission rates of suboptimum EPA strategies included for comparison. 50

Table 3.3. Rate maximizing $(B_{\mathrm{DC}}, \sigma)$ values and optimum rates for HD cooperative VLC with DF relaying. Transmission rates of suboptimum EPA strategies included for comparison. 50

Table 3.4. Rate maximizing $(B_{\mathrm{DC}}, \sigma)$ values and optimum rates for FD cooperative VLC with AF relaying. Transmission rates of suboptimum EPA strategies included for comparison. 51

Table 3.5. Rate maximizing $(B_{\mathrm{DC}}, \sigma)$ values and optimum rates for HD cooperative VLC with AF relaying. Transmission rates of suboptimum EPA strategies included for comparison. 51

Table 3.6. Rate maximizing $(B_{\mathrm{DC}}, \sigma)$ values and optimum rates for direct VLC. Transmission rates of suboptimum EPA strategies included for comparison. 52

Table 4.1. Optimal SCD for 2−User GSSK-VLC with $N_t = 6$, $N_a = 3$, $N_r = 3$. 73

Table 5.1. User configurations. 135

LIST OF SYMBOLS

a	Attenuation factor
$A[k]$	Received signal's magnitude at the frequency index k
A_{eff}	Effective signal collection area of the optical receiver
A_{PD}	Photodetector area
B_{DC}	DC bias level
$\mathbf{B}_{\mathrm{DC}}$	DC bias vector
BW	Bandwidth
$\mathbf{c}$	Random code symbol for NOMA
$\mathbf{C}$	Random constellation matrix for NOMA
$\mathbb{C}$	Covariance matrix
$\mathbb{C}$	Secrecy capacity
$\mathcal{C}$	Codebook
$\mathcal{C}_k$	Codebook for the kth user
d	Line-of-sight distance between terminals
$\mathrm{erfc}(\cdot)$	Gaussian error function
$F[k]$	The normalization coefficient at the frequency index k
$g(\cdot)$	Standard normal distribution
$\mathbf{h}$	Channel column vector
$h[n]$	Time-domain channel coefficient with the index n
$h(t)$	Impulse response of the visible light channel
h_k	Channel gain of the kth user
$\mathbb{H}(\cdot)$	Entropy
$\mathbb{H}(\cdot\|\cdot)$	Conditional entropy
$H[k]$	Frequency-domain channel coefficient with the index k
$\mathbf{H}_k$	Channel matrix between the access point and the kth user
$\mathbf{I}$	Identity matrix
$\mathbb{I}(\cdot;\cdot)$	Mutual information
$I_{\max}$	Upper limit of the LED driving current

$I_{\min}$	Lower limit of the LED driving current
$\mathbf{J}_k$	Jamming signal affecting Eve intercepting the kth user
K	Number of users
L_R	Number of LEDs at the relay
L_S	Number of LEDs at the source
M_k	Number of symbols in the kth user's codebook
N_a	Number of activated LEDs at the access point
N_B	Number of bits
$\mathbf{n}_k$	Additive white Gaussian noise vector at the kth user
N_r	Number of PDs at the user
N_t	Number of LEDs at the access point
$\mathbf{P}$	Channel precoding matrix
$P[k]$	Average bit error ratio per subcarrier
$P_n(\cdot)$	Total received power in the nth time interval
$\mathbf{q}$	LED intensity variation vector at the access point
$\mathbf{Q}$	NOMA PLS precoding matrix
$Q(\cdot)$	Tail distribution of the standard normal random variable
$\text{rect}(x)$	Rectangular function
$\mathcal{R}$	Transmission rate
$\Re$	Set of real numbers
$R_{T_1}(\cdot,\cdot)$	Generalized Lambertian model for the transmitting terminal
$\mathbf{s}_k$	Observed transmitted signal by the kth user
$\mathcal{S}$	NOMA received signal constellation
T_1	Transmitting terminal
T_2	Receiving terminal
T_s	Sampling period
$\mathbf{V}$	Effective channel matrix for the NOMA precoding vector
$\mathcal{V}_k$	Spatial constellation of user k
$w^{\text{cl}}[n]$	Additive Gaussian clipping distortion of time index n
$\mathbf{w}_k$	Total distortion in Eve's reception intercepting user k
$W[k]$	Frequency-domain effective noise with index k

$W^{\mathrm{AWGN}}[k]$	Additive white Gaussian noise at the frequency index k
$W^{\mathrm{cl}}[k]$	Additive clipping distortion at the frequency index k
$\mathbf{x}$	Magnitude vector of antenna radiation
$x[n]$	Time-domain information symbol of index n
$x^{\mathrm{cl}}[n]$	Clipped time-domain information symbol of index n
$\mathbf{X}$	Frequency-domain information block
$\hat{X}[k]$	Frequency-domain detected information symbol with index k
$X[k]$	Frequency-domain information symbol with index k
$X^{\mathrm{cl}}[k]$	Clipped frequency-domain information symbol of index k
$\mathbf{y}_k$	Received signal vector at the kth user
$y[n]$	Time-domain received signal with index n
$Y[k]$	Frequency-domain received signal with index k
α	NOMA power ratio
β	Lambertian emission order
γ	NOMA signal magnitude
ϵ	Regularization parameter
$\mathcal{E}$	NOMA spatial symbol constellation
θ	Angle of incidence
ρ	Power normalization coefficient
σ	Signal magnitude
σ_{cl}	Standard deviation of the clipping distortion
σ_R	Signal magnitude transmitted by the relay
σ_S	Signal magnitude transmitted by the source
τ_{max}	Multipath channel delay spread
ϕ	Angle of emergence
$\Phi_{1/2}$	Semi-angle of the transmitting LED's half-power
ψ	Angle of incidence
$\Psi_{1/2}$	Half-angle of the field-of-view of the PD

LIST OF ACRONYMS/ABBREVIATIONS

1G	First Generation of Mobile Cellular Technology
5G	Fifth Generation of Mobile Cellular Technology
ACO-OFDM	Asymmetrically Clipped Optical-OFDM
AF	Amplify-and-Forward
Alice	Access Point
AP	Access Point
AWGN	Additive White Gaussian Noise
BER	Bit Error Rate
Bob	Legitimate User
CSI	Channel State Information
DC	Direct Current
DCO-OFDM	Direct Current Biased Optical-OFDM
DF	Decode-and-Forward
EPA	Equal Power Allocation
EM	Electromagnetic
Eve	Eavesdropper
FD	Full-Duplex
FFT	Fast Fourier Transform
FOV	Field-of-View
GHz	Gigahertz
GSSK	Generalized Space Shift Keying
HD	Half-Duplex
IC	Information-carrying
ICI	Inter-channel Interference
IFFT	Inverse Fast Fourier Transform
IM/DD	Intensity Modulation/Direct Detection
IoT	Internet-of-Things
IR	Infrared

ISI	Inter-symbol Interference
LD	Laser Diode
LED	Light-emitting Diode
LiFi	Light Fidelity
MIMO	Multiple Input Multiple Output
MRC	Maximal Ratio Combining
MU	Multi User
MUI	Multi User Interference
NOMA	Nonorthogonal Multiple Access
OFDM	Orthogonal Frequency Division Multiplexing
OFDMA	Orthogonal Frequency Division Multiple Access
O-OFDM	Optical-Orthogonal Frequency Division Multiplexing
OOK	On-Off Keying
OPA	Optimal Power Allocation
OWC	Optical Wireless Communication
PD	Photodetector
PLS	Physical Layer Security
PPM	Pulse Position Modulation
PWM	Pulse Width Modulation
QoS	Quality-of-service
RF	Radio-Frequency
RLL	Run Length Limited
RX	Receiver
SCD	Spatial Constellation Design
SIC	Successive Interference Cancellation
SINR	Signal-to-Interference-and-Noise Ratio
SM	Spatial Modulation
SNR	Signal-to-Noise Ratio
SSK	Space Shift Keying
THz	Terahertz
TX	Transmitter

VL	Visible Light
VLC	Visible Light Communication

1. INTRODUCTION

Since the introduction of first-generation (1G) mobile networks in the 1980s, the services and applications relying on wireless communication technologies have grown tremendously. The data-rate and latency requirements of evolving multimedia applications, such as those involving augmented/virtual reality, are increasing exponentially, exceeding the capabilities of recent commercial mobile networks [1]. Additionally, the number of served users is expected to grow dramatically with the introduction of internet-of-things (IoT) technologies [2]. The increasing demand from the wireless communication technologies points to the direction of change: the future mobile networks (5G and beyond) have to exploit more resources for increasing data-rate and latency performance to the massive amount of users [1, 3–5].

The wireless network capacity can be significantly improved by expanding the portion of the electromagnetic spectrum for communication purposes [6]. In this context, visible light communication (VLC) is foreseen as a promising solution to the spectrum congestion problem in wireless networks [7]. The main idea of VLC is to exploit the fast-switching capabilities of the modern light-emitting diodes (LEDs) for digital data transmission, thereby realizing both illumination and wireless communication by the same LED infrastructure as visualized in Figure 1.1. The information is encoded on the variation of the light intensity around a constant level, which is insusceptible to humans, as the variation rate is larger than the response rate of the human eye. The transmitted data by VLC can be acquired by the end-users with photosensitive receiver circuits equipped with photodetectors (PDs). LED-based VLC is considered to be a complementary technology in light-fidelity (LiFi) systems, which is a complete wireless networking system supporting multi-user, multiple-input-multiple-output (MIMO), and uninterrupted communication with user mobility [8].

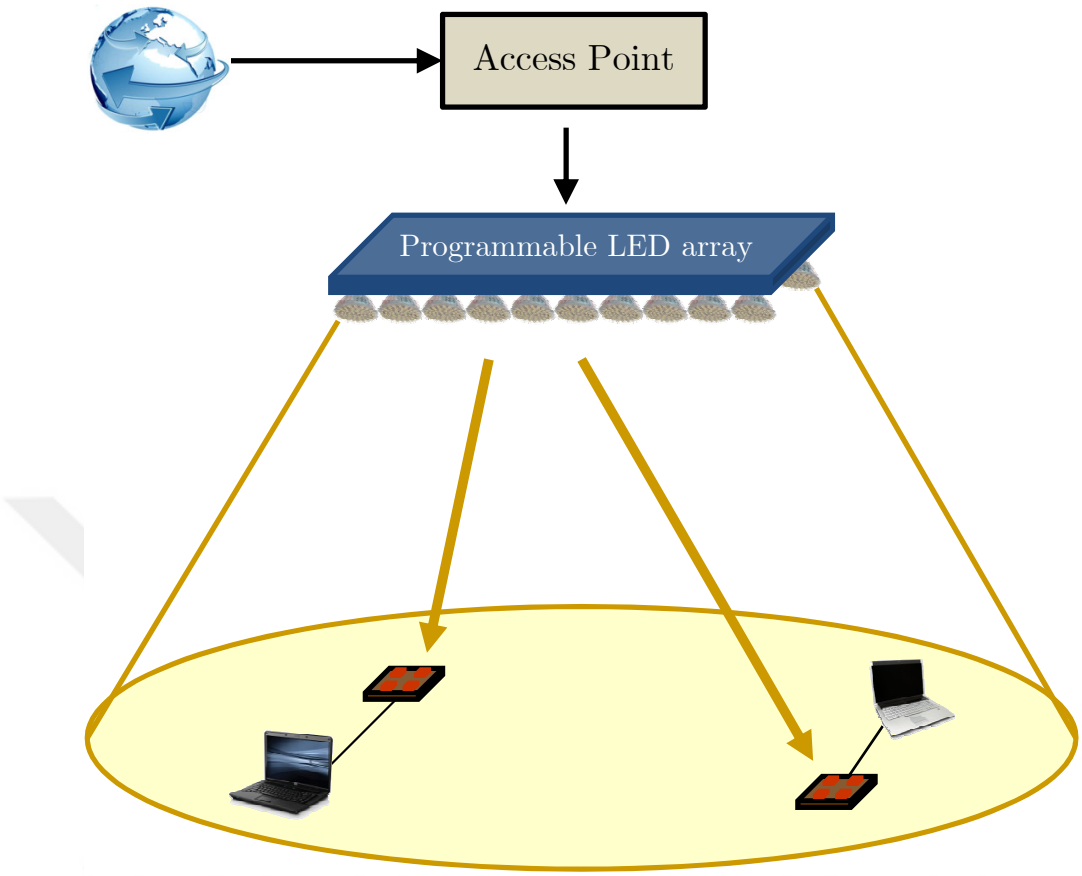

Figure 1.1. Visible light communication system for an indoor setting.

In the recent literature, the advantages and drawbacks of VLC are thoroughly investigated. The main drawback of VLC is that it provides short-range communication as light attenuates faster than RF signals and it cannot penetrate through walls. However, utilizing the optical spectrum on $400 - 800$ THz, the communication bandwidth offered by VLC is around 10^4 times larger than that of the radio-wave communication [9]. Even though the effective bandwidth of VLC is constrained by the modulation order of the LED transmitters, VLC is shown to be capable of providing a data rate of 100 Gb/s when the users are immobile and the laser diode (LD) and PD circuits are optimally aligned [10]. Also with mobile users, the research suggests promising performance results for VLC [11]. Data can be transmitted by VLC wherever there is light: homes, offices, classrooms, conference halls, hospitals, airplanes, trains, etc. [12] or between vehicles [13].

Along with the high data-rate transmission, VLC can be used for user positioning [14]. For all these reasons, VLC is a promising indoor communication solution for 5G networks.

A generic VLC system consists of LED luminaires at the transmitter and photodetectors at the receiver. In conventional RF systems, information is commonly encoded on the amplitude and phase of the electromagnetic signal. On the other hand, in VLC systems, the intensity variations of the emitted light convey information, which is referred to as *intensity modulation*. The emitted light experiences path loss until it reaches the receiving end, where the light beams cause fluctuating luminous flux on the PDs. Due to the major difference in the order of magnitudes between the PD surface area and the wavelength of the visible light, the average phase of the received light beams becomes zero, [15]. For this reason, the only way to extract information from the received light is by the direct detection of the fluctuating luminous flux. This type of information transmission technique is referred to as intensity modulation/direct detection (IM/DD).

In addition to information transmission, the design of VLC systems must satisfy the quality of service requirements of the environment. Firstly, the illumination provided by VLC has to be adjustable following the user preferences. Adjusting the average light intensity is possible in VLC, by dimming the state-of-the-art LEDs to - almost - any preferred illuminance level. It is worth noting that, there is a non-linear relationship between the illuminance of LEDs and the perceived illumination by humans. This is because the human eye can adapt to increased/decreased illuminance levels by adjusting the pupil size, [16]. It is imperative for VLC systems to accommodate for any dimming level by considering the perceived light, such that the speed and reliability of the wireless data transfer are minimally affected.

Secondly, any illumination source must be perceived as if it provides a constant illuminance level, to eliminate any possible physiological changes in humans, which may be elicited by perceivably frequent light intensity variations, [17].

Therefore, the frequency of the intensity variations of LEDs must be high enough that the changes are not detected by the human eye. In other words, the VLC source has to avoid *flickering*, [18]. Flickering can occur when the information encoding does not limit the run length, in which case the emitted light intensity level stays constant when the same information symbol happens to be transmitted consecutively. To mitigate flickering in such scenarios, *Run Length Limited (RLL)* codes can be employed, where each information symbol is represented by more than one intensity level [19]. A popular example for RLL codes is the Manchester encoding scheme, where the 0 and 1 bits are represented by the *down* and *up* transitions in the light intensity level, eliminating flickering for high data-rate applications. Whether or not Manchester coding is employed, any transmission strategy for intensity-modulated VLC systems must consider flicker mitigation, while providing uninterrupted data transfer.

There are various modulation schemes for VLC systems, which provide reliable and high data-rate communication while satisfying the mentioned illumination requirements. The simplest of such schemes is *on-off-keying, (OOK)*. Conventional OOK assigns information bits to ON and OFF states, where the presence and absence of the waveform convey information, respectively. However, in VLC systems, turning the LED entirely OFF is a second-best choice, since it triggers flickering and makes it harder to maintain a constant average intensity level. A better option is to *redefine the ON and OFF levels* and assign them to HIGH and LOW intensity levels to the information bits [20]. The advantage of this approach is that the HIGH and LOW levels can be picked such that the target dimming level is achieved without any further processing. However when low dimming levels are required, the data rate is negatively affected, [21]. Instead, one can apply OOK with ON and OFF levels, and add *compensation periods* to achieve the target dimming level [22]. In this approach, compensation periods are added when the LEDs are turned ON/OFF if the target dimming level is higher/lower than the provided dimming level without any compensation periods. With compensation periods, the overall data rate is reduced, however, the communication quality stays the same regardless of the target dimming level.

In addition to OOK, *pulse modulation* techniques are also simple modulation methods applicable to VLC. In pulse modulation, information is often encoded on either the width or the position of the pulse. In [23], it is shown that the target dimming level can be achieved with *pulse width modulation* without changing the intensity level of the light pulses. In pulse position modulation (PPM), the temporal position of the light pulse conveys information. Multi-level constellation can also be incorporated to PPM, through which higher spectral efficiency and flicker-free communication are achieved while illuminating at the required dimming level [24]. OOK, PWM and PPM are simple and effective communication regimes for VLC, however, these techniques may not provide very high data rates [25].

Similar to RF channels, VLC channels may also introduce inter-symbol interference (ISI) due to their nonlinear frequency response characteristics. The orthogonal frequency division multiplexing (OFDM) regime is well known to be very effective to combat ISI. For this reason, optical OFDM (O-OFDM) regimes are developed for VLC systems [26]. When OFDM is applied to RF systems, the complex time symbols outputted by the Inverse Fast Fourier Transform (IFFT) operation can easily be transmitted by electromagnetic signals. However, intensity-modulated LED signals cannot directly represent negative or complex values, therefore the IFFT symbols have to be processed such that they contain only real and positive values. There are two main approaches, which accommodate the IFFT symbols for IM/DD: *i)* Asymmetrically clipped O-OFDM (ACO-OFDM) [27], and *ii)* direct-current (DC) biased O-OFDM (DCO-OFDM) [28]. In both methods, the OFDM frame is constrained to have Hermitian symmetry, so that the time symbols have only real values. This is realized by generating the second half of each $N-$symbol OFDM frame, by the conjugate transposition of $N/2$ symbols from the first half. This means that the utilized bandwidth of the traditional OFDM is halved. The IFFT of the Hermitian symmetric frame has strictly real entries, however, some of them will be negative. To ensure positivity, a certain DC bias value is added to the time symbols in DCO-OFDM. The DC bias value must be known by the destination so that it is subtracted from the received signal before the detection.

In ACO-OFDM, in addition to the Hermitian symmetry property, the OFDM subcarriers with even numbers are deliberately set to zero, so that the IFFT/FFT procedures do not affect the values carried by the OFDM subcarriers with odd numbers. Due to the OFDM frame design procedures, in ACO-OFDM the utilized bandwidth is equivalent to the quarter of the bandwidth of the traditional OFDM. In DCO-OFDM, the bandwidth is doubled compared to ACO-OFDM in exchange for the transmission power spent for DC bias and not used for conveying information. In an ACO-OFDM VLC system, the receiver structure is identical for all constellations, therefore ACO-OFDM is preferable over DCO-OFDM for communication systems employing adaptive modulation [29]. Here, we note that DC-biased intensity modulation is employed not only in OFDM systems but also on any VLC system with real transmitted signals.

DC-biased intensity modulation is popular in VLC applications for other reasons as well. In DC-biased systems, the illumination is set by the number of LEDs and their DC bias points, which can be optimally selected to meet the illumination constraints. In addition, the intensity variation levels must also be designed properly to make sure that the light intensity emitted by LEDs is always in the dynamic range. If the required instantaneous intensity to be emitted by the LEDs is greater than the upper limit of the dynamic range, it is clipped at the maximum allowable intensity level of the LED. In that case, LEDs operate at the upper limit of their range, which makes them overheat and their efficacies drop. Another issue is that when the LED intensity is saturated, the information signal is clipped, which leads to a reduction in the quality of the transmitted information. This phenomenon is referred to as "clipping distortion" at the LED front-end, which is theoretically described by a random "clipping noise" added on the LED driving vector, to push the LED instantaneous intensity into the dynamic range. The signal clipping can be easily avoided by power normalization of the signal constellation if the VLC transmitter employs does not employ any sort of pre-processing. Otherwise, the pre-processed transmitted signal may have components that will be clipped. For example in DCO-OFDM systems, the peak-to-average power ratio is high due to the IFFT block, leading to some signal components in the driving vector force LEDs into saturation.

For multi-hop VLC systems, the signal clipping may be existent in all transmitting terminals, in which the transmitted SNR progressively worsens at each hop. For such systems, the VLC transmitters must be designed considering the clipping noise.

Indoor lighting systems are usually comprised of multiple LEDs to provide sufficient illumination to the environment. This is an opportunity to apply MIMO architecture to VLC systems [30]. In MIMO-VLC systems, the emitted light by each LED in the array is programmed separately to convey individual information signals to the receivers. At the destination, multiple PDs can be installed at the receivers, increasing the spatial diversity. The increased spatial diversity by MIMO improves the SNR of the VLC channel, its capacity, reliability, quality-of-service (QoS), and error performance. Moreover, MIMO-VLC can support multiple users with proper multiple access techniques [31, 32], over the communication resources such as frequency, space, time, and code [33–36]. Among these techniques, non-orthogonal multiple access (NOMA) stands out with its superior spectral efficiency [37]. By NOMA, the information for multiple users is multiplexed in the power-domain and transmitted using the shared communication resources. NOMA performs especially well when the received SNR is high [38], which is usually the case for indoor VLC systems with short transmitter-receiver distance. Therefore, the application of the MIMO-NOMA framework has gained significant attention in the VLC literature [39–42].

One of the main challenges of the VLC system design is to decrease shadowing as much as possible. In the shadowed regions, the communication performance is deteriorated due to the nonexistence of the line-of-sight (LoS) link from the VLC access point. In such cases, the average BER and throughput performance can be substantially improved by deploying VLC relays as pointed out in [43,44]. To the best of the researcher's knowledge, the work in [45] is one of the first works to consider relays in VLC systems. In that work, the authors propose a half-duplex (HD) mode amplify-and-forward (AF) relaying protocol for DCO-OFDM VLC with optimized power allocation. The authors extend their work to HD mode decode-and-forward (DF) relaying in [46], where the LED clipping distortion is introduced to the VLC access point.

A cooperative VLC system with multipath channels is considered in [47], where the performance degradation with respect to ideal single link VLC channels is quantified. There are many other works proposing effective transceiver architectures for cooperative VLC. A superimposed relaying scheme is proposed in [48], where the relay superimposes own information to the information from the source and then transmits. The full-duplex cooperation is introduced to VLC in [49], where the relay can transmit and receive simultaneously. A two-way relaying framework is proposed in [50], where the relay enables simultaneous communication to two VLC users. The VLC relay positioning problem is tackled in [51, 52] for linear and triangular system topologies. The aforementioned works show that utilizing relay-assistance improves VLC performance significantly. However, as it will be detailed in Chapter 3, most of the works in the cooperative VLC literature either omit or provide incomplete models for LED clipping distortion. LED distortion is more serious for the DC biased optical OFDM systems, since their peak-to-average-power ratio (PAPR) is high due to the inverse fast Fourier transform (IFFT) procedure at the VLC transmitter. Even though there are some works which do consider LED distortion, such as [46, 47], either the clipping effects are included for half-duplex mode and not full-duplex relaying or the clipping effects are omitted at the relay and only considered at the source. Therefore, a complete cooperative VLC system design is required, where LED distortion is carefully included at both the source and the relay and for both the half- and full-duplex relaying modes.

Another important challenge regarding the VLC system design is to ensure the security of the broadcasted private information. Even though VLC systems provide inherent security by the limited confinement of the optical signals, they may still be vulnerable to various security attacks, when the eavesdroppers are positioned in the VLC coverage area. Eavesdropping is a more serious threat for multiple access MIMO-VLC systems since they broadcast private information belonging to multiple users. A simple but effective security attack is passive eavesdropping, where an eavesdropper listens to the broadcasted information to extract confidential messages for various users.

Traditionally, information confidentiality is secured by cryptographic techniques, which involves ciphering techniques relying on publicly known algorithms and secretly shared secret keys by the communicating parties. Theoretically, cryptographic measures do not guarantee perfect secrecy, however, the utilized cyphering techniques exploit the lack of sufficient computational power of the eavesdroppers to decode the ciphered information reliably without the secret key. Hence, they have been very effective to this date. Another approach is to exploit the channel characteristics between the communicating parties to pre-process the transmitted signal at the transmitter. In the literature, this approach is referred to as *"physical layer security"* (PLS), and aims to ensure information security at the physical layer of the wireless network, by constructing the transmitted signals in such a way that the received SNR of the eavesdroppers are significantly corrupted and they cannot decode the confidential information reliably. PLS techniques are simpler to implement than ciphering procedures, and they are very effective in VLC systems.

In this thesis, the researcher proposes improvements to existing VLC systems for *i)* more efficient cooperation and *ii)* more secure transmission strategies. In the following section, the related background is given for these two main aspects.

1.1. Related Background

1.1.1. Cooperation via Relays

A relay is a terminal that processes and transmits its received signal from the source in an attempt to improve the communication performance at the destination. In this sense, the source cooperates with the relay to improve the received signal at the destination. Relay channels are extensively studied in [53]. In point-to-point communication, the destination receives only y_{SD}, which is a noisy version of the source's message signal x. In a generalized relay channel, the relay receives y_{SR}, which is a noisy version of x. Then, the relay constructs the relay signal x_R by processing y_{SR}, which is transmitted to the destination.

The destination receives a superposed signal y, which is the noisy sum of the relay signal x_R and the message x. The very first challenge in such a system is to find an effective method to construct x_R, such that the decoding performance of the destination based on y is improved compared to that of based on y_{SD}. This question leads us to the capacity of the relay channels, which are described by Thomas Cover in [54]. In that work, the channel capacities are formulated and proven for the degraded relay channel, arbitrary relay channel with feedback, and the general relay channel. It is also shown that the found capacities can be achieved when the relay employs superposition block Markov encoding. The findings in that work indicate that cooperation via relays can improve communication significantly when correct encoding schemes are used at the relay. Since then, relays are often utilized in RF systems, especially in wireless sensor networks [55].

Cooperation via relays can also improve communication performance in VLC systems. Different than RF waves, light signals are more easily obstructed by opaque objects, hence shadowing is more common in VLC systems. Therefore, cooperation in VLC systems not only improves BER and data rate but also provides communication with significantly less outage probability. The work in [56] considers a cooperative VLC system within a large indoor environment, where establishing an LoS link between the source and the destination terminals is a great challenge. To achieve a Gbps-level data rate, laser diodes and imaging receivers are utilized. In that work, the authors propose two relaying algorithms for various relay positionings within the environment. It is shown that when the source-relay distance is the largest, i.e. the worst-case configuration, the channel bandwidth of the proposed VLC system is increased to 26 GHz (about 0.006 ns delay spread) by cooperation. For cases in which the relay has its information to send to the destination, an effective superimposed relaying strategy is proposed in [48]. According to this strategy, the information generated at the relay is superposed on the received message from the source and then transmitted. This approach results in enlarging the symbol constellation due to the symbol superposition. The authors provide optimum power allocation at the relay for minimized BERs at the destination, subject to optical power constraints.

The work in [57] considers the relay positioning problem for an indoor VLC system to minimize the detrimental effects of the blockages. In particular, the blockages are modeled under two cases: *i)* blockage from standing people, and *ii)* blockage from sitting people. To establish LOS links around the blockages, a desk light is utilized as a relay terminal. For all cases, illumination constraints are applied to the LED distribution and the allocated power between the source and the relay. In the case of nonexistent LoS links, the light signals are assumed to reach the destination via reflections from various surfaces within the room. The simulation results show that cooperation via relays improves the BER at the destination by establishing LoS links between the source and the destination.

In general, there are two main options for relays in terms of the communication resources (time, frequency, etc.), they use for reception and transmission. Let the relay employ time-division multiple-access. One option is *i)* half-duplex (HD) mode, where the relay performs reception and transmission over non-intersecting time intervals. In this case, the relay stops transmitting while it is listening to the source. The other option is *ii)* full-duplex (FD) mode, where the relay transmits its message to the destination while receiving transmission from the source. Compared to the half-duplex mode, in the full-duplex mode, the data rate is theoretically doubled, since the time resource is not divided between transmission and reception. For RF systems, however, the relay might be experiencing self-interference in FD mode, since the RF signals transmitted by the relay can be received by its receiver circuits. In the literature, this is referred to as the *loop interference* and is a detrimental factor for the BER at the destination. Therefore, FD cooperative RF systems must mitigate the effects of loop interference for improved BER. FD relaying can be easily adapted to VLC systems since the light signals attenuate faster over the non-LoS links than the RF signals. An OFDM-based VLC system with FD relaying is proposed in [49], where the characterization of the loop interference channel is also provided. In that work, the BER performance of the proposed OFDM-VLC system is evaluated and compared with the direct transmission and HD relaying options. It is indicated that FD relaying outperforms both regimes and is more suitable for high modulation orders.

1.1.2. Physical Layer Security

In wireless communication systems, the transmission medium is accessible by many users including both legitimate and unauthorized ones. Considering that personal, banking, commercial and military data traffic involving private information has ever been increasing, it is vital for future technologies to ensure the *confidentiality* or *secrecy* of information. In general, eavesdroppers intercept the communication channel of the intended receiver, then attempt decoding the encoded information. In most wireless systems, channel interception is rather easy for eavesdroppers, due to the broadcast nature of the electromagnetic waves up to the gigahertz (GHz) band. After the interception, Eve can decode the received signal successfully if the information has not been encrypted or Eve has access to the private key. Traditionally, information is encrypted using sophisticated cryptographic techniques and the private key is safely shared with legitimate users. It is not practical for Eve to decrypt ciphers without the secret key since it would exhaust the computational resources at the receiver. Therefore, cryptography has become very useful to provide security in most wireless networks.

In recent literature, PLS has emerged as a potential approach to complement the security algorithms based on cryptographic techniques. PLS is envisioned as a required component of the future wireless systems since they provide secrecy on the physical layer - which is not covered by the existing security frameworks - and they rely on information-theoretic foundations. The concept of secrecy is introduced to information theory by Shannon in [58]. In that work, a three-terminal communication system is considered which is comprised of an access point, a legitimate receiver, and an eavesdropper. The access point intends to transmit a confidential message to the legitimate user, by pre-processing it with a one-time secret key, shared by the legitimate user. Shannon assumes that Eve has unlimited computational power and can receive an exact copy of the legitimate user's received signal. Eve is also aware of the pre-processing procedure adopted by the access point. As Eve is not aware of the secret key, it attempts to decode the confidential message by repeatedly "guessing" the secret key.

According to the *perfect secrecy* defined by Shannon, the mutual information between the encrypted message and the confidential message must be zero, which implies that the entropy of the secret key is at least equal to that of the original message. This notion of perfect secrecy is also referred to as "strong secrecy". Later, Wyner introduces the "wire-tap channel" in [59], where the eavesdropper receives the transmitted message over a degraded version of the legitimate user's channel. In that work, the purpose is to design an encoder-decoder pair that "confuses" the eavesdropper as much as possible. The level of "confusion" at the eavesdropper is quantified by the entropy of the message signal conditioned on the encoded signal, so perfect secrecy can be achieved when the "confusion" is equal to the unconditional source entropy. The analysis outlined by Wyner is used to develop the concept of "secrecy capacity", which is a measure for how much eavesdropper's reception is worsened while the message signal is delivered to the legitimate user with an acceptable error probability.

The concept of secrecy capacity can be utilized to ensure security at the physical layer. Specifically, the characteristics of the transmission medium can be exploited to design sophisticated encoder-decoder pairs for modern communication systems. In particular for optical communications, there has been a significant amount of work conducted on PLS for optical MIMO systems with single legitimate user, [60–69], and multiple legitimate users, [70–75]. Among many MIMO transmission techniques, GSSK stands forward with improved efficiency by activating only the selected transmit units every transmission [76–78]. In GSSK, information is transmitted by spatial symbols conveyed by the indices of the activated transmit units. This is different from the conventional wireless transmission, where the constellation symbol is encoded on the amplitude and phase of the transmitted waveform. The special case of GSSK with only one activated transmit unit is called SSK [79], which has lower spectral efficiency however simpler to employ for the transmitter. In this thesis, GSSK is utilized in the design of the proposed PLS precoder for the multi-user MIMO-VLC systems in Chapter 4.

Increased spectral efficiency can also be achieved by NOMA, by transmitting messages belonging to multiple users over the same communication resource blocks [4]. Ensuring PLS in NOMA-based systems is rather challenging since it relies on multiplexing individual messages on the power domain and transmitting them non-orthogonally, which has fused the research interest in secure NOMA-based communication systems. The secrecy capacity of MIMO-NOMA systems is derived in [80]. The expression found for the secrecy rates is then used to formulate problems for optimum power allocation policies which either aim to maximize the secrecy capacity [81], [82] or the minimum secrecy capacity [83].

In the following section, the motivating factors are explained which have led the researcher to address the problems that this thesis deals with.

1.2. Motivation for this Thesis

Intensity modulation is a simple yet effective method to convey information via visible light, however, some technical issues regarding the operational characteristics of LEDs require special consideration. One of these matters, the limited dynamic range of LEDs, poses importance. The intensity of the light emitted by LEDs has an upper and lower bound, defined by the LED dynamic range. If the modulating information symbols require an intensity level not supported by the LEDs, data cannot be properly transmitted since the information-carrying light intensity is clipped to fit the dynamic range. This clipping occurs at the LED front-end and causes a reduction in the transmitted SNR as well as a decrease in the decoding and BER performance at the receivers. The signal clipping can be easily avoided by a simple DC bias addition with magnitude normalization. However, signal clipping may be inevitable for most of the modern transmission techniques employing OFDM or any other methods involving pre-processing with a high peak-to-average power ratio. Similarly, the multi-hop cooperation design is also challenging for VLC, because at each inter-terminal transfer, the SNR is reduced by the LEDs' signal clipping, leading to the loss of cooperation gains.

Motivated by the need for a more efficient system design, in Chapter 3, optimal power allocation policies are sought for the cooperative VLC with the consideration of the signal clipping at the LED front-ends of all transmitting terminals.

Another important issue regarding the VLC system design is to secure the confidentiality of the transmitted information. The penetration of visible light is shorter than RF waves, therefore, the coverage area of a specific LED is more limited than that of RF systems, which makes VLC systems inherently more secure. However, information security may still be threatened if eavesdroppers are present in the VLC coverage area. For this reason, information must be processed before its transmission to maintain confidentiality. The traditional approach is to employ ciphering techniques based on cryptography, which rely on the limited computational power assumption of the eavesdroppers. By employing cryptographic techniques, information security can be practically unbreakable, however, they also require great computational resources. Recently, a new paradigm has been standing forward for information security over wireless media, namely physical layer security (PLS), which is based on information-theoretic foundations and also is less costly to apply, especially, to future communication systems with a massive amount of users. In PLS frameworks, the channel state information shared by the legitimate users and the transmitter - either complete or partial - is exploited, so that the transmitted information cannot be obtained by eavesdroppers, while successful decoding is practicable at the legitimate users. The security performance of PLS systems is quantifiable by secrecy rates and regions, which can be derived analytically for a given communication system. In Chapters 4,5 of this thesis, PLS ensuring precoding strategies are proposed for multi-user MIMO-VLC systems. The proposed precoding frameworks are also extended to multi-user RF systems. The proposed transmission schemes utilize several communication technologies such as generalized space shift keying (GSSK), NOMA, spatial modulation (SM), spatial constellation design (SCD), etc. More details on the contributions of this thesis are given in the following section.

1.3. Contributions of this Thesis

This thesis studies VLC systems in terms of two main aspects: cooperation and physical layer security. To summarize, the contributions of this thesis are as follows.

(i) In Chapter 3, a cooperative VLC system with 3 terminals is considered, and the transmission rate expressions are formulated for full-duplex AF and DF relays under the consideration of the signal clipping effects at the LED front-ends. Then, the DC bias values and information-carrying signal variances are optimized to find the achievable rate values for a given cooperative VLC system. The obtained achievable rates are then compared with those of the half-duplex cooperative and single-link VLC systems for different illumination preferences.

(ii) In Chapter 4, a novel PLS technique, namely MU-GSSK-SCD, is proposed to ensure the PLS of multi-user MIMO-VLC systems with an eavesdropper. The precoding scheme is based on GSSK, in which only the selected antennas are activated for information transmission. The intensity of each LED is adjusted such that the received spatial constellations of the legitimate users are optimally shaped in terms of their BER performance. Meanwhile, the received signal at the eavesdropper is significantly distorted due to the proposed precoding.

(iii) The secrecy rates and bounds are derived for VLC systems employing MU-GSSK-SCD, and its secrecy performance is obtained by computer simulations in terms of both the derived secrecy regions and BER performances. Its performance is also compared with conventional PLS methods based on artificial noise broadcast. This chapter is published in [84]. Motivated by the flexibility of the GSSK-based PLS system, the proposed MU-GSSK-SCD scheme is extended to multi-user MIMO-RF systems and published in [85]. The secrecy rates and bounds of MU-GSSK-SCD are derived for MIMO-RF systems, and its secrecy performance is compared with conventional GSSK and artificial noise-aided GSSK strategies.

(iv) In Chapter 5, a novel transmit precoding scheme based on receive SM is proposed for PLS provision of multi-user MIMO-NOMA-VLC systems. The proposed precoder employs randomized constellation coding and exploitation of the legitimate users' CSI. The secrecy performance of the proposed precoding system is obtained for various user locations and different LED/PD numbers. This chapter is presented in [86].

The outline of this thesis is as follows. In Chapter 2, the MIMO-VLC channel, cooperative VLC with LED distortion, GSSK-based VLC and NOMA-based VLC systems are described. In Chapter 3, the rate-maximizing VLC transmitter design problem is tackled and solved for a full-duplex cooperative system with the consideration of LED clipping distortion effects. Next, in Chapter 4, a novel GSSK-based PLS framework is proposed for multi-user MIMO-VLC systems with a single eavesdropper. Motivated by the flexibility of the GSSK-based PLS system, the precoding framework is extended to multi-user MIMO-RF systems. In Chapter 5, a new PLS precoding strategy is proposed for NOMA-based multi-user MIMO-VLC systems. This thesis is finalized in Chapter 6 with concluding remarks.

2. FUNDAMENTALS OF VISIBLE LIGHT COMMUNICATIONS

In this thesis, VLC systems are modeled within indoor environments using LED transmitters and PD receivers. The access point is equipped with N_t LEDs, whose emitted light intensities can be modulated by the incoming data while providing seamless illumination. Specifically, the driving current of each LED is varied around a preset DC bias level, which induces variations in the emitted light intensity and the received optical power on the PDs. The received optical power induces an output current from the PD, which is - ideally - proportional to the illumination on the PD. Then, the variations in the PD output current can be directly detected by the receiver circuits, and information is extracted. Since the LED light intensity is varied at a very high rate, the human eye perceives constant illumination, which is decided by the specified DC bias level for the driving currents of the LEDs. The PD output current is a function of the illumination on the PD surface, which is a function of several factors involving the relative positioning of the LED-PD pair and the LED radiation specifications. The relative positioning of the LED and PD effects is illustrated with a single ray in Figure 2.1.

In the following, Lambertian emission-based VLC channel model is described which is utilized in this thesis.

2.1. VLC Channel Model

In this thesis, it is assumed that LED radiation is characterized by the Lambertian emission pattern, according to which the luminous intensity on the LED depends on the cosine of the emittance angle, ϕ. Similarly, the illuminance on the PD is a function of the cosine of the incidence angle, θ.

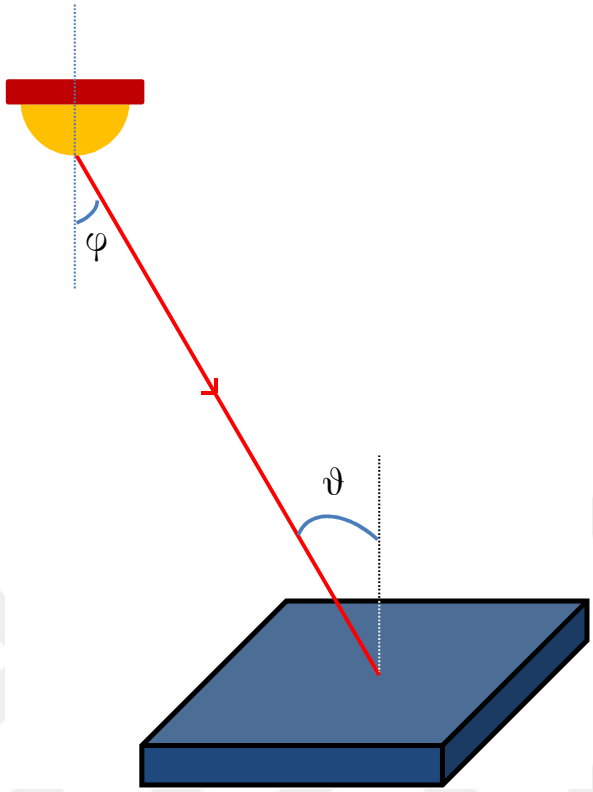

Figure 2.1. The emittance and incidence of a single ray for an LED - PD pair.

The received optical power, P_r, is proportional to the luminous flux incident on the PD, which is found by integrating the illuminance over the PD area. Therefore, P_r is calculated by

$$P_r = \frac{P_t \cos^m(\phi)(m+1)}{2\pi d^2} A_{\text{PD}} \cos(\theta), \tag{2.1}$$

where P_t is the emission power of the LED, m is the Lambertian emission order, and A_{PD} is the PD area. The Lambertian emission order is simply a measure for the rate of change of the LED emission power with respect to the emittance angle. This parameter depends on the LED's half-power angle of the LED, $\Phi_{1/2}$, and is given by

$$m = \frac{-1}{\log_2(\cos(\Phi_{1/2}))}. \tag{2.2}$$

The luminous intensity of an LED is maximum at its center and drops as ϕ increases.

The parameter $\Phi_{1/2}$ denotes the emittance angle at which the luminous intensity is halved. Hence, $\Phi_{1/2}$ can be used as a measure for the LED emission uniformity with changing ϕ. A low $\Phi_{1/2}$ value indicates that a change in ϕ results in a large decrease in the emitted power for that selected LED. Therefore, LEDs with larger $\Phi_{1/2}$ values have a wider FOV with little or no drop in emission power.

The channel gain between the LED-PD pair is the ratio of the received optical power to the emitted optical power from (2.1), which is found as

$$h = \left(\frac{\cos^m(\phi)(m+1)}{2\pi d^2} A_{\mathrm{PD}} \cos(\theta) \right) \mathbb{1}_{\Psi_{1/2}}(\theta), \tag{2.3}$$

where $\mathbb{1}_{\Psi_{1/2}}(\theta)$ is an indicator function, defined by

$$\mathbb{1}_{\Psi_{1/2}}(\theta) = \left\{ \begin{array}{ll} 1 & \theta \leq \Psi_{1/2} \\ 0 & \theta > \Psi_{1/2} \end{array} \right\}. \tag{2.4}$$

So, the PD output current will drop to zero if the incidence angle of the ray is larger than $\Psi_{1/2}$. Hence, it must be made sure that PDs must be placed such that LEDs are in their FOV. The channel model in (2.3) applies to cases where the users are static.

Using (2.3), one can find an analytical model for the VLC channel between an access point and a user, given the locations and orientations of the LEDs and PDs they are equipped with. Denoting the LED and PD indices with t and r respectively, the channel from the access point to the destination is described by

$$\mathbf{H} = \left[\begin{array}{cccc} h^{1,1} & h^{1,2} & \dots & h^{1,N_t} \\ h^{2,1} & h^{2,2} & \dots & h^{2,N_t} \\ \vdots & \vdots & \ddots & \vdots \\ h^{N_r,1} & h^{N_r,2} & \dots & h^{N_r,N_t} \end{array} \right], \tag{2.5}$$

where $h^{r,t}$ denotes the channel gain between the rth PD and tth LED. Also, N_r and N_t denote the number of PDs and LEDs, respectively.

In the following, the relay-equipped VLC system model is introduced.

2.2. Cooperative VLC with LED Distortion

In this section, the access point communicates with the user via a VLC relay as illustrated in Figure 2.2. The relay is a VLC transceiver, which can forward its received signal by AF or DF relaying. For the cooperative VLC model, the signal generated at the source is treated as a real Gaussian random variable denoted by x_S, which modulates the intensity of the transmitting LED. The variance of x_S is σ_S^2. According to the DC-biased IM, the driving current of the LED is found by the sum of x_S and B_{DC}, a positive DC bias value. However, the driving current is not allowed to result in "negative intensity", therefore x_S is clipped before the DC bias addition according to

$$x_S^{\mathrm{cl}} = \begin{cases} x_S, & x_S \geq -B_{\mathrm{DC}} \\ -B_{\mathrm{DC}} & x_S < -B_{\mathrm{DC}}. \end{cases} \tag{2.6}$$

Then the LED driving current is obtained by

$$x_S^{\mathrm{LED}} = x_S^{\mathrm{cl}} + B_{\mathrm{DC}}, \tag{2.7}$$

where x_S^{LED} modulates the LED.

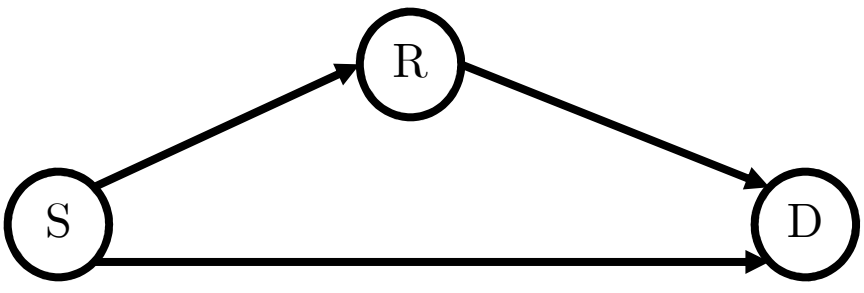

Figure 2.2. The source-relay-destination configuration.

The LED can transmit x_S^{LED} without clipping only if $x_S^{\mathrm{LED}} > 0$.

Since the input x_S is Gaussian, the clipping operation given above can be modelled as a Gaussian clipper, hence Bussgang's theorem from [87] can be applied on the statistical relationship between x_S and x_S^{cl} given in (2.6). We get

$$x_S^{\mathrm{cl}} = a_S x_S + w_S^{\mathrm{cl}}, \tag{2.8}$$

where a_S is the attenuation factor and w_S^{cl} is the Gaussian clipping distortion term. The attenuation factor and the clipping distortion variance are found at [87] as

$$a_S = 1 - Q\left(\frac{B_{\mathrm{DC}}}{\sigma_S}\right) \tag{2.9}$$

$$\begin{aligned}\sigma_{S,\mathrm{cl}}^2 = \sigma_S^2 \Bigg[1 + \left(\left(\frac{B_{\mathrm{DC}}}{\sigma_S}\right)^2 - 1\right) Q\left(\frac{B_{\mathrm{DC}}}{\sigma_S}\right) - \frac{B_{\mathrm{DC}}}{\sigma_S} g\left(\frac{B_{\mathrm{DC}}}{\sigma_S}\right) \\ - Q\left(-\frac{B_{\mathrm{DC}}}{\sigma_S}\right)^2 - \left(g\left(\frac{B_{\mathrm{DC}}}{\sigma_S}\right) - \frac{B_{\mathrm{DC}}}{\sigma_S} Q\left(\frac{B_{\mathrm{DC}}}{\sigma_S}\right)\right)^2 \Bigg],\end{aligned} \tag{2.10}$$

where $Q(\cdot)$ and $g(\cdot)$ are the tail distribution and the probability density function of the standard normal distribution respectively. It is assumed that B_{DC} is known by the receivers and can be removed prior to decoding. Then, the transmitted signal x_S^{cl} is received by the relay as

$$y_R = h_{SR}(a_S x_S + w_S^{\mathrm{cl}}) + w_R^{\mathrm{AWGN}}, \tag{2.11}$$

where y_R, h_{SR} and w_R^{AWGN} denote the relay's received signal, the channel gain from the source to the relay and the AWGN term due to thermal noise. Notice that y_R consists of the scaled information x_S and an effective noise, which is the sum of LED distortion and AWGN.

Hence y_R is rewritten as

$$y_R = A_{SR}x_S + w_{n,SR}, \tag{2.12}$$

where $A_{SR} = h_{SR}a_S\sigma_S$ is the effective signal amplitude and $w_{n,SR} = h_{SR}w_S^{cl} + w_R^{\text{AWGN}}$ is the effective noise at the relay which is a zero-mean Gaussian random variable with the variance of $\sigma_{n,SR}^2 = h_{SR}^2\sigma_{S,cl}^2 + \sigma_{\text{R,AWGN}}^2$. After its reception, the relay generates own signal x_R based on y_R either by amplification or decoding. The relay's LED may also introduce distortion to x_R, hence

$$x_{R,\text{cl}} = a_R x_R + w_R^{cl}, \tag{2.13}$$

is transmitted to the destination. Then, the destination receives $x_{R,\text{cl}}$ as

$$y_{\text{RD}} = A_{\text{RD}}x_R + w_{n,\text{RD}}, \tag{2.14}$$

where y_{RD} is the received signal from the relay, $A_{\text{RD}} = h_{RD}a_R\sigma_R$ denotes the effective signal amplitude of x_R, and $w_{n,\text{RD}} = h_{RD}w_R^{cl} + w_D^{\text{AWGN}}$ is the effective noise at the relay, which is a zero-mean Gaussian random variable with the variance of $\sigma_{n,RD}^2 = h_{RD}^2\sigma_{R,cl}^2 + \sigma_{\text{D,AWGN}}^2$. Now, based on y_{RD}, the destination can decode x_S. The cooperative system model introduced here will be extended to half-duplex and full-duplex DCO-OFDM VLC systems in Chapter 3.

2.3. GSSK-based VLC

Let the access point and the destination communicate using a codebook, $\mathcal{C}$, which consists of M information symbols denoted by $\mathbf{s}_i$ for $i = 1, \ldots, M$. In intensity-modulated DC-biased VLC systems, information is encoded on the varying light intensity around a constant DC bias level. Let $\mathbf{x} \in \Re^{N_t \times 1}$ denote the information-carrying LED intensity variation vector. The selected information symbol $\mathbf{s}_i$ from $\mathcal{C}$ shapes the vector $\mathbf{x}$. The way $\mathbf{x}$ is shaped depends on the adapted transmission technique.

Let $\mathbf{J} = [j_1, j_2, \ldots, j_{N_a}]$ be a set of LED indices with $j_t \in \{1, 2, \ldots, N_t\}$ for $t = 1, \ldots, N_a$. The set $\mathbf{J}$ indicates the activated LED indices for a transmission. Let $\mathcal{J}$ be the collection of all distinct $\mathbf{J}$ sets. For GSSK-VLC, every symbol $\mathbf{s}_i$ in $\mathcal{C}$ is assigned a set $\mathbf{J}$ in $\mathcal{J}$. The activated LEDs indicated by the selected $\mathbf{J}$ set are assigned an intensity variation of I_a, while the deactived LEDs are assigned an intensity variation of 0. For instance, the intensity variation vector for a randomly selected symbol $\mathbf{s}_i$ would be

$$\mathbf{x} = \begin{bmatrix} 0 & I_a & \ldots & 0 & \ldots & I_a & \ldots & 0 & \ldots & I_a & \ldots \\ & \uparrow & & & & \uparrow & & & & \uparrow & \\ & j_1 & & & & j_2 & & & & j_{N_a} & \end{bmatrix}^T, \tag{2.15}$$

where j_t for $t = 1, \ldots, N_a$ stands for the activated LED index. The receiver obtains the transmitted GSSK signal as

$$\mathbf{y} = \mathbf{H}(\mathbf{x} + \mathbf{B}_{\mathrm{DC}}) + \mathbf{n}, \tag{2.16}$$

where $\mathbf{y} \in \Re^{N_r \times 1}$ is the received signal at the destination, $\mathbf{B}_{\mathrm{DC}}$ is the $N_t \times 1$ DC-bias vector, and $\mathbf{n} \in \Re^{N_r \times 1}$ is the additive white Gaussian noise (AWGN) vector. The receiver has the prior information for $\mathbf{H}$ and B_{DC}, hence it can decode $\mathbf{y}$ to extract the message $\mathbf{s}_i$ using $\mathcal{C}$ and $\mathcal{J}$ via maximum likelihood detection. Notice that, in RF-GSSK systems, deactivated antennas do not emit any sort of waveform, while in GSSK-VLC, deactivated LEDs emit the intensity produced by the DC bias current. This is necessary to provide stable illumination without any flickering. GSSK-VLC can be adapted to multi-user downlink communication by using joint codebooks and joint collection of LED indices. Secure communication is also possible with GSSK-VLC with proper pre-processing. A novel framework for GSSK-based secure multi-user VLC is proposed in Chapter 4. In the following, NOMA signaling is described for VLC.

2.4. NOMA-based VLC

For a NOMA-based VLC system, the information symbols for multiple users are superposed in power-domain and encoded on the intensity variation vector, $\mathbf{x}$. Assume that there are 2 users communicating with the access point in a NOMA-VLC system without any pre-processing. Let the user codebooks be defined as

$$\mathcal{C}_k = \{\mathbf{s}_k^1, \mathbf{s}_k^2, \ldots, \mathbf{s}_k^M\}, \tag{2.17}$$

where $k = 1, 2$ denotes the user index, $\mathcal{C}_k$ denotes user k's codebook, and $\mathbf{s}_k^r \in \{\Re_{N_t \times 1}\}$ denotes user k's rth information symbol for $r = 1, \ldots, M$. Superposing both symbols non-orthogonally yields

$$\mathbf{x} = \sqrt{\alpha}\mathbf{s}_1 + \sqrt{(1-\alpha)}\mathbf{s}_2, \tag{2.18}$$

where $0 < \alpha < 1$ is the NOMA power coefficient. According to the NOMA principles, the user with the lower channel gains (weak user) is assigned a higher power coefficient to improve the overall communication performance. Assume that user 1 is the strong user in (2.18), hence $\alpha < 0.5$ is selected. The received signals at the users become

$$\mathbf{y}_k = \mathbf{H}_k(\mathbf{x} + \mathbf{B}_{\mathrm{DC}}) + \mathbf{n}_k. \tag{2.19}$$

Again, the effects of the channel and the DC bias can be removed at the users with the prior information on $\mathbf{H}_k$ and B_{DC}. Since the access point assigns $\mathbf{s}_1$ a lower NOMA coefficient, $\mathbf{s}_2$ is the strong signal in $\mathbf{x}$ and can be directly detected. Therefore, user 2 can recover its signal by ML detection. On the other hand, $\mathbf{s}_1$ is the weak signal in $\mathbf{x}$, therefore user 1 must first decode $\mathbf{s}_2$ then remove it from its received signal. This operation is referred to as successive interference cancellation (SIC). User 1 can apply ML detection to extract its signal after SIC is complete. In Chapter 4, a secure precoded NOMA strategy is developed for multi-user MIMO-VLC systems.

2.5. Conclusion

In this chapter, the fundamentals of VLC systems are introduced. First, the MIMO-VLC channel model is formulated under the Lambertian emission model at the source. Secondly, the cooperative VLC signal model is developed considering the clipping noise effects at the transmitting terminals. Next, the GSSK-based VLC model is constructed, which utilizes DC-biased intensity modulation. Finally, a NOMA-based VLC signal model is established, which enables spectrally efficient multiple access. These key models form the foundation for the VLC system designs in the upcoming chapters. In the following chapter, efficient relaying strategies are proposed for full-duplex cooperative VLC systems, which are affected by clipping noise.

3. FULL DUPLEX COOPERATIVE VISIBLE LIGHT COMMUNICATIONS WITH CLIPPING NOISE EFFECTS

3.1. Introduction

Visible light communication (VLC) is an energy-efficient solution for indoor short-range communication as it provides simultaneous illumination and communication via programmable light-emitting diode (LED) arrays and offers high data rates over a very large bandwidth [7, 9]. The existing LED lighting infrastructure can be used as both illuminators and wireless transmitters as noted in [88], which is rendered possible by the latest LED technologies, which provide high dimming speed as reported in [89], [90]. Research also shows that VLC communication can offer high-speed data transmission, as the area spectral efficiency is improved by VLC in [91], which can be utilized for increased data rate. In [56] and [92], it is shown that 10 - 15 Gb/s data rates can be achieved by VLC, using enhanced optical transmitters and receivers.

As in its radio-frequency counterparts, incorporating the relay assistance and forming cooperative VLC systems bring further improvements in terms of fundamental performance metrics such as the bit error rate (BER) and network coverage as shown in [43] and [44], respectively. Relay-assisted VLC channels are already included in the IEEE 802.15.7r1 VLC standardization group for short-range optical wireless communications as noted in [93]. Designing effective transceiver architectures for relay-aided VLC has also spun significant research interest. For instance, BER minimization is considered in [57] by optimum relay positioning for indoor cooperative VLC systems, in [48] for superimposed relaying and in [94] for underwater VLC channels. Then BER minimization for half-duplex (HD) cooperative VLC systems by power allocation among the source and relay is considered in [45] for amplify-and-forward (AF) relaying and in [47] for decode-and-forward (DF) relaying. BER minimization for a similar system is also considered for full-duplex (FD) relaying in [49]. Similarly, relay positioning for BER minimization is proposed for FD relaying in [51] and [52].

All these works demonstrate the comparative advantages of utilizing cooperation in VLC and for this reason, in this chapter, we also consider 3-terminal (relay-aided) cooperative VLC, for which we address the transmission rate maximizing power allocation problem.

In this regard, some design challenges need careful consideration. For instance, both direct link and cooperative VLC systems suffer from intersymbol interference (ISI) whose severity depends on the environment characteristics, as revealed in [9, 95, 96]. To mitigate the ISI, optical orthogonal frequency division multiplexing (O-OFDM) systems are developed, by adapting the conventional OFDM to optical communications for intensity-modulated LED transmission, as presented in [97–101]. Among the proposed adaptations, the direct current (DC) biased O-OFDM (DCO-OFDM) has the maximum achievable spectral efficiency as noted in [100] and is necessary to satisfy the indoor illumination requirements as noted in [101]. As a result, DCO-OFDM became the underlying technology in various VLC applications such as the works in [46, 102–104]. Nevertheless, DCO-OFDM has a non-trivial drawback, which is the clipping distortion. In VLC systems, time-domain symbols are required to be real and positive due to the light intensity requirements. Hence, in DCO-OFDM, the complex frequency-domain OFDM symbols are constrained to be Hermitian symmetric, which results in the time-domain signals being real. To ensure positivity, a DC bias is added in the time-domain, however, in cases where the peak-to-average-power ratio (PAPR) is large, the DCO-OFDM signal may still take negative values, which is clipped during the intensity modulation, leading to the clipping distortion effect. Thus, the high transmission rates obtained by DCO-OFDM come at the expense of the clipping distortion, which may seriously damage the communication quality and needs to be considered in the VLC system design.

Notice that all of the aforementioned works in [43–45, 47–49, 51, 52, 57, 94], which report significant performance improvements for various cooperative VLC system configurations, have overlooked the LED clipping and the resulting clipping noise effects, despite it having significantly detrimental effects on the transmitted signal quality.

Among the limited number of works where the signal clipping is considered, such as [47] and [46], either the clipping effects are considered only on the source side (and not on the relay), or the signal model includes only HD relaying and not FD transmission.

In summary, the current state of the art on cooperative VLC communications is limited in one or more of the following aspects:

- As mentioned above, the clipping noise is usually overlooked in cooperative VLC systems, as done in [43–45, 47–49, 51, 52, 57, 94].
- Most works are limited to either direct VLC or HD relaying and do not consider FD relaying, as in [43–48, 57, 94, 105].
- BER minimization is considered as the main performance improvement objective and transmission rate maximization is generally not studied, as done in [43, 45–49, 51, 52, 57, 94].
- The DC-bias levels are usually set *a priori* to constant levels or to deterministic variable models and power allocation is only performed over the IC signal variances, as in [43–49, 51, 52, 57, 94].

Given this background, the first contribution of this chapter, which is also on DCO-OFDM based cooperative VLC systems, is the consideration of the LED clipping effects at all transmitters, i.e. in both the source and the relay. Within this framework, we develop the FD cooperative VLC signal models and derive the corresponding signal-to-interference-noise ratio (SINR) expressions for both AF and DF relaying strategies. Then, as the second important contribution of this chapter, we consider the transmission rate maximization problem for FD relaying and propose an optimum rate maximizing power allocation approach which jointly optimizes the DC bias level and the IC signal variance together. We also characterize the bit error rate (BER) expressions for the considered communication settings with maximal ratio combining (MRC) detection.

We show with extensive simulation results that under high illumination preferences, the FD cooperative VLC system together with the proposed optimum power allocation (OPA) strategy achieves significantly better transmission rates than those of both direct communications and also the alternative HD relaying approach. Our contributions to the state of the art of the cooperative VLC literature are summarized in Table 3.1.

Table 3.1. Comparison of the work in this chapter to the state of the art of the cooperative VLC literature.

Reference Number	**SYSTEM MODEL**					**PERFORMANCE METRIC**		**OPTIMIZATION VARIABLES**	
	COOPERATION				Clipping noise	Transmission Rates	BER	IC Signal Variances	DC Bias Values
	Full Duplex	Half Duplex	Amplify and Forward	Decode and Forward					
43	NO	NO	NO	NO	NO	NO	NO	NO	NO
44	NO	NO	NO	NO	NO	YES	YES	NO	NO
45	NO	YES	YES	NO	NO	NO	YES	YES	NO
46	NO	YES	YES	YES	YES	NO	YES	YES	NO
47	NO	YES	YES	YES	NO	NO	YES	YES	NO
48	NO	NO	NO	NO	NO	NO	YES	YES	NO
49	YES	YES	YES	NO	NO	NO	YES	YES	NO
51	YES	NO	YES	YES	NO	NO	YES	NO	NO
52	YES	NO	YES	YES	NO	NO	YES	NO	NO
57	NO	YES	YES	NO	NO	NO	YES	YES	NO
94	NO	NO	YES	YES	NO	NO	YES	NO	NO
105	NO	NO	NO	NO	YES	YES	NO	YES	YES
This Work	YES	YES	YES	YES	YES	YES	YES	YES	YES

The rest of this chapter is organized as follows: The VLC channel model together with the clipping noise characteristics are presented in Section II. The signal model, SNR expressions for direct and HD cooperative communication modes are described in Section III. Then, in Section IV the proposed FD cooperative relaying strategy is introduced and the corresponding rate expressions are derived. The proposed joint transmission rate optimization framework is presented in Section V, together with the BER expressions, followed by the simulation results in Section VI. Finally, our conclusions are given in Section VII.

3.2. VLC System Model

3.2.1. Channel Model

In this chapter, the communication is assumed to take place in a rectangular indoor environment, between a source and a destination via a relaying terminal, which is shown in Figure 3.1. These indoor VLC models are designed according to the Configuration 8 in [95] and Scenario 2 in the IEEE 802.15.7r1 VLC standard, [93]. In these configurations, the source illuminates the entire room and the relay illuminates the workspace while both are operating as VLC transmitters as presented in [57, 100]. The channel impulse responses of the three communication links (S-R, R-D, S-D) can be obtained separately by non-sequential ray tracing methods as presented in [106]. In this system, the receivers at the relay and the destination collect the optical radiation emitted by its transmitter over a multipath channel with a total of N_n rays. For a transmitting terminal $T_1 \in \{S, R\}$ and a receiving terminal $T_2 \in \{R, D\}$, the principal ray is the one that is received over the LOS.

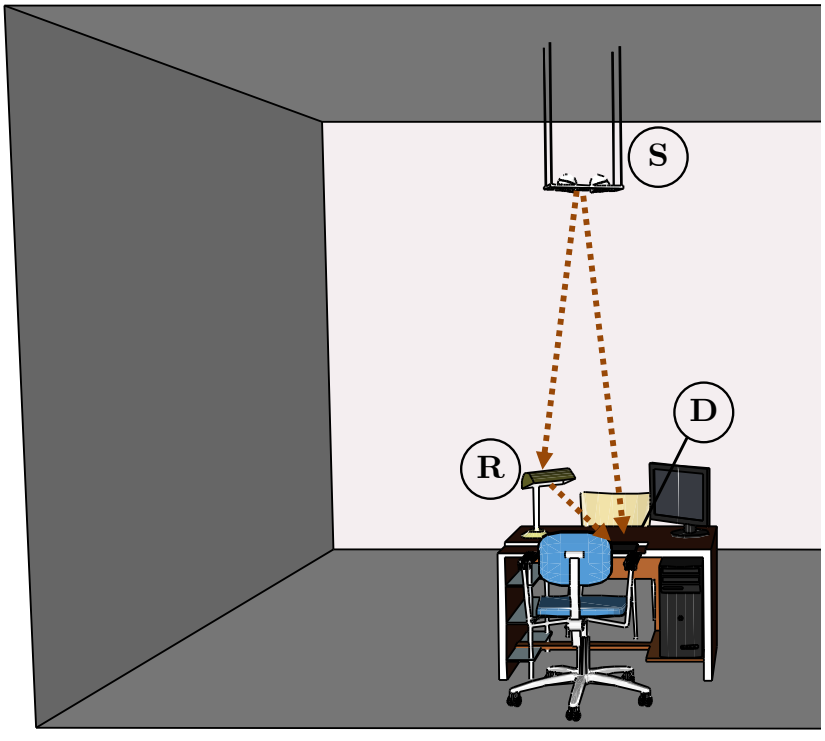

Figure 3.1. Cooperative VLC terminal placement model.

The angle of incidence and emittance of this ray are denoted by ψ and ϕ, respectively. Assuming that both transmitting terminals are monochromatic light sources, the channel impulse response can be calculated as in [106], such that

$$h(t) = \frac{A_{\mathit{eff}}(\psi)}{d^2} R_{T_1}(\phi, n)\delta(t) + \sum_{n=1}^{\frac{\tau_{max}}{\Delta t}-1} P_n(T_1, T_2)\delta(t - n\Delta t). \tag{3.1}$$

Here $P_n(T_1, T_2)$ is the total received power in the nth time interval, $R_{T_1}(\phi, n)$ is the generalized Lambertian model for the transmitting terminal and d is the LOS distance between terminals. τ_{max} is the delay spread of the multipath channel. $A_{\mathit{eff}}(\psi)$ the effective signal collection area of the optical receiver and is given by

$$A_{\mathit{eff}}(\psi) = A_{T_2} \cos(\psi) \mathrm{rect}\left(\frac{\psi}{\mathrm{FOV}}\right), \tag{3.2}$$

where A_{T_2} is the total area of the optical receiver, FOV is its field of view and $\mathrm{rect}(x) = \left\{ \begin{array}{ll} 1 & |x| < 1 \\ 0 & |x| \geq 1 \end{array} \right\}$ is the rectangular function. Furthermore, $P_n(T_1, T_2)$ can be obtained by

$$P_n(T_1, T_2) = \sum_{i=1}^{N_n} P_{i,n}(T_1, T_2). \tag{3.3}$$

For this configuration, $P_n(T_1, T_2)$ can safely be assumed to stay invariant during all communication sessions, since all terminals are immobile and the environment is indoors.

The terminals in Figure 3.1 are equipped with VLC transmitters and receivers whose design is shown in Figure 3.2. The VLC source is equipped with an LED array, which consists of L_S perfectly synchronized LEDs. The information symbols are generated at the source and are encoded on the emitted light by modulating its intensity.

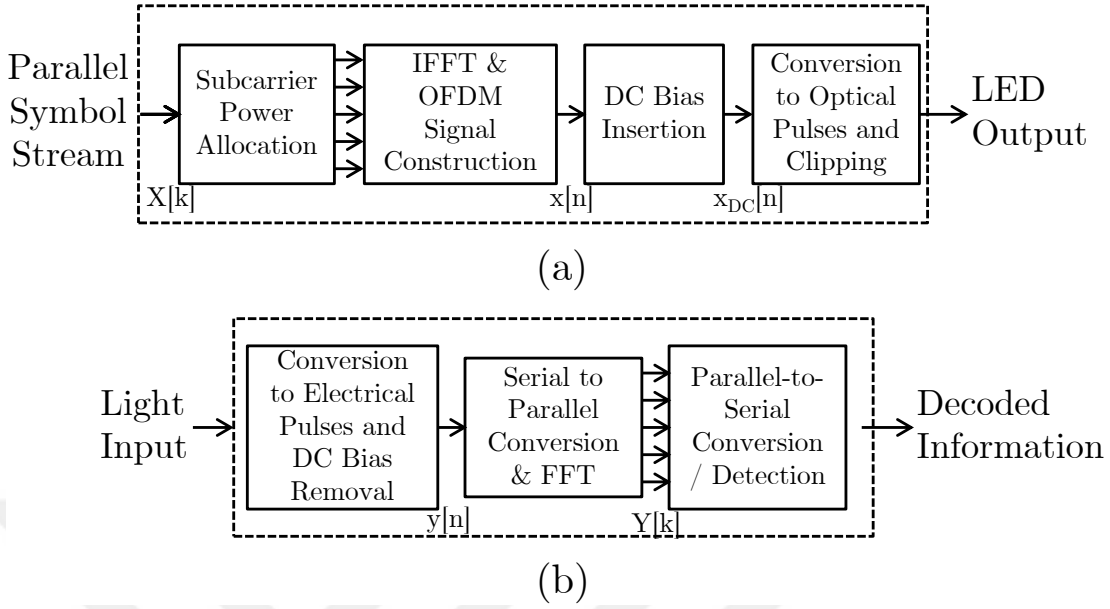

Figure 3.2. a) Transmitter and b) receiver design for DCO-OFDM VLC.

The transmitters at the source and the relay can operate in two modes: *active mode*, where the LED light is modulated and carries information, and *silent mode*, where the emitted light is not modulated, therefore no information is transmitted. The VLC relay terminal consists of a VLC transmitter, equipped with an array of L_R synchronous LEDs a receiver, working in coordination to forward the message it receives from the source by either amplification (AF) or decoding (DF), whose designs are shown in Figure 3.3. The VLC receivers at the relay and the destination can perform direct detection of the information symbols encoded on the light intensity. In this chapter, we adopt the DC-biased optical orthogonal frequency division multiplexing (DCO-OFDM) transmission model, which is shown to provide higher throughputs than other modulation schemes as given in [107].

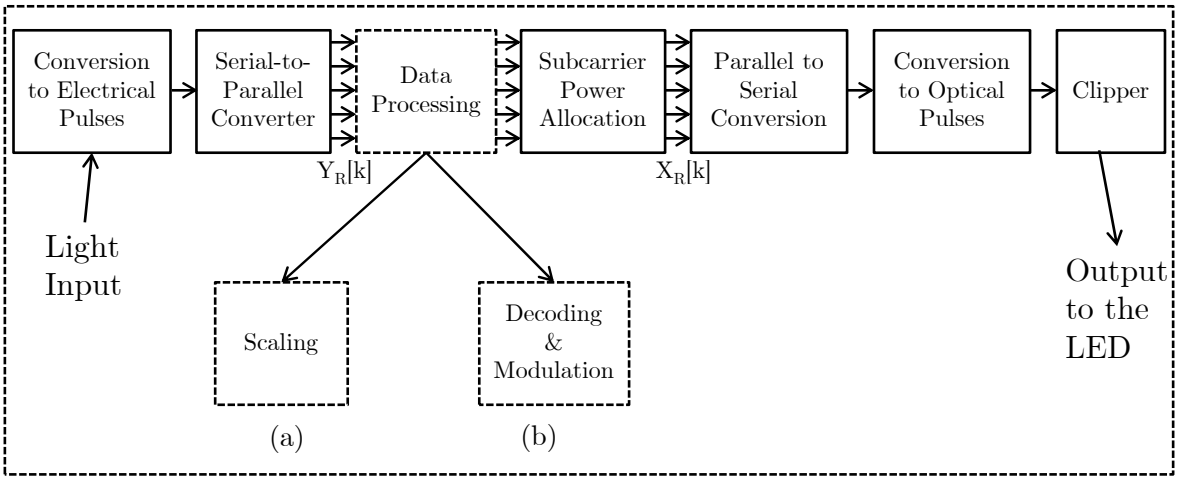

Figure 3.3. a) AF relay design and b) DF relay design for DCO-OFDM VLC.

3.2.2. LED Clipping Model

The information symbols are generated at the source in blocks of length $N/2-1$ from a Gaussian codebook, $\mathcal{C}$. Then, the generated symbols are converted into the frequency-domain information block, $\tilde{\mathbf{X}} = \left[\tilde{X}[1], \tilde{X}[2], \ldots, \tilde{X}[N]\right]$, which is forced to be Hermitian-symmetric for DCO-OFDM transmission, therefore

$$\tilde{X}[k] = \tilde{X}[N-k]^*, \tag{3.4}$$

for $0 < k < N/2$ $\tilde{X}[0] = \tilde{X}[N/2] = 0$. This is mandatory so that the IFFT output sequence,

$$x[n] = \frac{1}{\sqrt{N}} \sum_{k=0}^{N-1} X[k] e^{j\frac{2\pi}{N}nk} \tag{3.5}$$

consists of real values only. Here, $X[k] = \sigma\tilde{X}[k]$ and σ^2 is the power loaded on $X[k]$. Hence, the variance of $x[n]$, the IC signal variance, is denoted by σ^2. The IC signal variances of the source and the relay are denoted by σ_S^2 and σ_R^2, respectively.

Since an intensity modulated LED is capable of transmitting only the magnitude of the input signal, the negative values in $x[n]$ are clipped prior to the transmission, hence the clipping distortion is introduced. In order to reduce this distortion, the values in $x[n]$ are first clipped at the negative DC bias level, $-B_{\mathrm{DC}}$, then increased by B_{DC} to ensure unipolarity of $x[n]$. Applying signal clipping on the sequence of $x[n]$ gives

$$x^{\mathrm{cl}}[n] = \begin{cases} x[n], & x[n] \geq -B_{\mathrm{DC}} \\ -B_{\mathrm{DC}} & x[n] < -B_{\mathrm{DC}}. \end{cases} \tag{3.6}$$

Then the required DC bias, B_{DC} is added on $x[n]$ so that $x_{\mathrm{DC}}[n] = x^{\mathrm{cl}}[n] + B_{\mathrm{DC}}$. The clipping operation given in (3.6) can be modelled as a Gaussian clipper, provided that the input, $x[n]$, is Gaussian as it is the case in our model. Thus, Bussgang's theorem from [87] can be applied on the statistical relationship between $x[n]$ and $x^{\mathrm{cl}}[n]$, hence we get

$$x^{\mathrm{cl}}[n] = ax[n] + w^{\mathrm{cl}}[n], \tag{3.7}$$

where a is the attenuation factor and $w^{\mathrm{cl}}[n]$ is the Gaussian clipping distortion term. The attenuation factor and the clipping distortion variance are found at [87] as

$$a = 1 - Q\left(\frac{B_{\mathrm{DC}}}{\sigma}\right) \tag{3.8}$$

$$\begin{aligned} \sigma_{\mathrm{cl}}^2 = \sigma^2 \Bigg[1 + \left(\left(\frac{B_{\mathrm{DC}}}{\sigma}\right)^2 - 1 \right) Q\left(\frac{B_{\mathrm{DC}}}{\sigma}\right) - \frac{B_{\mathrm{DC}}}{\sigma} g\left(\frac{B_{\mathrm{DC}}}{\sigma}\right) \\ - Q\left(-\frac{B_{\mathrm{DC}}}{\sigma}\right)^2 - \left(g\left(\frac{B_{\mathrm{DC}}}{\sigma}\right) - \frac{B_{\mathrm{DC}}}{\sigma} Q\left(\frac{B_{\mathrm{DC}}}{\sigma}\right) \right)^2 \Bigg], \end{aligned} \tag{3.9}$$

where $Q(\cdot)$ and $g(\cdot)$ are the tail distribution and the probability density function of the standard normal distribution respectively.

Then assuming that $X[k]$ and $W^{\text{cl}}[k]$ are the DFT's of $x[n]$ and $w^{\text{cl}}[n]$, respectively, the the frequency domain representation of the clipped signal in (3.7) becomes

$$X^{\text{cl}}[k] = aX[k] + W^{\text{cl}}[k]. \tag{3.10}$$

Note that, $w^{\text{cl}}[n]$ and $W^{\text{cl}}[k]$ have the same clipping distortion variance, σ^2_{cl}, which depends solely on B_{DC} and σ of the transmitted signal.

Before we develop the signal model for FD relaying, we first present the signal model for direct communication and HD cooperation. From this point on, $X^{\text{cl}}[k]$ is taken as the transmitted signal, since B_{DC} and the cyclic prefix are removed at the receiver and do not contribute to decoding.

3.3. Benchmark Derivations: Direct Link and HD Relaying with Clipping Noise

In this section, we present the system model and derive the SNR and achievable rate expressions for both direct link and HD relaying modes, which serve as benchmarks for the corresponding derivations for the proposed FD relaying model that will be presented in the next section. Notice that the derivations in this section of HD relaying, which are included here for benchmarking purposes are new to the literature, as they are obtained with the assumption of the presence of the clipping noise effects at both the source and the relay.

3.3.1. Direct Link

The clipped transmitted signal by a single LED at the source can be expressed as

$$X_S^{cl}[k] = a_S \sigma_S \tilde{X}_S[k] + W_S^{cl}[k], \quad k = 0, \ldots, N-1. \tag{3.11}$$

Then the received signal at the destination becomes

$$Y_{\mathrm{SD}}[k] = A_{SD}[k]\tilde{X}_S[k] + W_{n,SD}[k], \tag{3.12}$$

where $A_{SD}[k] = L_S H_{SD}[k] a_S \sigma_S$ is the received signal amplitude and

$$W_{n,SD}[k] = L_S H_{SD}[k] W_S^{cl}[k] + W_D^{\mathrm{AWGN}}[k]$$

is the effective noise at the destination, which is composed of the clipping and thermal noise components. Note that, the transmitted light intensity is proportional to L_S. The variance of $W_{n,SD}[k]$ becomes $\sigma^2_{\mathrm{n,SD}}[k] = L_S^2 |H_{SD}[k]|^2 \sigma^2_{S,\mathrm{cl}} + \sigma^2_{\mathrm{D,AWGN}}$. The effective noise is a function of the frequency response of the channel and therefore varies over the spectrum. The receiver can optimally use maximum likelihood detection to decode the kth symbol as

$$\hat{X}^{\mathrm{DIR}}[k] = \arg\min_{\mathcal{X}\in\mathcal{C}} \left| Y_{SD}[k] - A_{SD}[k]\mathcal{X} \right|, \quad \forall k = 1, 2, \ldots, N/2 - 1. \tag{3.13}$$

Thus, the received SNR per subcarrier for direct communication becomes

$$\mathrm{SNR}_{\mathrm{SD}}[k] = \frac{|A_{SD}[k]|^2}{\sigma^2_{\mathrm{n,SD}}[k]}. \tag{3.14}$$

Now, the corresponding transmission rate per subcarrier can be found by using Shannon's capacity formula as $\mathcal{R}^{\mathrm{DIR}}[k] = 1/2 \log_2(1 + \mathrm{SNR}_{\mathrm{SD}}[k])$, hence we get

$$\mathcal{R}^{\mathrm{DIR}} = \frac{BW}{2} \sum_{k=1}^{N/2-1} \log_2(1 + \mathrm{SNR}_{\mathrm{SD}}[k]), \tag{3.15}$$

as the transmission rate for the direct communication. Here BW stands for the bandwidth.

3.3.2. Half Duplex Cooperation

When the HD cooperation mode is employed, the communication is perpetuated in two-phased intervals, where each phase consists of N time slots with a duration of T_s seconds. In an interval i, the source terminal transmits the ith information block during Phase I (active mode) and remains silent during Phase II, whereas the relay remains silent during Phase I and transmits during Phase II. While the source operates in silent mode during Phase I, it generates the $(i+1)^{th}$ information block for the next interval. Similarly, during Phase II, the relay processes the ith information block it received during Phase I, to formulate the transmitted signal for the next interval. In the ith interval, the destination terminal listens to the source during Phase I and to the relay during Phase II, also decoding the $(i-1)^{th}$ information block by using the signals it received from both links during the previous interval. In HD mode, signals from the source and the relay are ensured to be transmitted in different phases, therefore they never interfere at the destination. On the other hand, the average transmission rate is halved, since a single block is sent over two phases. In this chapter, we consider a relay with amplify-and-forward and decode-and-forward capabilities.

3.3.2.1. AF Relaying. The transmitted signal by the source in (3.11) is received by the relay as

$$Y_R[k] = A_{SR}[k]\tilde{X}_S[k] + W_{n,SR}[k], \tag{3.16}$$

where $A_{SR}[k] = L_S H_{SR}[k] a_S \sigma_S$ and

$$W_{n,SR}[k] = L_S H_{SR}[k] W_S^{cl}[k] + W_R^{\text{AWGN}}[k]$$

is the effective noise at the relay that is assumed to be zero-mean Gaussian with the variance of

$$\sigma^2_{n,SR}[k] = L_S^2 |H_{SR}[k]|^2 \sigma^2_{S,cl} + \sigma^2_{\text{R,AWGN}}.$$

The AF relay scales and amplifies the signal and then transmits

$$X_R^{\mathrm{AF}}[k] = a_R \sigma_R F_R[k] Y_R[k] + W_R^{cl}[k] \tag{3.17}$$

through each of its LEDs. Here,

$$F_R[k] = 1/\sqrt{|A_{SR}[k]|^2 + \sigma_{n,SR}^2[k]} \tag{3.18}$$

normalizes the received signal from the source. $X_R^{\mathrm{AF}}[k]$ is received at the destination as

$$Y_{\mathrm{SRD}}^{\mathrm{AF}}[k] = A_{\mathrm{SRD}}^{\mathrm{AF}}[k] \tilde{X}_S[k] + W_{\mathrm{SRD}}^{\mathrm{AF}}[k], \tag{3.19}$$

where the signal amplitude and the effective noise are represented by

$$A_{\mathrm{SRD}}^{\mathrm{AF}}[k] = L_R H_{RD}[k] a_R \sigma_R F_R[k] A_{SR}[k], \tag{3.20}$$

$$\begin{aligned} W_{\mathrm{SRD}}^{\mathrm{AF}}[k] &= L_R H_{RD}[k] a_R \sigma_R F_R[k] W_{n,SR}[k] \\ &\quad + L_R H_{RD}[k] W_R^{cl}[k] + W_D^{\mathrm{AWGN}}[k]. \end{aligned} \tag{3.21}$$

Now, the received SNR per subcarrier over the S-R-D link can be found as

$$\mathrm{SNR}_{\mathrm{SRD}}^{\mathrm{AF}}[k] = \frac{|A_{SRD}^{AF}[k]|^2}{\sigma_{\mathrm{n,SRD,AF}}^2[k]}. \tag{3.22}$$

When the AF relay is employed in addition to the direct link, the destination will have 2 pieces of received symbols to decode every k^{th} symbol. In this case, the receiver can employ maximum ratio combining, which results in the detection rule given by

$$\hat{X}^{\mathrm{AF}}[k] = \arg\min_{\mathcal{X}\in\mathcal{C}} \left| \mathcal{X} - \frac{\dfrac{(A_{\mathrm{SD}}[k])^* Y_{\mathrm{SD}}[k]}{\sigma_{\mathrm{n,SD}}^2[k]} + \dfrac{(A_{\mathrm{SRD}}^{\mathrm{AF}}[k])^* Y_{\mathrm{SRD}}^{\mathrm{AF}}[k]}{\sigma_{\mathrm{n,SRD,AF}}^2[k]}}{\dfrac{|A_{\mathrm{SD}}[k]|^2}{\sigma_{\mathrm{n,SD}}^2[k]} + \dfrac{|A_{\mathrm{SRD}}^{\mathrm{AF}}[k]|^2}{\sigma_{\mathrm{n,SRD,AF}}^2[k]}} \right|. \tag{3.23}$$

So the received SNR per subcarrier by AF relaying is obtained by

$$\mathrm{SNR}^{\mathrm{AF}}[k] = \mathrm{SNR}^{\mathrm{AF}}_{\mathrm{SRD}}[k] + \mathrm{SNR}_{\mathrm{SD}}[k]. \tag{3.24}$$

Then the achievable transmission rate with a HD AF relay becomes

$$\mathcal{R}^{\mathrm{HD}}_{\mathrm{AF}} = \frac{BW}{4} \sum_{k=1}^{N/2-1} \log_2(1 + \mathrm{SNR}^{\mathrm{AF}}[k]). \tag{3.25}$$

3.3.2.2. DF Relaying. The received signal by the relay in (3.16) is first decoded by the DF relay and then forwarded with

$$X^{\mathrm{DF}}_R[k] = a_R \sigma_R \hat{X}^{DF}_R[k] + W^{cl}_R[k], \tag{3.26}$$

where $\hat{X}^{\mathrm{DF}}_R[k]$ is the decoded symbol at the relay. $X^{\mathrm{DF}}_R[k]$ is received at the destination as

$$Y^{\mathrm{DF}}_{\mathrm{RD}}[k] = A^{\mathrm{DF}}_{\mathrm{RD}}[k] \hat{X}^{\mathrm{DF}}_R[k] + W_{\mathrm{n,RD}}[k] \tag{3.27}$$

with the signal amplitude and effective noise given by

$$A^{\mathrm{DF}}_{\mathrm{RD}}[k] = L_R H_{RD}[k] a_R \sigma_R, \tag{3.28}$$

$$W^{\mathrm{DF}}_{\mathrm{RD}}[k] = L_R H_{RD}[k] W^{cl}_R[k] + W^{\mathrm{AWGN}}_D[k]. \tag{3.29}$$

Here, $W^{\mathrm{DF}}_{\mathrm{RD}}[k]$ is a zero mean Gaussian random variable with the variance of

$$\sigma^2_{\mathrm{n,RD,DF}}[k] = L^2_R |H_{RD}[k]|^2 \sigma^2_{R,cl} + \sigma^2_{\mathrm{D,AWGN}}. \tag{3.30}$$

By (3.16) and (3.27), the relay and the destination will perform decoding according to

$$\hat{X}_R^{\mathrm{DF}}[k] = \arg\min_{\mathcal{X}\in\mathcal{C}} \left| Y_{SR}[k] - A_{SR}[k]\mathcal{X} \right|, \tag{3.31}$$

$$\hat{X}_{\mathrm{D}}^{\mathrm{DF}}[k] = \arg\min_{\mathcal{X}\in\mathcal{C}} \left| \mathcal{X} - \frac{\dfrac{(A_{\mathrm{SD}}[k])^* Y_{\mathrm{SD}}[k]}{\sigma^2_{\mathrm{n,SD}}[k]} + \dfrac{(A^{\mathrm{DF}}_{\mathrm{RD}}[k])^* Y^{\mathrm{DF}}_{\mathrm{RD}}[k]}{\sigma^2_{\mathrm{n,RD,DF}}[k]}}{\dfrac{|A_{\mathrm{SD}}[k]|^2}{\sigma^2_{\mathrm{n,SD}}[k]} + \dfrac{|A^{\mathrm{DF}}_{\mathrm{RD}}[k]|^2}{\sigma^2_{\mathrm{n,RD,DF}}[k]}} \right|, \tag{3.32}$$

respectively. Hence, the source-to-relay and the relay-to-destination SNRs become

$$\mathrm{SNR}^{\mathrm{DF}}_{\mathrm{SR}}[k] = \frac{|A^{\mathrm{DF}}_{\mathrm{SR}}[k]|^2}{\sigma^2_{\mathrm{n,SR,DF}}[k]}, \quad \mathrm{SNR}^{\mathrm{DF}}_{\mathrm{RD}}[k] = \frac{|A^{\mathrm{DF}}_{\mathrm{RD}}[k]|^2}{\sigma^2_{\mathrm{n,RD,DF}}[k]}. \tag{3.33}$$

In DF relaying, the relay is required to decode the transmitter's signal completely. Therefore the transmission rate at the destination in this case is bounded by the maximum rate at which the relay can decode the transmitter's signal. So, the transmission rate becomes

$$\mathcal{R}^{\mathrm{HD}}_{\mathrm{DF}} = \frac{BW}{4} \sum_{k=1}^{N/2-1} \min \left\{ \log_2(1+\mathrm{SNR}^{\mathrm{DF}}_{\mathrm{SR}}[k]), \log_2(1+\mathrm{SNR}_{\mathrm{SD}}[k]+\mathrm{SNR}^{\mathrm{DF}}_{\mathrm{RD}}[k]) \right\}, \tag{3.34}$$

where the second term in the brackets give the maximum rate at which the destination decodes the transmitter's signal.

3.4. Full Duplex Cooperative VLC with Clipping Noise

To improve the transmission rate of the considered VLC system, we enable FD relaying, where the relay is always in the active mode. The comparison of FD and HD relaying modes are presented in Figure 3.4. In FD mode, the transmission duration of one information block is halved compared to the HD relaying. We will also show that the source signal may interfere with the relay's signal at the receiver's photodetector, resulting in a reduction in SNR.

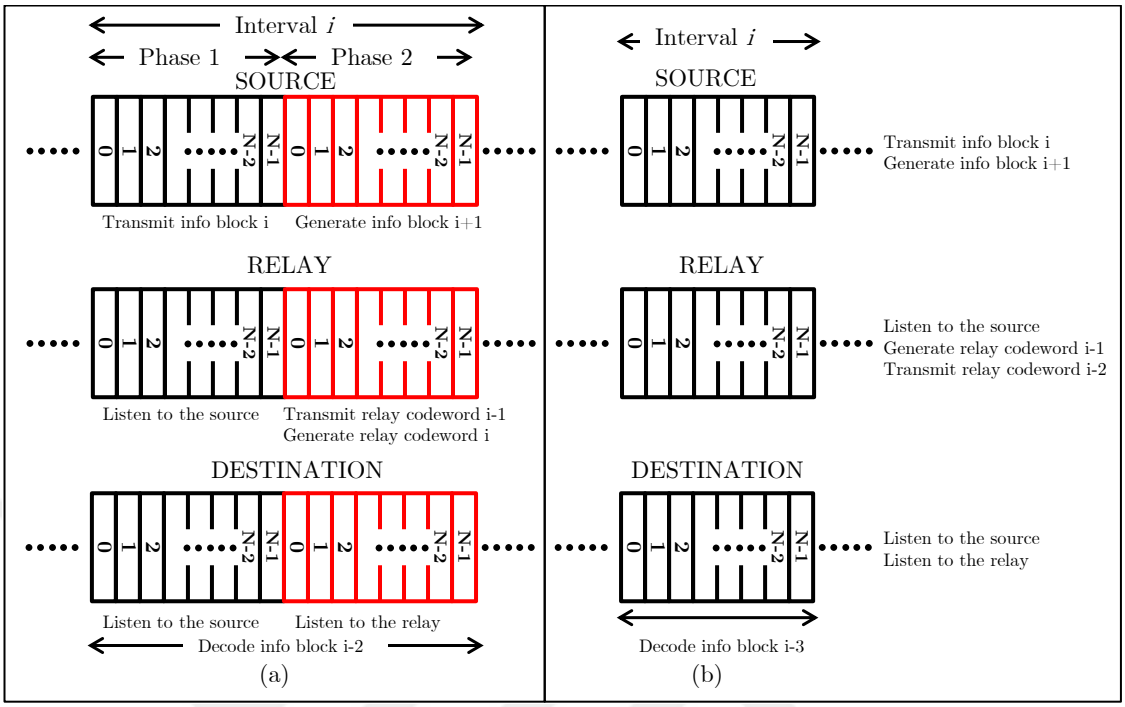

Figure 3.4. Comparison of a) HD and b) FD modes in cooperative VLC.

In accordance with Figure 3.4b, during an interval i, the source transmits the ith information block both to the relay and the destination, also generates the $(i+1)^{th}$ information block for the next interval. Meanwhile, the relay listens to the source to get the ith information block, also processes its received signal during the previous phase to form its message for the $(i+1)^{th}$ interval. For this reason, during the interval i, the relay can forward the $(i-2)^{th}$ information block from the source. As a result, the destination receives the ith block from the source and $(i-2)^{th}$ block from the relay. The destination decodes the $(i-3)^{th}$ information blocks by using its received signals from the source and the relay during the $(i-3)^{th}$ and $(i-1)^{th}$ intervals. In the following, we present the signal models for AF and DF relaying.

3.4.1. AF Relaying

The ith OFDM block transmitted by the source can be expressed as

$$X_S^i[k] = a_S \sigma_S \tilde{X}_S^i[k] + W_S^{cl}[k], \quad k = 0, \ldots, N-1. \tag{3.35}$$

This block is received by the relay as

$$Y_R^i[k] = A_{SR}[k]\tilde{X}_S^i[k] + W_{n,SR}[k], \tag{3.36}$$

where $A_{SR}[k] = L_S H_{SR}[k] a_S \sigma_S$ is the signal amplitude and $W_{n,SR}[k] = L_S H_{SR}[k] W_S^{cl}[k] + W_R^{\mathrm{AWGN}}[k]$ is the effective noise at the relay, which is a zero-mean Gaussian random variable with the variance of $\sigma_{n,R}^2[k] = L_S^2 |H_{SR}[k]|^2 \sigma_{S,cl}^2 + \sigma_{\mathrm{R,AWGN}}^2$. The AF relay scales forwards $Y_R^i[k]$ as in the HD mode. However, the relay's signal interferes with $(i+1)^{\mathrm{th}}$ block transmitted by the source. Therefore, the received signal at the destination becomes

$$Y_D^{\mathrm{AF}}[k] = A_{\mathrm{SRD}}^{\mathrm{AF}}[k]\tilde{X}_S^i[k] + A_{\mathrm{SD}}[k]\tilde{X}_S^{i+1}[k] + W_{\mathrm{SRD}}[k], \tag{3.37}$$

where the second term is the interference caused by the source's signal at the destination. Now, the received SINR per subcarrier for AF relaying is obtained by

$$\mathrm{SINR}_{\mathrm{AF}}^{\mathrm{FD}}[k] = \frac{|A_{\mathrm{SRD}}[k]|^2}{|A_{\mathrm{SD}}[k]|^2 + \sigma_{\mathrm{n,SRD}}^2[k]}. \tag{3.38}$$

The maximum likelihood detection at the destination for AF relaying is given by

$$\hat{X}_{\mathrm{AF}}^{\mathrm{FD}}[k] = \arg\min_{\mathcal{X} \in \mathcal{C}} \left| Y_D^{\mathrm{AF}}[k] - A_{\mathrm{SRD}}^{\mathrm{FD}}[k]\mathcal{X} \right|. \tag{3.39}$$

Then the achievable transmission rate for FD AF relaying becomes

$$\mathcal{R}_{\mathrm{AF}}^{\mathrm{FD}} = \frac{BW}{2} \sum_{k=1}^{N/2-1} \log_2 \left(1 + \mathrm{SINR}_{\mathrm{D}}^{\mathrm{AF}}[k]\right). \tag{3.40}$$

Note that, in the conventional FD radio frequency communication, the signal reception usually suffers from self-interference, however in VLC, this does not have to be the case, because the transmitter and the receiver circuits can be placed on opposite sides of the relay. Thus, the LOS component of the transmitted light signals is prevented to travel to its receiver, unlike radio signals.

3.4.2. DF Relaying

When DF relaying is employed in FD mode, the received signal at the destination becomes the superposition of $\hat{X}_R^i[k]$ and $X_S^{i+1}[k]$ as in

$$Y_{\mathrm{D}}^{\mathrm{DF}}[k] = A_{\mathrm{RD}}^{\mathrm{DF}}[k]\hat{X}_R^i[k] + A_{\mathrm{SD}}[k]\tilde{X}_S^{i+1}[k] + W_{\mathrm{n,D}}[k], \tag{3.41}$$

where $\hat{X}_R^i[k]$ is decoded by the DF relay. $W_{\mathrm{n,D}}[k]$ is a zero mean Gaussian with the variance of

$$\sigma_{\mathrm{n,D}}^2[k] = L_S^2|H_{SD}[k]|^2\sigma_{S,cl}^2 + L_R^2|H_{RD}[k]|^2\sigma_{R,cl}^2 + \sigma_{\mathrm{D,AWGN}}^2 \tag{3.42}$$

with the following signal amplitudes and the effective noise.

$$A_{RD}[k] = L_R H_{RD}[k] a_R \sigma_R, \tag{3.43}$$

$$A_{SD}[k] = L_S H_{SD}[k] a_S \sigma_S, \tag{3.44}$$

$$W_{n,D}[k] = L_S H_{SD}[k] W_S^{cl}[k] + L_R H_{RD}[k] W_R^{cl}[k] + W_D^{\mathrm{AWGN}}[k]. \tag{3.45}$$

Here, $W_{n,D}[k]$ is a zero mean Gaussian with the variance of

$$\sigma^2_{\mathrm{n,D}}[k] = L_S^2|H_{SD}[k]|^2\sigma^2_{S,cl} + L_R^2|H_{RD}[k]|^2\sigma^2_{R,cl} + \sigma^2_{\mathrm{D,AWGN}}. \tag{3.46}$$

Note that, the term with $\tilde{X}_S^{i+1}[k]$ in (3.41) is the interference from the source, since in the destination aims to decode $X_R^i[k]$. Thus, the signal-to-interference-noise ratio at the destination becomes

$$\mathrm{SINR}_{\mathrm{D}}^{\mathrm{FD,DF}}[k] = \frac{L_R^2|H_{RD}[k]|^2 a_R^2\sigma_R^2}{L_S^2|H_{SD}[k]|^2(a_S^2\sigma_S^2 + \sigma^2_{S,cl}) + L_R^2|H_{RD}[k]|^2\sigma^2_{R,cl} + \sigma^2_{\mathrm{D,AWGN}}}, \tag{3.47}$$

where the first term in the denominator is the power of interference caused by the direct link and the rest is the total power of clipping noise at the relay LEDs and the AWGN at the receiver. The maximum likelihood decoding at the destination is specified by

$$\hat{X}_{\mathrm{DF}}^{\mathrm{FD}}[k] = \arg\min_{\mathcal{X}\in\mathcal{C}} |Y_D[k] - A_{RD}[k]\mathcal{X}|\,, \tag{3.48}$$

In DF relaying, the transmission rate at the destination is bounded by the maximum rate at which the relay can decode the transmitter's signal. Hence, the total transmission rate is found by

$$\mathcal{R}_{\mathrm{DF}}^{\mathrm{FD}} = \frac{BW}{2}\sum_{k=1}^{N/2-1}\log_2\left(1 + \min\left\{\mathrm{SNR}_{\mathrm{SR}}^{\mathrm{DF}}[k], \mathrm{SINR}_{\mathrm{D}}^{\mathrm{DF}}[k]\right\}\right). \tag{3.49}$$

In the following, we propose OPA strategies, which maximize the transmission rate obtained by VLC under illumination constraints.

3.5. Transmission Rate Maximization

In this section, the OPA strategies are formulated to maximize $\mathcal{R}^{\mathrm{DIR}}$, $\mathcal{R}_\lambda^{\mathrm{FD}}$, $\mathcal{R}_\lambda^{\mathrm{HD}}$, for a relaying mode $\lambda \in \{\mathrm{HD}, \mathrm{FD}\}$. The transmission rate maximization has to provide a constant illumination, which is specified by the user preferences and environmental conditions.

The illumination of the room can be controlled by the illuminance of a surface, which is the received light energy per second per unit surface area [108]. Although different LEDs may have different power functions, the illuminance level can generally be stabilized by fixing the radiated power of the LEDs, which is proportional to the emitted signal power, which is proportional to the square sum of the DC bias level and the IC signal standard deviation. Hence, we impose

$$\mathcal{I}_{\mathrm{DIR}}: \quad B_{\mathrm{DC,s}}^2 + \sigma_S^2 = \sigma_T^2, \tag{3.50}$$

for direct communication. In HD mode, the DC bias level stays constant during all phases, however, the IC signal variances of the source and the relay are set to zero during their silent phases. Therefore the illuminance constraint becomes

$$\mathcal{I}_{\mathrm{HD}}: \quad B_{\mathrm{DC,s}}^2 + B_{\mathrm{DC,r}}^2 + \frac{1}{2}(\sigma_R^2 + \sigma_S^2) = \sigma_T^2. \tag{3.51}$$

When FD relaying is employed, the source and relay terminals are always in active mode, therefore we impose

$$\mathcal{I}_{\mathrm{FD}}: \quad B_{\mathrm{DC,s}}^2 + \sigma_S^2 + B_{\mathrm{DC,r}}^2 + \sigma_R^2 = \sigma_T^2. \tag{3.52}$$

Next, we formulate the optimization problem, that solves for the optimum DC bias levels and IC signal variances, which achieve the maximum transmission rates for all communication modes. The optimization problem is stated as

$$\mathcal{P}_{\lambda'}: \qquad \max_{\mathcal{V}} \mathcal{R}_{\lambda}^{\lambda'} \tag{3.53a}$$

$$\text{s.t.} \quad \mathcal{I}_{\lambda'}, \quad \& \quad 0 \leq \mathcal{V} \tag{3.53b}$$

where $\lambda' \in \{\mathrm{DIR}, \mathrm{HD}, \mathrm{FD}\}$ and $\mathcal{V} = \{B_{DC,s}, \sigma_S, B_{DC,r}, \sigma_R\}$ is the optimization variable set. The solution to (3.53) is the proposed OPA strategy, which consists of the optimum $(B_{\mathrm{DC}}, \sigma)$ values for a given illuminance level σ_T, a communication mode λ' and a relaying strategy λ. Note that, if λ' is selected as DIR, $\lambda \in \emptyset$ and $\sigma_R = B_{\mathrm{DC,r}} = 0$.

The problem $\mathcal{P}_{\lambda'}$ is nonconvex for all modes, because the optimization variables, $\{\sigma_S, \sigma_R, B_{DC,s}, B_{DC,r}\}$ appear in the nonconvex clipping noise parameters in (3.8). However, we can still find rate-optimum DC bias and IC signal variances by performing a global search over the feasible region, specified by (3.53b).

3.5.1. Equal Power Allocation Policies

We also propose a simple power allocation policy, where the illuminance constraints are satisfied distributing the power σ_T^2 to $\{\sigma_S, \sigma_R, B_{DC,s}, B_{DC,r}\}$ equally for all phases. Hence, the EPA strategies become

$$\mathcal{E}^{\mathrm{DIR}}: \quad \sigma_S = B_{DC,s} = \sigma_T/\sqrt{2}, \tag{3.54}$$

$$\mathcal{E}^{\mathrm{FD}}: \quad \sigma_S = \sigma_R = B_{DC,s} = B_{DC,r} = \sigma_T/2, \tag{3.55}$$

$$\mathcal{E}^{\mathrm{FD}}: \quad \sigma_{S,1} = \sigma_{R,2} = B_{DC,S,1} = B_{DC,S,2} = B_{DC,R,1} = B_{DC,R,2} = \sigma_T/\sqrt{6}, \tag{3.56}$$

for direct communication, FD and HD cooperation respectively. Here, $i \in \{1, 2\}$ in $\sigma_{X,i}$ and $B_{DC,X,i}$ stands for the phase index.

3.5.2. Theoretical bit error rates

The solution to the optimization problem in (3.53) gives the rate-maximizing DC bias and IC signal variances along with the optimum received SNR values. The optimum value of (3.53) is the maximum achievable transmission rate for the considered communication setting. Next, we formulate the theoretical BERs for those regimes as a function of the received SNR.

When the symbol constellation is 16-QAM and the number of transmitted blocks, M, is very large, the average BER per subcarrier can be found by using the analysis in [109] and it becomes

$$P_e[k] = \frac{3}{8}\text{erfc}\left(\sqrt{\frac{2\text{SNR}[k]}{5}}\right) + \frac{1}{4}\text{erfc}\left(3\sqrt{\frac{2\text{SNR}[k]}{5}}\right) - \frac{1}{8}\text{erfc}\left(5\sqrt{\frac{2\text{SNR}[k]}{5}}\right), \tag{3.57}$$

where $\text{erfc}(x) = \frac{2}{\pi}\int_x^\infty e^{-u^2}du$ is the error function and $\text{SNR}[k]$ denotes the received SNR per subcarrier for the enabled communication mode as given in Sections III and IV. Then the average BER can be found by

$$P_e^{\lambda'} = \frac{2}{N-2}\sum_{k=1}^{N/2-1} P_e[k], \tag{3.58}$$

where $\lambda' \in \{\text{DIR}, \text{FD}, \text{HD}\}$ denotes the considered communication setting.

3.6. Simulation Results

In this section, the transmission rate and BER performances of the proposed OPA strategies are presented in comparison to the suboptimum EPA strategies, under FD and HD communication modes and both relaying strategies (AF, DF). The communication takes place in a practical indoor office environment, where the channel impulse responses are given as in (3.1). The channel coefficients can be deduced from the coordinates of the terminals, size of the optical receivers and the wavelength of the emitted light's wavelength. However $P_{i,n}(T_1, T_2)$ and therefore $P_n(T_1, T_2)$ depend on the indoor environment conditions such as the dimensions of the room, surface materials, location and size of obstacles like as furniture as mentioned in [110].

In this regard, we make use of the VLC channel estimation results obtained in [95] and assume that the channel impulse responses are

$$h_{sd}[n] = 10^{-7}\times\{6.54,\ 2.43,\ 0.05\ 0.05\}, \tag{3.59}$$

$$h_{sr}[n] = 10^{-6}\times\{1.71\ 0.57\ 0.01\ 0\ 0\ 0\ 0.01\ 0.01\ 0.01\ 0.01\ 0.01\}, \tag{3.60}$$

$$h_{rd}[n] = 10^{-4}\times\{0.55\ 0.01\ 0.01\ 0\ 0.01\ 0.01\ 0.01\ 0.01\ 0.01\ 0.01\ 0.01\}, \tag{3.61}$$

where $h[n] = h(nT_s)$ and T_s is the sampling period. The channel state information for this configuration is assumed to remain constant during all communication sessions since $P_n(T_1, T_2)$ does not change.

We consider a DCO-OFDM VLC with $N = 256$ subcarriers and a bandwidth of $BW = 20$ MHz. The source illuminates with $L_S = 8$ LEDs and the relay with $L_R = 2$ LEDs for cooperative VLC and with $L_S = 10$ for direct VLC. The AWGN power spectral density is $N_0 = 8.1 \times 10^{-19}$ W/Hz, which results in $\sigma_{D,\mathrm{n}} = \sigma_{R,\mathrm{n}} = N_0 * BW = 4.0249 \times 10^{-6}$. This communication environment and the given parameters are typical for an indoors setting as given in [95].

For the given VLC system, the rate-maximizing $\{B_{\mathrm{DC}}, \sigma\}$ values along with the optimum rates are presented in Tables 3.2 - 3.6 for each σ_T value. The transmission rates achieved by the suboptimal EPA strategies are also presented in the tables for comparison. The performance comparison of cooperative and direct VLC shows that introducing an HD relay to the VLC system with the proposed OPA strategy improves the achieved transmission rate significantly for all σ_T values. Even with a suboptimum PA strategy, the use of cooperation outperforms direct VLC for low σ_T.

Table 3.2. Rate maximizing $(B_{\mathrm{DC}}, \sigma)$ values and optimum rates for FD cooperative VLC with DF relaying. Transmission rates of suboptimum EPA strategies included for comparison.

σ_T^2 per LED		FD Mode, DF, OPA					EPA
(dBm)		$B_{\mathrm{DC,s}}$ (V)	$B_{\mathrm{DC,r}}$ (V)	σ_S (V)	σ_R (V)	Rate	Rate
0	0.001	0.0094	0.0038	0.0278	0.0112	4×10^{-5}	8×10^{-6}
5	0.0032	0.0168	0.0067	0.0494	0.0199	4×10^{-4}	8×10^{-5}
10	0.01	0.0299	0.0131	0.0876	0.0355	0.0044	8×10^{-4}
15	0.0316	0.0531	0.0255	0.155	0.0642	0.0418	0.0082
20	0.1	0.0983	0.0605	0.2702	0.117	0.3693	0.081
25	0.3162	0.1815	0.1748	0.4635	0.1947	2.6147	0.7612
30	1	0.3705	0.4064	0.7739	0.3142	11.7191	5.6555
35	3.1623	0.8502	0.8502	1.1779	0.5739	28.6087	22.121
40	10	1.8520	1.663	1.5915	1.1276	47.8279	45.184

Table 3.3. Rate maximizing $(B_{\mathrm{DC}}, \sigma)$ values and optimum rates for HD cooperative VLC with DF relaying. Transmission rates of suboptimum EPA strategies included for comparison.

σ_T^2 per LED		HD Mode, DF, OPA					EPA
(dBm)		$B_{\mathrm{DC,s}}$ (V)	$B_{\mathrm{DC,r}}$ (V)	σ_S (V)	σ_R (V)	Rate	Rate
0	0.001	0.015	0.0023	0.0388	0.0058	0.0586	0.0218
5	0.0032	0.0267	0.0041	0.069	0.0103	0.1827	0.0687
10	0.01	0.0475	0.0073	0.1227	0.0183	0.5535	0.2142
15	0.0316	0.0844	0.013	0.2182	0.0325	1.5524	0.6503
20	0.1	0.1732	0.0231	0.3686	0.0554	3.7242	1.8374
25	0.3162	0.3696	0.0616	0.5887	0.0711	7.1874	4.4694
30	1	0.8033	0.1095	0.8206	0.1095	11.5766	8.7265
35	3.1623	1.5584	0.2597	1.147	0.1299	16.679	13.5038
40	10	2.8868	0.4619	1.6852	0.2582	22.4219	17.2007

Table 3.4. Rate maximizing $(B_{\mathrm{DC}}, \sigma)$ values and optimum rates for FD cooperative VLC with AF relaying. Transmission rates of suboptimum EPA strategies included for comparison.

σ_T^2 per LED		FD Mode, AF, OPA					EPA
(dBm)		$B_{\mathrm{DC,s}}$ (V)	$B_{\mathrm{DC,r}}$ (V)	σ_S (V)	σ_R (V)	Rate	Rate
0	0.001	0.0072	0.0072	0.0213	0.0211	9×10^{-10}	2×10^{-10}
5	0.0032	0.0128	0.0134	0.0381	0.037	8×10^{-8}	2×10^{-8}
10	0.01	0.0227	0.0251	0.069	0.064	7×10^{-6}	2×10^{-6}
15	0.0316	0.0425	0.0531	0.1259	0.1056	5×10^{-4}	2×10^{-4}
20	0.1	0.0832	0.1172	0.2305	0.1619	0.0244	0.0128
25	0.3162	0.1613	0.2487	0.4205	0.227	0.6774	0.364
30	1	0.3586	0.49	0.7236	0.3282	6.7219	4.215
35	3.1623	0.8289	0.9565	1.1138	0.5655	21.995	18.49
40	10	1.852	1.8142	1.4861	1.0344	40.799	38.45

Table 3.5. Rate maximizing $(B_{\mathrm{DC}}, \sigma)$ values and optimum rates for HD cooperative VLC with AF relaying. Transmission rates of suboptimum EPA strategies included for comparison.

σ_T^2 per LED		HD Mode, AF, OPA					EPA
(dBm)		$B_{\mathrm{DC,s}}$ (V)	$B_{\mathrm{DC,r}}$ (V)	σ_S (V)	σ_R (V)	Rate	Rate
0	0.001	0.0127	0.0081	0.0336	0.0205	0.0117	0.0066
5	0.0032	0.0226	0.0164	0.0582	0.0372	0.0595	0.0347
10	0.01	0.0402	0.0292	0.1083	0.0579	0.2793	0.1638
15	0.0316	0.0779	0.0519	0.1978	0.0811	1.0566	0.6151
20	0.1	0.1501	0.1039	0.3495	0.1058	3.0455	1.8651
25	0.3162	0.3285	0.1848	0.5735	0.1393	6.5461	4.542
30	1	0.6938	0.3651	0.8532	0.2066	11.1059	8.6247
35	3.1623	1.4285	0.6493	1.1433	0.3046	16.3291	12.9922
40	10	2.6558	1.1547	1.7321	0.4761	22.0617	16.6601

Table 3.6. Rate maximizing $(B_{\mathrm{DC}}, \sigma)$ values and optimum rates for direct VLC. Transmission rates of suboptimum EPA strategies included for comparison.

σ_T^2 per LED		Direct Comm., OPA			EPA
(dBm)		$B_{\mathrm{DC,s}}$ (V)	σ_S (V)	Rate	Rate
0	0.001	0.0167	0.0269	0.0168	0.0153
5	0.0032	0.0297	0.0477	0.0529	0.0483
10	0.01	0.053	0.0848	0.1663	0.1521
15	0.0316	0.0946	0.1506	0.516	0.4737
20	0.1	0.1707	0.2662	1.5442	1.4308
25	0.3162	0.3166	0.4647	4.2172	3.993
30	1	0.6173	0.7868	9.7144	9.5134
35	3.1623	1.2593	1.2555	18.1525	18.1524
40	10	2.5288	1.8987	28.5875	27.5737

The transmission rates achieved by OPA strategies are presented in Figure 3.5 for DF relaying and direct communication, in comparison with the suboptimum EPA strategies. First of all, the results show that optimizing the power allocation among the DC bias levels and IC signal variances is beneficial in terms of transmission rates for all communication settings. The results also show that for low σ_T values, all communication modes provide very little transmission rates (around several *kbps*). It is also observed that FD relaying provides almost zero rates for $\sigma_T < 20$ dBm/LED. This can be explained by two factors. First, when σ_T is low, the DC bias level must also be low, which results in severe clipping by the LEDs. Secondly, for FD relaying, the SNR reduction introduced by the interference from the source is very large for 30 dBm/LED $< \sigma_T <$ 30 dBm/LED. However when illumination requirements are increased, the doubled transmission duration becomes dominant, and the transmission rate is improved significantly compared to HD relaying. Therefore it is beneficial to employ HD relaying when illumination requirements are low and switch to FD relaying when illumination requirements are high.

The BER performances of the OPA strategies for DF relaying are presented in Figure 3.6 and compared to the suboptimum EPA strategies. These BER curves are obtained by (3.58) using the optimum B_{DC} and σ values in Tables 3.2-3.6. The BER results indicate that when the OPA strategy is employed, the HD relaying provides the lowest BER for a given σ_T value. This implies that, switching from HD relaying to FD relaying at high σ_T values provides rate gains in exchange for an increase in BERs. The transmission rates achieved by OPA and EPA strategies are presented in Figure 3.7 for AF relaying. It is observed that maximum transmission rates achievable with AF relaying are smaller than those with DF relaying. It is also observed that FD cooperation improves the transmission rates with AF relaying as well, this time with a smaller increase in BER, compared to the case with DF relaying.

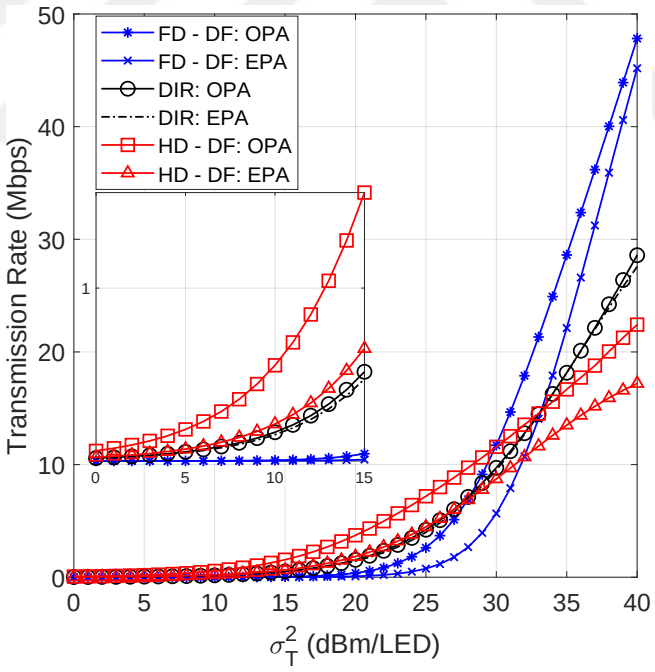

Figure 3.5. Transmission rate performances of OPA and EPA strategies for DF relaying along with direct communication.

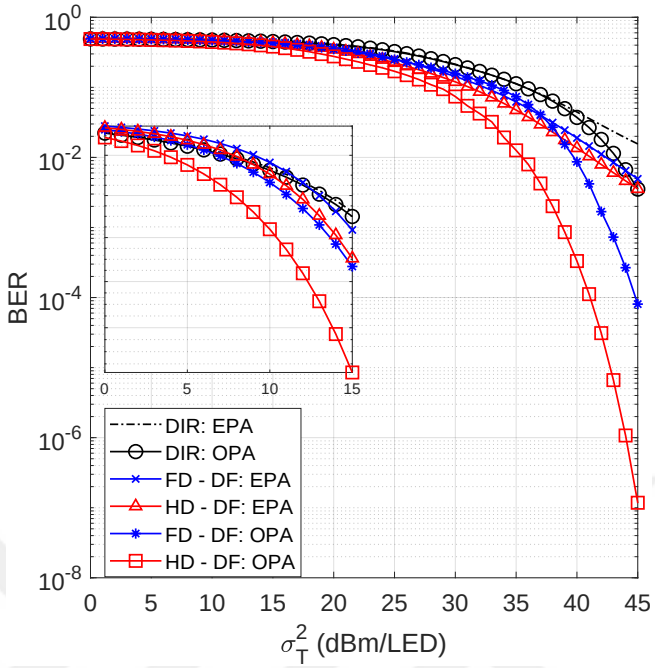

Figure 3.6. BER performances of OPA and EPA strategies for DF relaying along with direct communication.

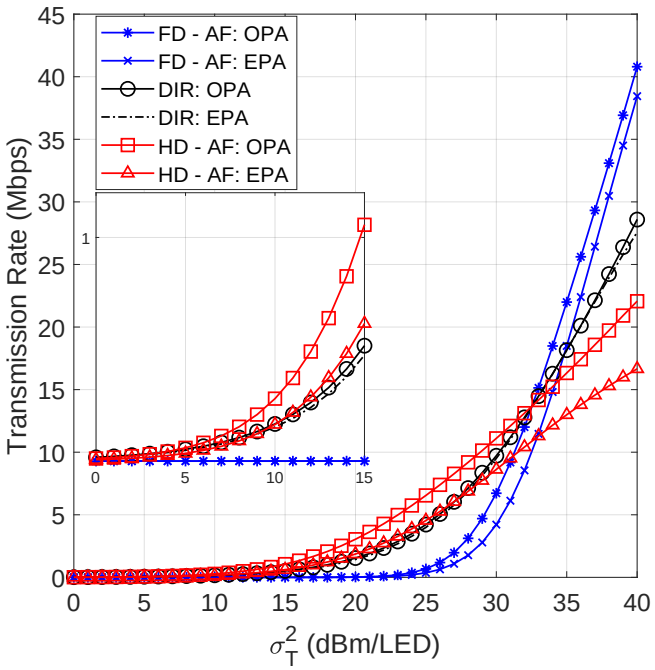

Figure 3.7. Transmission rate performances of OPA and EPA strategies for AF relaying along with direct communication.

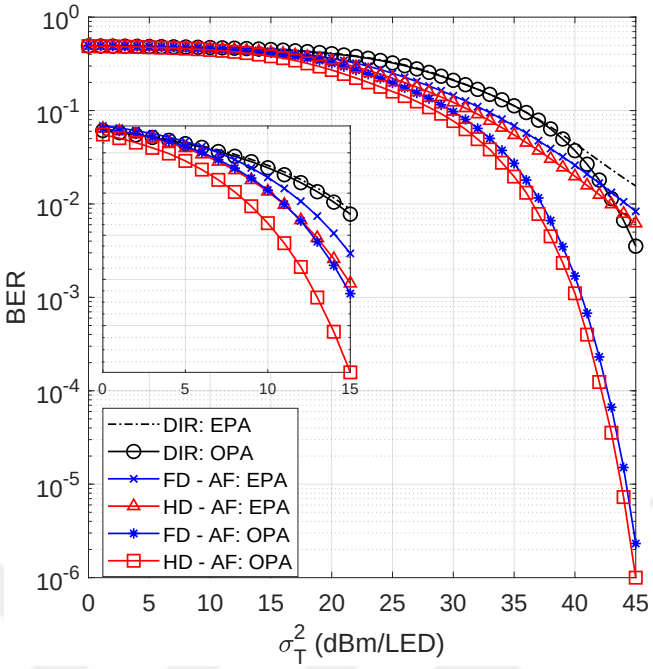

Figure 3.8. BER performances of OPA and EPA strategies for AF relaying along with direct communication.

In Figure 3.9 and 3.10, we present the optimum performance comparisons for AF and DF relaying in FD and HD modes. In addition, we present the optimum performance curves for FD relaying, in which the operational delay at the relay terminal is zero. Hence, the black curves stand for the ideal case with zero interference at the destination. Notice that, the achievable transmission rates with an ideal FD relay are significantly larger than the realistic case for the lower σ_T values, which is outperformed by the optimum communication with the realistic relay for larger σ_T values. The results also show that employing a relay improves both the transmission rate and BER performances of the VLC system, compared to direct communication. DF relaying generally provides greater transmission rates compared to the AF relaying, with larger gains for high σ_T values when FD mode is employed. However, at the high σ_T band, AF relaying provides $1-2$ orders of magnitude smaller BERs in FD mode. Hence, DF relaying provides larger rate gains, but at the expense of greater BER increase.

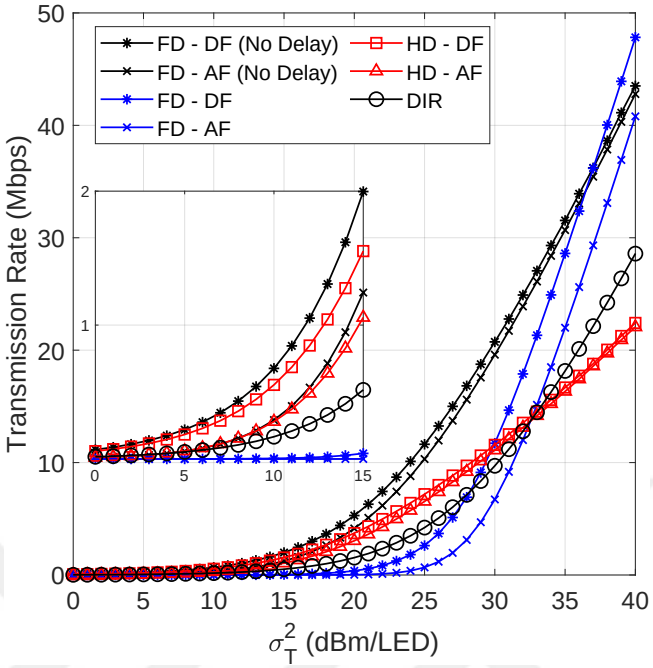

Figure 3.9. Transmission rate performances of rate maximizing OPA strategies for all communication settings.

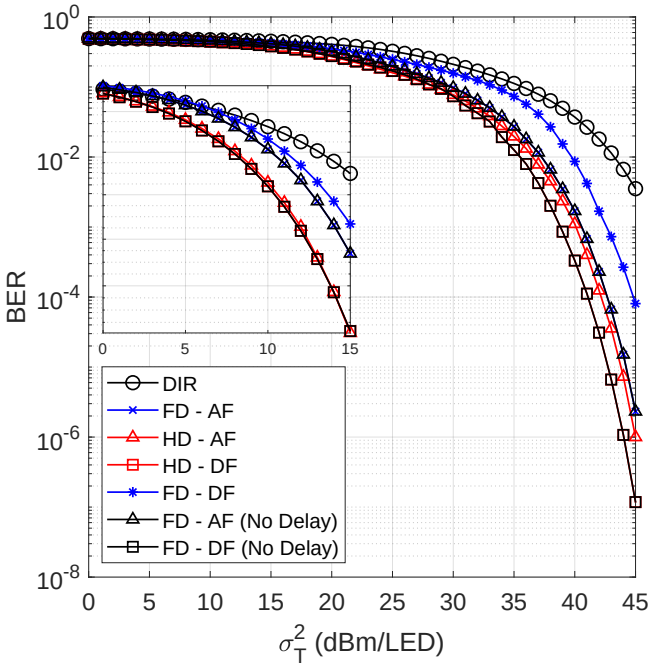

Figure 3.10. BER performances of rate maximizing OPA strategies for all communication settings.

Finally, the optimal $\{B_{\mathrm{DC}}, \sigma\}$ values under LED clipping effects, which is obtained by solving (3.53), are applied on the considered 3-terminal VLC systems with and without LED clipping. The corresponding transmission rate and BER results are presented for FD and HD cooperative modes in Figures 3.11 - 3.14 for DF and AF relaying respectively. In this figure, the *ideal case* curves are obtained with the assumption of zero LED clipping at both the source and the realistic relay with non-zero delay. The transmission rates are expected to be lower in the realistic VLC systems, also suggested by the results in Figure 3.11, since LED clipping is ignored in the ideal case. However, this loss decreases with increasing σ_T for both the FD and HD cooperation modes, when the realistic VLC system employs the OPA strategy. Inspecting the simulation results in Figure 3.12, it is observed that with the OPA strategy, the BERs are also improved and brought closer to the ideal case with increasing σ_T for both the FD and HD cooperation. The simulations performed with AF relaying provide similar outcomes as shown in Figures 3.13 3.14. These simulation results show that the LED clipping has a detrimental effect on the communication performance of VLC systems, which can be mitigated by the joint $\{B_{\mathrm{DC}}, \sigma\}$ optimization. As a result, the transmission rates and BERs can be brought closer to the ideal case with increasing σ_T, while the suboptimal EPA strategies suffer under LED clipping.

The exhibited transmission rate and BER performance results have the following outcomes. The proposed OPA strategy is beneficial for all communication modes and σ_T values. This is shown through evaluating the performance of OPA with the EPA strategy, which involves no optimization. Furthermore, the signal clipping introduced by the VLC transmitters is shown to have a detrimental effect on the communication performance, which can be reduced by employing the OPA strategies. The OPA strategy also brings improvement compared to the partially optimized power allocation strategies with preset DC bias levels, since it maximizes the transmission rate by controlling the clipping noise effects through the joint optimization of DC bias levels and IC signal variances.

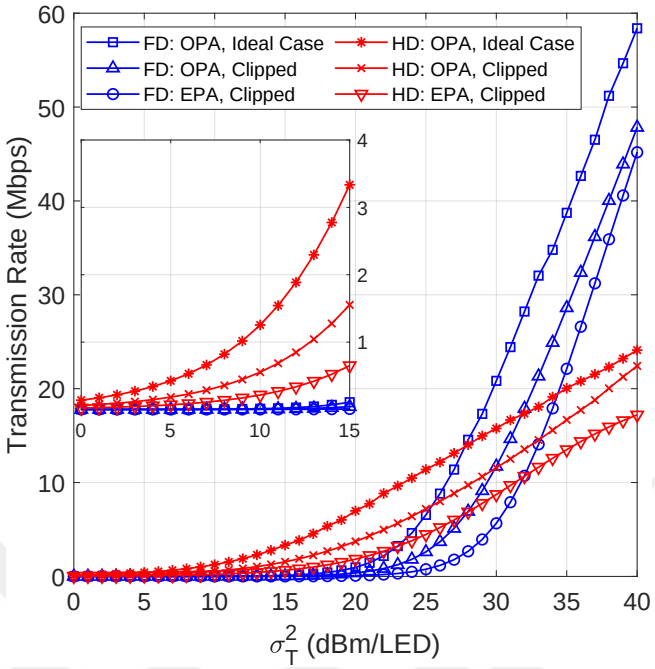

Figure 3.11. Transmission rate performances with no clipping (ideal) and with clipping (realistic) for DF relaying.

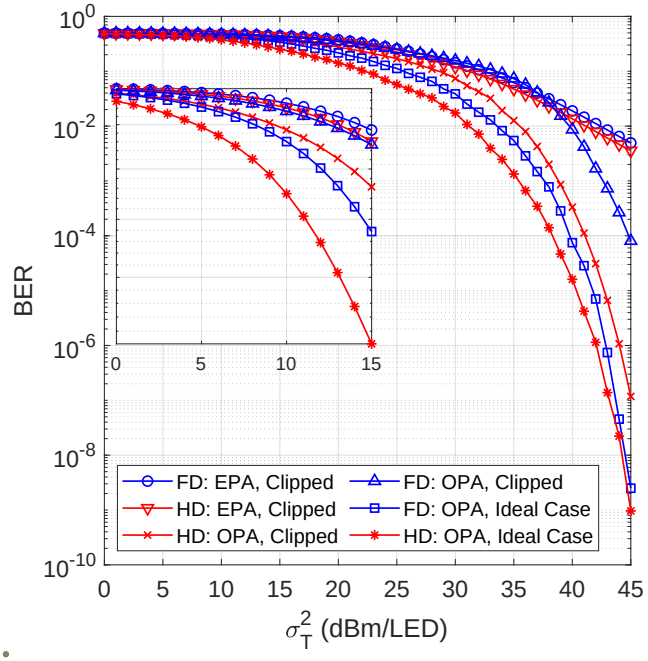

Figure 3.12. BER performances with no clipping (ideal) and with clipping (realistic) for DF relaying.

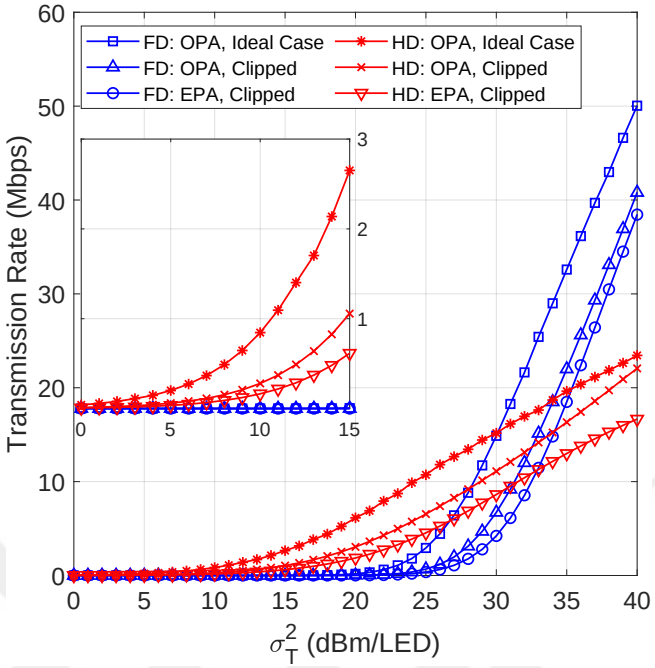

Figure 3.13. Transmission rate performances with no clipping (ideal) and with clipping (realistic) for AF relaying.

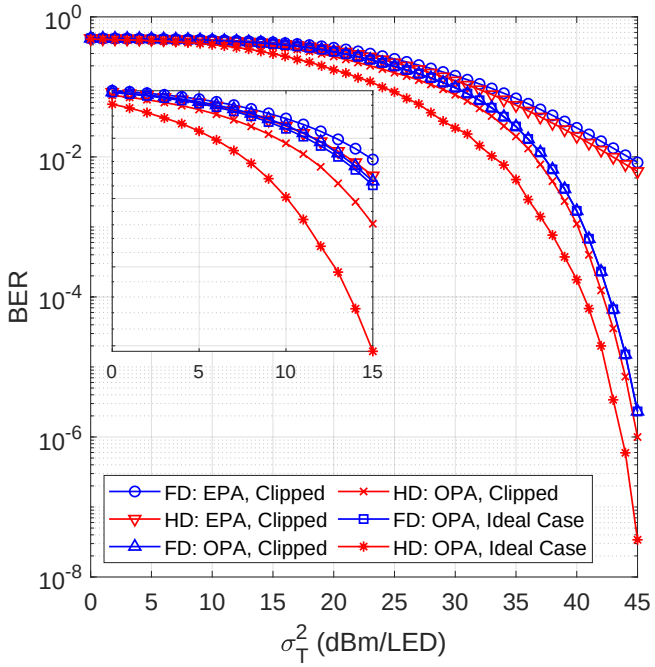

Figure 3.14. BER performances with no clipping (ideal) and with clipping (realistic) for AF relaying.

The OPA strategy does not bring additional computational costs during the communication, because the optimum $\{B_{\mathrm{DC}}, \sigma\}$ values are found offline and valid for a typical indoor VLC at all times, since the VLC channel is static as described in Section II. Our results also suggest that employing a relay to the VLC system improves both the transmission rates and BER. The FD relaying is shown to be superior to HD relaying in terms of transmission rates when the illumination requirements are high. When DF relaying is employed, switching to FD mode brings larger gains in transmission rates, when compared to AF relaying. However, this additional benefit is obtained at the expense of reduced BER performance.

3.7. Conclusion

In this chapter, FD relaying is described for 3-terminal indoor DCO-OFDM VLC systems with LED signal clipping at both the source and the relay. The achievable transmission rates and the rate maximizing communication strategies are characterized under illumination constraints. For both the FD and HD modes, AF and DF relaying capabilities are studied. It is shown that LED clipping greatly worsens the VLC performance, however by the proposed OPA strategies, both transmission rates, and BER can be improved for all communication settings. In FD cooperation, the source's signal interferes with the relay's signal at the destination, which has a detrimental effect on the transmission rates especially when the required illumination level is low. However, when the required illumination is high, cooperation in FD mode is shown to improve the transmission rates significantly, compared to HD relaying. According to the simulation results, FD mode can improve the VLC performance in terms of both the transmission rates and BER, depending on the illumination preferences.

4. PHYSICAL LAYER SECURITY FOR MULTI USER MIMO VISIBLE LIGHT COMMUNICATION SYSTEMS WITH GENERALIZED SPACE SHIFT KEYING

4.1. Introduction

The evolution of wireless communication systems and the way people use their mobile devices are constantly inducing one another for high data rates, low latency, high reliability, and availability. To address this data-centric era of wireless connectivity demands efficiently, two important factors; (i) utilization of a higher frequency portion of the spectrum and (ii) deployment of multiple transmitter (TX) / receiver (RX) units are set to be the core components of fifth generation (5G) and beyond wireless communication networks [111]. Firstly, the frequencies above 30 GHz, referred to as the mm-Wave band, is started to be considered as a viable solution for delivering broadband wireless data access in the literature. However, due to the high path loss characteristic of the electromagnetic (EM) wave in the $30 - 300$ GHz band, mmWave systems would require the deployment of many access points (APs) even for a very small area, compared to conventional radio systems. Here, the optical wireless communications (OWC), in a broader extend light fidelity (LiFi), offers the utilization of both visible light (VL) and infrared (IR) bands to address the mentioned problems in an radio frequency (RF) non-interfering way. Since LiFi networks utilize the existing illumination infrastructure for seamless broadband data transmission, it offers energy and cost efficiency along with significant deployment ease. Furthermore, a significant area of spectral efficiency and secrecy could be achieved as the light cannot penetrate through opaque objects [91,112]. Secondly, the utilization of multiple elements at both TX and RX sides, namely multiple-input-multiple-output (MIMO), have its distinct potential to increase the system capacity [113]. Also, multiple transmit and receive units could also be used to increase the system reliability and quality of service (QoS) as well as the achievable signal-to-noise ratio (SNR) and error performance.

More recently, the MIMO systems are started to be used to enhance the achievable secrecy of the wireless communication systems [114, 115].

The amalgamation of both the nm-wave signalling and MIMO transmission creates the physical layer security (PLS) for the optical systems with multiple TX and/or RX units [60–69]. Moreover, PLS for multi-user MIMO networks for in RF and optical bands have recently drawn a significant attention from the researchers [70–75]. Particularly, spatial modulation (SM) is a promising MIMO transmission technique which is able to achieve enhanced error performance by deactivating some of the transmit units in an energy efficient manner [116]. Accordingly, both the signal itself (constellation symbol) and the active transmit unit index (spatial symbol) carry information in SM per transmission instant. Since only a transmit unit per symbol transmission is activated in SM, the inter-channel-interference (ICI) caused by the channel coupling is completely mitigated. The application of SM in the optical domain is also proposed in [117]. For further simplification in SM transmission, space shift keying (SSK) method, which omits the constellation symbols completely, is proposed in [79, 118]. However, the system simplification is obtained in exchange for the reduced spectral efficiency in SSK. Therefore, a system with high spectral efficiency and less transmission complexity, referred to as generalized space shift keying (GSSK), is proposed in [76–78]. In GSSK, multiple transmit units are activated per transmission instant, which essentially extends the number of transmit possibilities that could be sent by using the transmit unit indexes. Although the PLS for the SM, SSK and GSSK systems are investigated in the literature [119–123], there are only a few works that considered multi-user SM based systems. [124, 125].

In this chapter, we extend the work in [68] to an indoor multi-user MIMO-VLC (MU-MIMO-VLC) scenario and propose the MU-GSSK-SCD technique to enhance the PLS. In this system, the AP is located on the ceiling, which is equipped with multiple transmitting light-emitting diodes (LEDs) for illumination and wireless data transfer purposes. A fixed number of the LEDs are activated for each channel use, while the rest operates for illumination only.

The legitimate users and the eavesdropper are scattered within the environment and equipped with multiple photodetectors (PDs) for data reception. In order to satisfy the eye-safety requirements of the visible light communication (VLC) system, the illumination level is constrained in a preset interval by adjusting the direct-current (DC) bias level accordingly. We optimize the received signal constellations at the legitimate users jointly by adjusting the emission power of each transmitting LEDs with the channel state information (CSI) of the legitimate users. This power allocation introduces jamming for the eavesdropper only, while the legitimate users get an undistorted signal. The proposed strategy also ensures zero user-interference and does not require CSI exchange between the legitimate users. Furthermore, the achievable secrecy rate region for MU-MIMO-VLC is derived analytically. The proposed multi user-GSSK with spatial constellation design (MU-GSSK-SCD) system is simulated in a practical indoor VLC environment for various user configurations, which shows that the bit error ratio (BER) of the eavesdropper is significantly degraded. The simulation results also show that the improvement in the secrecy rate depends on the user positions relative to each other. However, the full secrecy is indeed attainable at 0 dB SNR with a user separation of 90 cm. The BER and secrecy rate results prove that the PLS of the multi user-MIMO-VLC (MU-MIMO-VLC) system is ensured with the MU-GSSK-SCD approach. The contributions of this chapter can be summarized as follows:

- A novel multidimensional lattice design technique for multi-user GSSK system, namely MU-GSSK-SCD, is proposed to improve the PLS of the MU-MIMO-VLC transmission. According to our proposed approach, the emitted light intensity of the transmitting LEDs is adjusted by using the legitimate users CSI, such that the received signal constellations at the legitimate users are optimized in terms of BER.

- Multi user RF- or VLC-based MIMO communications is generally based on assigning disjoint sets of transmit antennas or LEDs to each user or cluster of users. Conversely, the multi user PLS technique proposed in this chapter does not require such clustering approach. Instead, by means of a properly designed precoding at the transmitter, all available LEDs are used simultaneously for reliable and secure information transmission to each user without any multi user interference (MUI) with higher spectral efficiency.
- The proposed MU-GSSK-SCD scheme inherently generates a friendly jamming signal by the random switching of the LED, preventing any meaningful confidential information leakage to Eve. Whereas, in classical PLS- based systems, a separate jamming signal is generated for this purpose at the expense of resorting to highly directive LED arrays, suitable beamforming techniques and requiring the CSI of Eve by the transmitter as well as higher signal energy for transmission of the jamming signal.
- The achievable secrecy rate region of MU-MIMO-VLC systems by the MU-GSSK-SCD technique is derived analytically for a given number of LEDs and PDs and the secrecy performance is presented for different user separations and varying number of PDs.

The outline of this chapter is as follows. In Section II, we introduce the MU-MIMO-GSSK-VLC system model. Next in Section III, the MU-GSSK-SCD technique is explained in detail. The analytical secrecy rate upper bounds and the secrecy rate regions are derived in Section IV. The performance evaluations of the proposed MU-GSSK-SCD technique are presented in Section IV for various parameters and with both perfect and imperfect CSI at the legitimate users. We finalize this chapter with concluding remarks in Section V.

Notation: Throughout the chapter, matrices and column vectors are in bold uppercase and lowercase letters, respectively. Unless stated otherwise, $\mathbf{A}_k$ and $\mathbf{a}_k$ denote the matrix $\mathbf{A}$ and the vector $\mathbf{a}$ designated to User k. The mth row and n^{th} column element of the matrix $\mathbf{A}_k$ is denoted by $a_k^{m,n}$.

Similarly, the mth element of the vector $\mathbf{a}_k$ is given by a_k^m. The transpose, Euclidean norm, determinant and Cartesian product operations are expressed by $(\cdot)^{\mathrm{T}}$, $\|\cdot\|$, $|\cdot|$ and $\times$, respectively. The natural logarithm is denoted by $\ln(\cdot)$. The interval of numbers between a and b, including a and b, is denoted by $[a, b]$. The element-wise inequality between two vectors is given by $\preceq$. The set of all real $m \times n$ matrices are denoted by $\mathcal{R}^{m\times n}$. Statistical expectation, argument maximum, argument minimum, floor and ceiling operations are represented by $\mathrm{E}\{\cdot\}$, $\arg\max\{\cdot\}$, $\arg\min\{\cdot\}$, $\lfloor\cdot\rfloor$ and $\lceil\cdot\rceil$, respectively. Mutual information, entropy and conditional entropy are denoted by $\mathbb{I}(\cdot;\cdot)$, $\mathbb{H}(\cdot)$ and $\mathbb{H}(\cdot|\cdot)$, respectively.

4.2. Multi User MIMO-GSSK-VLC System Model

In this chapter, we consider an indoor VLC system, where the AP (Alice) is equipped with N_t LEDs, and K legitimate users and Eve are equipped with N_r PDs each. The most straightforward approach for realizing the VLC with off-the-shelf optical components is intensity-modulation-direct-detection (IM/DD). Accordingly, the information is encoded onto changes in instantaneous light intensity at the TX side. As the rate of change of light intensity is in the order of MHz region, this changes are not visible to the human eye. However, the subtle changes in the instantaneous light intensity can be detected by the PDs at the RX side to retrieve the information. Unlike the conventional RF systems, the small scale fading effects are lacking in IM/DD systems. The reason for this is the significantly large area of the PD devices compared to the operation wavelength (nm). Therefore, the integration of spontaneously emitted light-waves, whose phase values are uniformly distributed between $[-\pi, \pi]$, over a large area yields an average phase of zero. Furthermore, it has been reported in [15, 126] that the majority of the users experience a line-of-sight (LoS) channel as long as they are from the corners of the room. Hence, we can deduce that the multipath richness is minimal in MIMO-VLC applications, in other words, LoS component dominates the effective channel. The LoS channel coefficients are practically taken as the effective OWC channel in this chapter without loss of generality.

As reported in [127], we can describe the LoS coefficients between the tth transmitter of Alice and the rth receiver of the kth user as

$$h_k^{r,t} = \frac{(\beta+1)A_{\text{PD}}}{2\pi(d_k^{r,t})^2}\cos^{\beta}(\phi_k^{r,t})\cos(\theta_k^{r,t})\mathbb{1}_{\Psi_{1/2}}(\theta_k^{r,t}), \tag{4.1}$$

where $\beta = -1/\log_2(\cos(\Phi_{1/2}))$ is the Lambertian emission order of the light source, with $\Phi_{1/2}$ being the semi-angle of the half-power of the transmitting LED. A_{PD} stands for the effective area of the non-imaging PD. The parameters $d_k^{r,t}$, $\phi_k^{r,t}$ and $\theta_k^{r,t}$ indicate the distance, the angle of emergence and the angle of incidence between the tth transmitter and the rth receiver of the kth user, respectively. The function

$$\mathbb{1}_{\Psi_{1/2}}(\theta_k^{r,t}) = \left\{ \begin{array}{ll} 1, & \text{if } ||\theta_k^{r,t}|| \leq \Psi_{1/2} \\ 0, & \text{otherwise} \end{array} \right\} \tag{4.2}$$

indicates whether the incidence angle is within the field-of-view (FOV) of the PD. The parameter $\Psi_{1/2}$ is the half-angle of the FOV of the PD. The channel matrix between Alice and k^{th} user can be constructed as

$$\mathbf{H}_k = \begin{bmatrix} h_k^{1,1} & h_k^{1,2} & \dots & h_k^{1,N_t} \\ h_k^{2,1} & h_k^{2,2} & \dots & h_k^{2,N_t} \\ \vdots & \vdots & \ddots & \vdots \\ h_k^{N_r,1} & h_k^{N_r,2} & \dots & h_k^{N_r,N_t} \end{bmatrix}. \tag{4.3}$$

The complete architecture for the proposed multi-user MIMO-GSSK-VLC system is shown in Figure 4.1. This architecture is distinguished from the conventional MU-MIMO-GSSK systems with the novel SCD and the corresponding power optimization technique, which will be discussed in the next section. We employ intensity modulated VLC, where the information is encoded on the emitted light intensity around a constant level. This is provided by driving the LEDs with a varying current around a DC bias level (B_{DC}), so that bipolar signals are encoded on the unipolar light intensity as reported in [88].

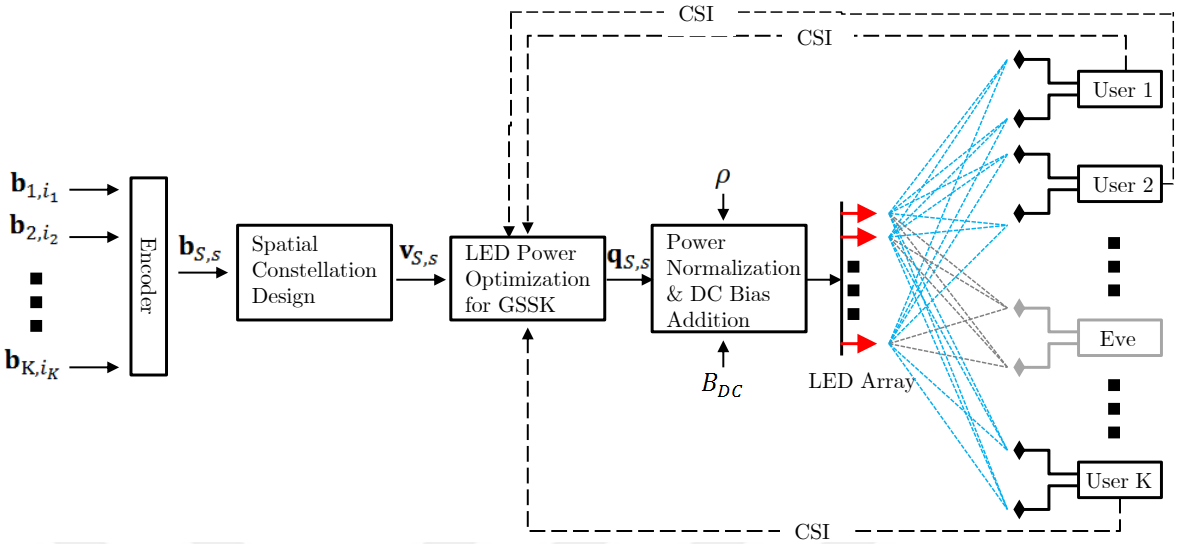

Figure 4.1. System architecture for the multi-user MIMO-GSSK-VLC with SCD.

In GSSK-VLC, N_a LEDs are activated (intensity modulated) for each channel's use, while the other LEDs provide illumination only. For MU-GSSK, a joint bit sequence is broadcasted over the active LEDs to all users. For a GSSK system, the total number of bits that can be broadcasted by the AP per channel use is

$$N_B = \left\lfloor \log_2 \binom{N_t}{N_a} \right\rfloor . \tag{4.4}$$

Each broadcast is designed to deliver every user its designated information only, which is equal to $N_B^{(k)}$ bits per channel use (bpcu). Therefore

$$N_B = \sum_{k=1}^{K} N_B^{(k)}. \tag{4.5}$$

For each channel use, an information symbol is generated for the kth user, from their designated symbol alphabet, $\mathcal{C}_k$, which is defined as

$$\mathcal{C}_k = \{\mathbf{b}_{k,1}, \mathbf{b}_{k,2}, \ldots, \mathbf{b}_{k,i_k}, \ldots, \mathbf{b}_{k,M_k}\}. \tag{4.6}$$

Here, $M_k = 2^{N_B^{(k)}}$ is the number of symbols in $\mathcal{C}_k$ and $i_k \in \{1, 2, \ldots, M_k\}$. The variable $\mathbf{b}_{k,i_k}$ denotes the bit sequence that corresponds to the i_k^{th} information symbol of the kth user and is defined as

$$\mathbf{b}_{k,i_k} = [b_{k,i_k}^{(1)}, b_{k,i_k}^{(2)}, \ldots, b_{k,i_k}^{(\ell)}, \ldots, b_{k,i_k}^{N_B^{(k)}}], \tag{4.7}$$

where ℓ is the bit index. For each channel use, a joint bit sequence is constructed by concatenating $\mathbf{b}_{k,i_k}$ for $k = 1, 2, \ldots, K$ in the given order. The constructed joint bit sequence represents a joint symbol from the joint symbol alphabet,

$$\mathcal{C}_{\mathcal{S}} = \mathcal{C}_1 \times \mathcal{C}_2 \times \cdots \times \mathcal{C}_k \times \cdots \times \mathcal{C}_K = \{\mathbf{b}_{\mathcal{S},1}, \mathbf{b}_{\mathcal{S},2} \ldots, \mathbf{b}_{\mathcal{S},s}, \ldots, \mathbf{b}_{\mathcal{S},M_{\mathcal{S}}}\}, \tag{4.8}$$

where $\times$ denotes the Cartesian product operation and $M_{\mathcal{S}} = \prod_k M_k$. The element $\mathbf{b}_{\mathcal{S},s}$ is the bit sequence, representing s^{th} joint symbol, and defined as

$$\mathbf{b}_{\mathcal{S},s} = [\mathbf{b}_{1,i_1}, \mathbf{b}_{2,i_2}, \ldots, \mathbf{b}_{k,i_k}, \ldots, \mathbf{b}_{K,i_K}]. \tag{4.9}$$

Note that as mentioned above, $\mathbf{b}_{k,i_k}$ is the bit sequence for the i_k^{th} information symbol of the kth user from (4.6). The symbol index s can be found by modified base conversion as

$$s = \sum_{k=1}^{K-1} \left((i_k - 1) \prod_{j=k+1}^{K} M_j \right) + i_K. \tag{4.10}$$

Therefore, a joint bit sequence $\mathbf{b}_{\mathcal{S},s}$ conveys the information symbols $\{i_1, i_2, \ldots, i_K\}$ of Users $k = 1, 2, \ldots, K$ respectively.

For each channel use, a selected $\mathbf{b}_{\mathcal{S},s}$ is broadcasted over the MU-GSSK-VLC channel by activating N_a out of N_t LEDs, whose indices are chosen randomly and stored in

$$\mathbf{I}_{\mathcal{S},s} = [I_{\mathcal{S},s}^{(1)}, I_{\mathcal{S},s}^{(2)}, \ldots, I_{\mathcal{S},s}^{(\ell)}, \ldots, I_{\mathcal{S},s}^{(N_a)}]^T, \tag{4.11}$$

where the indices of the active LEDs, $I_{\mathcal{S},s}^{(\ell)}$ and $I_{\mathcal{S},s}^{(\ell')}$, are distinct random integers from $[1, N_t]$ for $\ell \neq \ell'$ and $\ell, \ell' = 1, \ldots, N_a$.

The emitted light intensity of all LEDs are determined by a constant DC bias level, B_{DC}, and the intensity variations around it that carry information for $\mathbf{b}_{\mathcal{S},s}$. It is denoted by $\mathbf{q}_{\mathcal{S},s} \in \mathcal{R}^{N_t \times 1}$. Both $\mathbf{q}_{\mathcal{S},s}$ and B_{DC} are designed according to the proposed MU-GSSK-SCD scheme in the following section. Consequently, the corresponding received signals by the kth user and Eve become

$$\mathbf{y}_k = \mathbf{H}_k \left(\mathbf{q}_{\mathcal{S},s} + [(B_{\mathrm{DC}})_{\times N_t}]^T \right) + \mathbf{n}_k, \tag{4.12}$$

$$\mathbf{y}_e = \mathbf{H}_e \left(\mathbf{q}_{\mathcal{S},s} + [(B_{\mathrm{DC}})_{\times N_t}]^T \right) + \mathbf{n}_e, \tag{4.13}$$

where $\left(\mathbf{q}_{\mathcal{S},s} + [(B_{\mathrm{DC}})_{N_t \times 1}]^T \right)$ denotes the emitted light intensity of all LEDs, and $[(B_{\mathrm{DC}})_{N_t \times 1}]^T$ is the DC bias vector. In (4.12), $\mathbf{H}_k$, $\mathbf{H}_e \in \mathcal{R}^{N_r \times N_t}$ are the CSI of the kth legitimate user and Eve. These channel matrices are obtained from (4.3) and are available at the AP. The variables $\mathbf{y}_k, \mathbf{y}_e \in \mathcal{R}^{N_r \times 1}$ are the received signal vectors at the kth user and Eve. The noise vectors, $\mathbf{n}_k, \mathbf{n}_e \in \mathcal{R}^{N_r \times 1}$, are zero mean Gaussian random vectors with the covariance matrices $\sigma_k^2 \mathbf{I}_{N_r}$ and $\sigma_e^2 \mathbf{I}_{N_r}$, where $\mathbf{I}_{N_r}$ is the identity matrix of size $N_r \times N_r$. In the proposed MU-GSSK-SCD, the information symbols for all users are broadcasted jointly via all LEDs with $\mathbf{q}_{\mathcal{S},s}$, unlike the LED clustering approach in such as [128–130], where certain LEDs are designated for a single user or group of users. Notice that, only N_a LEDs are activated per channel use by (4.11), therefore only those entries of $\mathbf{q}_{\mathcal{S},s}$ are non-zero. Hence the columns of $\mathbf{H}_k$, which are multiplied with the remaining zero entries of $\mathbf{q}_{\mathcal{S},s}$, do not contribute to $\mathbf{y}_k$.

In this chapter, the legitimate users are assumed to be aware of their own channel that is the case in practical communication systems, so the DC bias can be removed from $\mathbf{y}_k$ at the receiver. Therefore, the received signals can be rewritten as

$$\begin{bmatrix} \mathbf{y}_1 \\ \mathbf{y}_2 \\ \vdots \\ \mathbf{y}_K \end{bmatrix} = \rho \begin{bmatrix} \tilde{\mathbf{H}}_1 \\ \tilde{\mathbf{H}}_2 \\ \vdots \\ \tilde{\mathbf{H}}_K \end{bmatrix} \tilde{\mathbf{q}}_{\mathcal{S},s} + \begin{bmatrix} \mathbf{n}_1 \\ \mathbf{n}_2 \\ \vdots \\ \mathbf{n}_K \end{bmatrix}, \tag{4.14}$$

where $\tilde{\mathbf{H}}_1, \tilde{\mathbf{H}}_2, \ldots, \tilde{\mathbf{H}}_K \in \mathcal{R}^{N_r \times N_a}$ are the relevant channel state matrices of the Users $1, 2, \ldots, K$, which are constructed by N_a columns of $\mathbf{H}_k$, indicated by the entries of $\mathbf{I}_{\mathcal{S},s}$ from (4.11). The variable $\tilde{\mathbf{q}}_{\mathcal{S},s} \in \mathcal{R}^{N_a \times 1}$ is the intensity vector of the selected N_a LEDs before the DC bias addition. The transmit power vector is normalized with ρ, which will be detailed in the following section.

4.3. Spatial Constellation Design for Enhanced PLS

In conventional GSSK downlink communication, spatial constellation points are specified by a set of active transmitters. For each transmitted constellation point, the destinations receive the superposition of the channel outputs of the transmitted signals. As a result, a transmitted constellation point is detected based on a received signal constellation, whose elements mainly depend on the channel coefficients, given by (4.1) in our case. Hence, when conventional GSSK is employed for VLC, PLS would depend on the features of the system configuration such as location and orientation of transmitters and receivers, which determine the channel conditions. However, it is possible to design the users' received signal constellations to remove the mentioned channel dependence and minimize their BERs. In fact, the BER of an optical MIMO-GSSK system is minimized in [68] for a single user by intelligent selection of the received signal constellation points at the legitimate user. In this part, we consider a multi-user MIMO-GSSK-VLC system, and minimize the BER at all legitimate users by joint spatial constellation design of all users, namely MU-GSSK-SCD.

According to MU-GSSK-SCD, for every channel use, the LED intensity vector $\tilde{\mathbf{q}}_{\mathcal{S},s}$ is designed so that the received signals from (4.14) become

$$\mathbf{y}_k = \rho \mathbf{v}_{k,i_k} + \mathbf{n}_k, \quad 1 \leq k \leq K, \tag{4.15}$$

where $\mathbf{v}_{k,i_k}$ is the received signal at user k, corresponding to the i_k^{th} information symbol and ρ is the power normalization coefficient. The received signal vector $\mathbf{v}_{k,i_k}$ belongs to

$$\mathcal{V}_k : \left\{ \mathbf{v}_{k,i_k} = [v_{k,i_k}^{(1)}, v_{k,i_k}^{(2)}, \ldots, v_{k,i_k}^{(N_r)}]^T, 1 \leq i_k \leq M_k \right\}, \tag{4.16}$$

which is the received spatial constellation of the User k. The selection of the elements in $\mathcal{V}_k$ is crucial because it directly affects the BER performance of the kth legitimate user and also Eve. In [131], it is shown that the SCD approach minimizes the BER of a user with $N_r = 1$ in an optical spatial modulation (OSM) system by maximizing the minimal pairwise Euclidean distance of the received signal constellation points while their average norm is fixed. The work in [68] generalizes the SCD framework to the MIMO setting, and shows that bipolar signal constellation is optimal in an N_r-space. In this chapter, the SCD approach is applied to the multi-user setting, therefore the received spatial constellations $\mathcal{V}_k$ for all k are optimally chosen to be M-ary signal constellations in N_r-space. In order for (4.15) to hold, $\tilde{\mathbf{q}}_{\mathcal{S},s}$ is formed such that

$$\tilde{\mathbf{H}}_k \tilde{\mathbf{q}}_{\mathcal{S},s} = \mathbf{v}_{k,i_k}, \quad 1 \leq k \leq K. \tag{4.17}$$

The condition in (4.17) should be satisfied jointly for all users.

For this purpose it is rewritten as

$$\begin{bmatrix} \tilde{\mathbf{H}}_1 \\ \tilde{\mathbf{H}}_2 \\ \vdots \\ \tilde{\mathbf{H}}_K \end{bmatrix} \tilde{\mathbf{q}}_{\mathcal{S},s} = \begin{bmatrix} \mathbf{v}_{1,i_1} \\ \mathbf{v}_{2,i_2} \\ \vdots \\ \mathbf{v}_{K,i_K} \end{bmatrix} \quad \rightarrow \quad \tilde{\mathbf{H}}\tilde{\mathbf{q}}_{\mathcal{S},s} = \mathbf{v}_{\mathcal{S},s}, \tag{4.18}$$

where $\tilde{\mathbf{H}}$ denotes the general channel matrix and $\mathbf{v}_{\mathcal{S},s}$ is the joint received signal vector. Note that $\mathbf{v}_{\mathcal{S},s}$ is mapped to s^{th} element in the joint symbol alphabet $\mathcal{C}_{\mathcal{S}}$ from (4.8), just like $\mathbf{v}_{k,i_k}$ is mapped to the i_k^{th} element in User k's symbol alphabet $\mathcal{C}_k$ from (4.6).

In Table 4.1, an example for the optimal 2−user GSSK-SCD is provided. In this setting, $N_t = 6$, $N_a = 3$, $N_r = 3$ and $K = 2$, and $N_B^{(1)} = N_B^{(2)} = 2$ bpcu is transmitted to the users, satisfying (4.4). Thus, both users have $M_k = 2^{N_B^{(k)}} = 4$ symbols in $\mathcal{C}_k$, given by (4.6). In a 3-dimensional space, 4 constellation points with unit energy have the maximal Euclidean distance from each other, when they lie on the vertices of a regular tetrahedron. Therefore, the optimal spatial constellation points are found as

$$\mathbf{v}_{k,1} = [\sqrt{\frac{8}{9}}, 0, -\frac{1}{3}], \qquad \mathbf{v}_{k,2} = [-\sqrt{\frac{2}{9}}, \sqrt{\frac{2}{3}}, -\frac{1}{3}],$$
$$\mathbf{v}_{k,3} = [-\sqrt{\frac{2}{9}}, -\sqrt{\frac{2}{3}}, -\frac{1}{3}], \qquad \mathbf{v}_{k,4} = [0, 0, 1],$$

for $k = 1, 2$. The transmit power vector that achieves the optimal received signal in (4.18) can be obtained by a zero forcing precoder, which is found by

$$\tilde{\mathbf{q}}_{\mathcal{S},s} = \left(\tilde{\mathbf{H}}^T\tilde{\mathbf{H}}\right)^{-1} \tilde{\mathbf{H}}^T\mathbf{v}_{\mathcal{S},s}. \tag{4.19}$$

Substituting (4.19) into (4.14), the received signals at the legitimate users become

$$\begin{bmatrix} \mathbf{y}_1 \\ \mathbf{y}_2 \\ \vdots \\ \mathbf{y}_K \end{bmatrix} = \rho \begin{bmatrix} \mathbf{v}_{1,i_1} \\ \mathbf{v}_{2,i_2} \\ \vdots \\ \mathbf{v}_{K,i_K} \end{bmatrix} + \begin{bmatrix} \mathbf{n}_1 \\ \mathbf{n}_2 \\ \vdots \\ \mathbf{n}_K \end{bmatrix}. \tag{4.20}$$

Table 4.1. Optimal SCD for 2−User GSSK-VLC with $N_t = 6$, $N_a = 3$, $N_r = 3$.

i_1	i_2	s	$\mathbf{b}_{\mathcal{S},s}$ (4.9)	$\mathbf{I}_{\mathcal{S},s}$ (4.11)	$\mathbf{v}_{\mathcal{S},s}$ (4.16)
1	1	1	$[[0,0],[0,0]]$	$[1,2,3]$	$[\mathbf{v}_{1,1}, \mathbf{v}_{2,1}]$
1	2	2	$[[0,0],[0,1]]$	$[1,2,4]$	$[\mathbf{v}_{1,1}, \mathbf{v}_{2,2}]$
1	3	3	$[[0,0],[1,0]]$	$[1,2,5]$	$[\mathbf{v}_{1,1}, \mathbf{v}_{2,3}]$
1	4	4	$[[0,0],[1,1]]$	$[1,2,6]$	$[\mathbf{v}_{1,1}, \mathbf{v}_{2,4}]$
2	1	5	$[[0,1],[0,0]]$	$[1,3,4]$	$[\mathbf{v}_{1,2}, \mathbf{v}_{2,1}]$
2	2	6	$[[0,1],[0,1]]$	$[1,3,5]$	$[\mathbf{v}_{1,2}, \mathbf{v}_{2,2}]$
2	3	7	$[[0,1],[1,0]]$	$[1,3,6]$	$[\mathbf{v}_{1,2}, \mathbf{v}_{2,3}]$
2	4	8	$[[0,1],[1,1]]$	$[1,4,5]$	$[\mathbf{v}_{1,2}, \mathbf{v}_{2,4}]$
3	1	9	$[[1,0],[0,0]]$	$[1,4,6]$	$[\mathbf{v}_{1,3}, \mathbf{v}_{2,1}]$
3	2	10	$[[1,0],[0,1]]$	$[1,5,6]$	$[\mathbf{v}_{1,3}, \mathbf{v}_{2,2}]$
3	3	11	$[[1,0],[1,0]]$	$[2,3,4]$	$[\mathbf{v}_{1,3}, \mathbf{v}_{2,3}]$
3	4	12	$[[1,0],[1,1]]$	$[2,3,5]$	$[\mathbf{v}_{1,3}, \mathbf{v}_{2,4}]$
4	1	13	$[[1,1],[0,0]]$	$[2,3,6]$	$[\mathbf{v}_{1,4}, \mathbf{v}_{2,1}]$
4	2	14	$[[1,1],[0,1]]$	$[2,4,5]$	$[\mathbf{v}_{1,4}, \mathbf{v}_{2,2}]$
4	3	15	$[[1,1],[1,0]]$	$[2,4,6]$	$[\mathbf{v}_{1,4}, \mathbf{v}_{2,3}]$
4	4	16	$[[1,1],[1,1]]$	$[2,5,6]$	$[\mathbf{v}_{1,4}, \mathbf{v}_{2,4}]$

The expression in (4.20) follows, because for any matrices $\mathbf{A} \in \mathcal{R}^{N\times N}$ and $\mathbf{B} \in \mathcal{R}^{N\times M}$ for $N \leq M$, it is true that $\mathbf{A} = \mathbf{B}\left(\mathbf{B}^T\mathbf{B}\right)^{-1}\mathbf{B}^T = \mathbf{I}_N$. This can be shown easily by multiplying $\mathbf{A}$ with $\mathbf{B}^T$ from the left side and observing that $\mathbf{B}^T\mathbf{A} \equiv \mathbf{B}^T$ if $\mathbf{A} = \mathbf{I}_N$. It is also worth noting that in OWC the channels between different LEDs and PDs may be closely related depending on the user locations. Therefore, the channel coefficients are functions of the terminal locations and orientations as given in (4.1). In some cases, this may result in linearly dependent rows or columns in $\tilde{\mathbf{H}}$ as reported in [132] and $\mathbf{B} = \tilde{\mathbf{H}}^T\tilde{\mathbf{H}}$ may be ill-conditioned. In that case, a small perturbation ϵ, called *regularization parameter* is inserted to make the resulting matrix full rank as in

$$\tilde{\mathbf{q}}_{\mathcal{S},s} = \left(\tilde{\mathbf{H}}^T\tilde{\mathbf{H}} + \epsilon\mathbf{I}_{N_a}\right)^{-1}\tilde{\mathbf{H}}^T\mathbf{v}_{\mathcal{S},s}, \tag{4.21}$$

where $\mathbf{I}_{N_a} \in R^{N_a\times N_a}$ denotes the unit diagonal matrix. Notice that the transmit power vector given in (4.21), not only achieves the optimal received signal at each legitimate user, but it also ensures zero inter-user interference as it is evident in (4.20). Also notice that for $K = 1$, the general channel matrix $\tilde{\mathbf{H}}$ is reduced to $\tilde{\mathbf{H}}_1$ and $\mathbf{v}_{\mathcal{S},s}$ to $\mathbf{v}_1$ by (4.18). In this case, the optimal transmit power vector in (4.21) ensures the received signals to be (4.20) for $K = 1$, which is identical to the solution proposed in (13) of [68]. Therefore, the proposed MU-GSSK-SCD in this chapter is the generalization of the single user GSSK-SCD strategy proposed in [68].

4.3.1. Transmit Power Normalization

In this section, we design the DC bias level, B_{DC}, and the power normalization coefficient, ρ. The driving current of the LEDs must stay below a certain threshold to prevent overheating and reduction in electro-optical efficiency, as reported in [133]. Also, LEDs are expected to support communication while maintaining a constant illumination level, [134]. Therefore, the driving current must always be in $[I_{\min}, I_{\max}]$, so that both constraints are satisfied.

To ensure that, the elements in the transmit power vector, $\tilde{\mathbf{q}}_{\mathcal{S},s}$, are constrained such that

$$I_{\min} < \tilde{q}_{\mathcal{S},s}^{(\ell)} < I_{\max}, \quad \ell = 1, \ldots, N_a. \tag{4.22}$$

For the jointly optimal $\mathcal{V}_k$'s for $k = 1, 2, \cdots, K$, it follows from (4.21) that $E\{\tilde{\mathbf{q}}_{\mathcal{S},s}\} = 0$. Hence, we set $B_{\mathrm{DC}} = (I_{\min} + I_{\max})/2$. It is worth to note that, off-the-shelf white LEDs usually work below $I_{\max} = 100$ mA in average, [133]. If, for example, the preferred illumination level in the communication environment requires $B_{\mathrm{DC}} = 75$ mA, then $I_{\min}$ is set to 50 mA. The power normalization coefficient is calculated by $\rho = (I_{\max} - I_{\min})/\max\{||\tilde{\mathbf{q}}_{\mathcal{S},s}||\}$, where $\max\{||\tilde{\mathbf{q}}_{\mathcal{S},s}||\}$ is the maximum value, the norm of the transmit power vector can take for any symbol i_k. An upper bound for this term is found by

$$\begin{aligned} \max\{||\tilde{\mathbf{q}}_{\mathcal{S},s}||\} &= \max\left\{\left|\left|\left(\tilde{\mathbf{H}}^T\tilde{\mathbf{H}}\right)^{-1}\tilde{\mathbf{H}}^T\mathbf{v}_{\mathcal{S},s}\right|\right|\right\} \\ &\prec \max\left\{\left|\left|\left(\tilde{\mathbf{H}}^T\tilde{\mathbf{H}}\right)^{-1}\tilde{\mathbf{H}}^T\right|\right|\right\}\max\{||\mathbf{v}_{\mathcal{S},s}||\}. \end{aligned} \tag{4.23}$$

Consequently, the received signal at the kth legitimate user can be completely expressed as

$$\mathbf{y}_k = \mathbf{s}_k + \mathbf{n}_k, \tag{4.24}$$

where $\mathbf{s}_k$ is the observed transmitted signal by the kth user and given by

$$\mathbf{s}_k = \rho\tilde{\mathbf{H}}_k\left(\tilde{\mathbf{H}}^T\tilde{\mathbf{H}} + \epsilon\mathbf{I}_{N_a}\right)^{-1}\tilde{\mathbf{H}}^T\mathbf{v}_{\mathcal{S},s} + B_{\mathrm{DC}}\tilde{\mathbf{H}}_k = \rho\mathbf{v}_{k,i_k} + B_{\mathrm{DC}}\tilde{\mathbf{H}}_k, \tag{4.25}$$

from which the DC bias part can be extracted with receiver's knowledge of its own channel. The transmitted signal is received by the eavesdropper as

$$\mathbf{y}_e = \rho\mathbf{H}_e\mathbf{q}_{\mathcal{S},s} + \mathbf{n}_e = \rho\mathbf{H}_e\left(\tilde{\mathbf{H}}^T\tilde{\mathbf{H}} + \epsilon\mathbf{I}_{N_a}\right)^{-1}\tilde{\mathbf{H}}^T\mathbf{v}_{\mathcal{S},s} + \mathbf{n}_e. \tag{4.26}$$

Hence, $\mathbf{v}_{k,i_k}$ cannot be perfectly recovered at Eve for any k. The received signal $\mathbf{y}_e$ can also be expressed as

$$\mathbf{y}_e = \mathbf{s}_k + \mathbf{J}_k + \mathbf{n}_e, \tag{4.27}$$

where $\mathbf{J}_k$ is the jamming signal at Eve, wiretapping User k. The jamming signal $\mathbf{J}_k$ is found by

$$\mathbf{J}_k = \rho \left(\mathbf{H}_e - \mathbf{H}_k \right) \mathbf{q}_{\mathcal{S},s}. \tag{4.28}$$

At the legitimate users and the eavesdropper, the GSSK signal is decoded by maximum likelihood (ML) detection, which is performed according to

$$\hat{\mathbf{v}}_k = \arg \min_{\mathbf{v}_{k,i_k}} \left\{ ||\mathbf{y}_k - \rho \mathbf{v}_{k,i_k}|| \right\}, \tag{4.29}$$

$$\hat{\mathbf{v}}_{e,k} = \arg \min_{\mathbf{v}_{k,i_k}} \left\{ ||\mathbf{y}_e - \rho \mathbf{v}_{k,i_k}|| \right\}, \tag{4.30}$$

where $\hat{\mathbf{v}}_k$ and $\hat{\mathbf{v}}_{e,k}$ are the detected symbols at User k and the eavesdropper that wiretaps User k.

4.4. Secrecy Rate Region of MU-GSSK-VLC System

The secrecy capacity of the kth user for the proposed system in (4.24) and (4.27) is given in [135] and defined by

$$\mathbb{C}_{\text{GSSK}}^{(k)} = \mathbb{I}(\mathbf{s}_k; \mathbf{y}_k) - \mathbb{I}(\mathbf{s}_k; \mathbf{y}_e) = \mathbb{H}(\mathbf{y}_k) - \mathbb{H}(\mathbf{y}_k|\mathbf{s}_k) - \left(\mathbb{H}(\mathbf{y}_e) - \mathbb{H}(\mathbf{y}_e|\mathbf{s}_k) \right), \tag{4.31}$$

where $\mathbb{H}(\cdot)$ and $\mathbb{H}(\cdot|\cdot)$ stand for the entropy and conditional entropy, respectively. The mutual information is represented by $\mathbb{I}(\cdot;\cdot)$.

Following (4.24), $\mathbb{H}(\mathbf{y}_k|\mathbf{s}_k)$ is found to be Gaussian entropy with

$$\mathbb{H}(\mathbf{y}_k|\mathbf{s}_k) = \frac{N_r}{2}\log_2(2\pi e\sigma_k^2). \tag{4.32}$$

The jamming vector in (4.28) can be approximated as a zero mean Gaussian random vector with the covariance matrix $\mathbb{C}_{\mathbf{J}_k}$. Then, the total noise in Eve's received signal, (4.27) becomes another zero mean Gaussian random vector, $\mathbf{w}_k = \mathbf{J}_k + \mathbf{n}_e$, with the covariance matrix

$$\mathbb{C}_{\mathbf{w}_k} = \mathbb{C}_{\mathbf{J}_k} + \sigma_e^2\mathbf{I}_{N_r}. \tag{4.33}$$

Therefore,

$$\mathbb{H}(\mathbf{y}_e|\mathbf{s}_k) = \frac{1}{2}\log_2(2\pi e|\mathbb{C}_{\mathbf{w}_k}|). \tag{4.34}$$

Then the secrecy capacity in (4.31) becomes

$$\mathbb{C}_{\text{GSSK}}^{(k)} = \frac{N_r}{2}\log_2\left(\frac{|\mathbb{C}_{\mathbf{w}_k}|^{1/N_r}}{\sigma_k^2}\right) - \left(\mathbb{H}(\mathbf{y}_e) - \mathbb{H}(\mathbf{y}_k)\right). \tag{4.35}$$

Since the received signal $\mathbf{y}_k$ is a mixture of M Gaussian random vectors, its entropy can be upper bounded by

$$\mathbb{H}(\mathbf{y}_k) \leq \log_2(M) + \frac{N_r}{2}\log_2\left(2\pi e\sigma_k^2\right) = \frac{N_r}{2}\log_2\left(2\pi e\sigma_k^2 M^{2/N_r}\right). \tag{4.36}$$

A lower bound for $\mathbb{H}(\mathbf{y}_e)$ can be found by applying the entropy power inequality (EPI) to $\mathbf{y}_e = \mathbf{y}_k + \hat{\mathbf{n}}_k$, where $\hat{\mathbf{n}}_k = \mathbf{w}_k - \mathbf{n}_k$ is the significant noise term in Eve's received signal.

Then by EPI, [136], we have

$$\begin{aligned}\mathbb{H}(\mathbf{y}_e) = \mathbb{H}(\mathbf{y}_k + \hat{\mathbf{n}}_k) &\geq \frac{N_r}{2}\log_2\left(2^{(2/N_r)}\mathbb{H}(\hat{\mathbf{n}}_k) + 2^{(2/N_r)}\mathbb{H}(\mathbf{y}_k)\right) \\ &= \frac{N_r}{2}\log_2\left(2\pi e|\mathbb{C}_{\hat{\mathbf{n}}_k}|^{(1/N_r)} + 2^{(2/N_r)}\mathbb{H}(\mathbf{y}_k)\right),\end{aligned} \tag{4.37}$$

where $\mathbb{C}_{\hat{\mathbf{n}}_k} = \mathbb{C}_{\mathbf{w}_k} - \sigma_k^2\mathbf{I}_{N_r}$ is the covariance matrix of $\hat{\mathbf{n}}_k$. Now, applying (4.36) and (4.37) to (4.35), we get

$$\mathbb{C}_{\text{GSSK}}^{(k)} \leq \frac{N_r}{2}\log_2\left(\frac{|\mathbb{C}_{\mathbf{w}_k}|^{(1/N_r)}M^{(2/N_r)}}{\sigma_k^2 M^{(2/N_r)} + |\mathbb{C}_{\mathbf{n}_k}|^{(1/N_r)}}\right). \tag{4.38}$$

The achievable secrecy rate region is defined by all User secrecy rates, $\left(R^{(1)}, \ldots, R^{(K)}\right)$ as reported in [137], which jointly satisfy

$$\sum_{k=1}^{K} 2^{R^{(k)}} \leq \sum_{k=1}^{K} 2^{\mathbb{C}_{\text{GSSK}}^{(k)}}, \tag{4.39}$$

where $\mathbb{C}_{\text{GSSK}}^{(k)}$ obeys (4.38) for $k = 1, 2, \ldots, K$. In the following, the BER and PLS performances of MU-GSSK-SCD is presented under various user configurations.

4.5. Simulation Results

In this section, we present the communication performances of the legitimate users and the eavesdropper under different VLC scenarios. We assume that the communication takes place in a 6 m ×6 m ×3 m indoor environment, where $N_t = 8$ LEDs are located on the ceiling. The LEDs are located at

$$\text{LED}_{\text{loc}}(x, y) = \begin{bmatrix} -2.25, & -0.75, & 0.75, & 2.25, & -2.25, & -0.75, & 0.75, & 2.25 \\ 1.5, & 1.5, & 1.5, & 1.5, & -1.5, & -1.5, & -1.5, & -1.5 \end{bmatrix}^T \text{m}. \tag{4.40}$$

The location vectors of the LEDs and the users are given in meters and their units will be dropped from this point on.

The locations of the legitimate users and the eavesdropper differ for each scenario and are indicated in the rest of this section. The LoS channel coefficients are obtained by (4.1) as a function of the parameters

$$\Phi_{1/2} = 60^\circ, \quad \Psi_{1/2} = 70^\circ, \quad A_{\text{PD}} = 1 \text{ cm}^2. \tag{4.41}$$

The other channel parameters, $\beta, d_k^{r,t}, \phi_k^{r,t}, \theta_k^{r,t}$, are obtained from the locations of the LEDs, users and the eavesdropper. Also, the emission power is assumed to be 1 W per LED.

For simulation purposes, we activate $N_a = 4$ LEDs per channel use. The reception at $K = 2$ legitimate users and the eavesdropper is performed by $N_r = 2$ PDs. The total number of bits sent per channel use is $N_B = 6$ by (4.4). N_B is divided evenly among the legitimate users, hence $M = 2^{N_B/2} = 8$ for both users. Thus, $\mathcal{C}_1$ and $\mathcal{C}_2$ have the cardinality of $M = 8$ and consist of the bit vectors of length $N_B/2 = 3$. The joint symbol alphabet is the Cartesian product of $\mathcal{C}_1$ and $\mathcal{C}_2$, therefore $\mathcal{C}_\mathcal{S}$ consists of $M^2 = 64$ bit vectors of length $N_B = 6$. Since $N_r = 2$ and $M = 8$, $\mathcal{V}_1$ and $\mathcal{V}_2$ are chosen to be 8−QAM symbol constellations. For each channel use, random bit vectors $\mathbf{b}_{1,i_1}$ and $\mathbf{b}_{2,i_2}$ are chosen from $\mathcal{C}_1$ and $\mathcal{C}_2$ respectively and their corresponding joint bit vector $\mathbf{b}_{\mathcal{S},s}$ is found from $\mathcal{C}_\mathcal{S}$. Then, $\tilde{\mathbf{q}}_{\mathcal{S},s}$ is calculated according to (4.21) for a signal amplitude ρ and the received signal $\mathbf{v}_{\mathcal{S},s}$, which is mapped to $\mathbf{b}_{\mathcal{S},s}$. Finally, the GSSK signal is received by all users according to (4.12).

4.5.1. BER Performance of MU-GSSK-SCD with Perfect CSI

In the first scenario presented in Figure 4.2, the legitimate users are located at opposing corners of the room, precisely at $[-2, 2, 0.85]$ and $[2, -2, 0.85]$. For this scenario, the eavesdropper is located in three different locations: *a*) closer to User 1, *b*) in the middle of the users, *c*) closer to User 2. The corresponding BER curves are obtained and presented in Figures 4.5 - 4.7, in the given order. In all BER graphs, four curves are generated: two of them represent the BERs of User 1 and User 2.

Eve's performance is exhibited in two distinct cases, where it wiretaps User 1 and User 2 respectively, hence two BER curves are obtained for Eve. The simulation results indicate that the eavesdropper suffers from high BERs, which are around the 0.5 level, regardless of the user Eve is wiretapping. Another observation is that the impact of Eve's location on its BER is not significant.

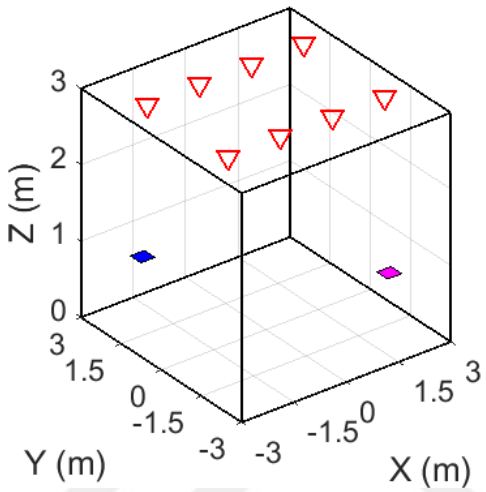

Figure 4.2. Scenario 1 for the evaluated MIMO-VLC system. User 1 and 2 are represented with blue and magenta squares, respectively.

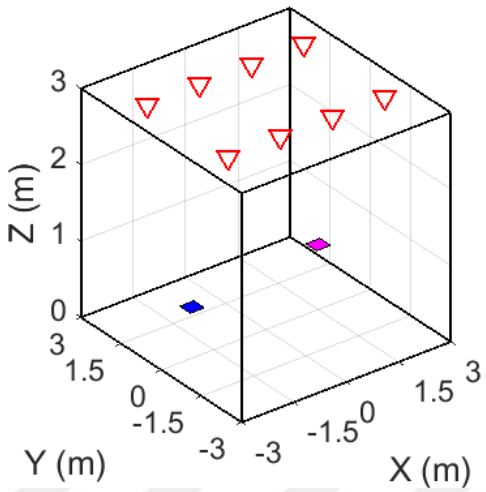

Figure 4.3. Scenario 2 for the evaluated MIMO-VLC system. User 1 and 2 are represented with blue and magenta squares, respectively.

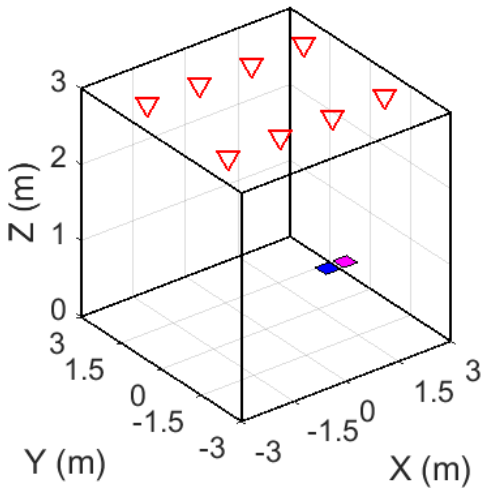

Figure 4.4. Scenario 3 for the evaluated MIMO-VLC system. User 1 and 2 are represented with blue and magenta squares, respectively.

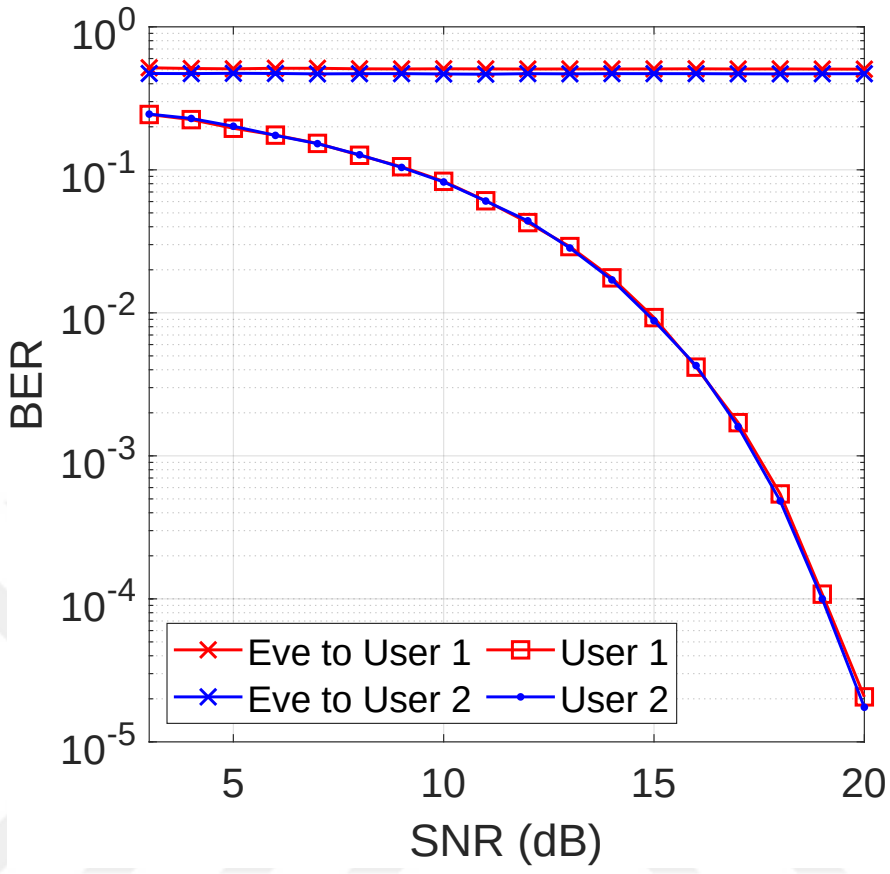

Figure 4.5. BER vs. SNR for Scenario 1. Eve is located at [-1, 1, 0.85].

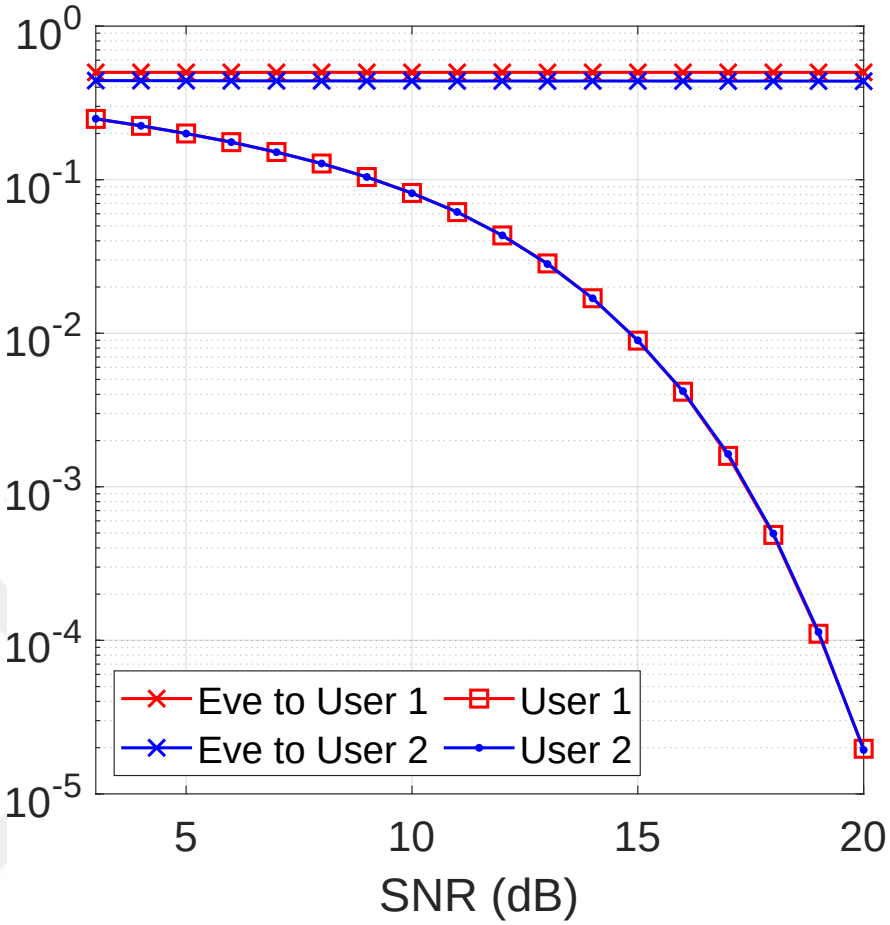

Figure 4.6. BER vs. SNR for Scenario 1. Eve is located at [0, 0, 0.85].

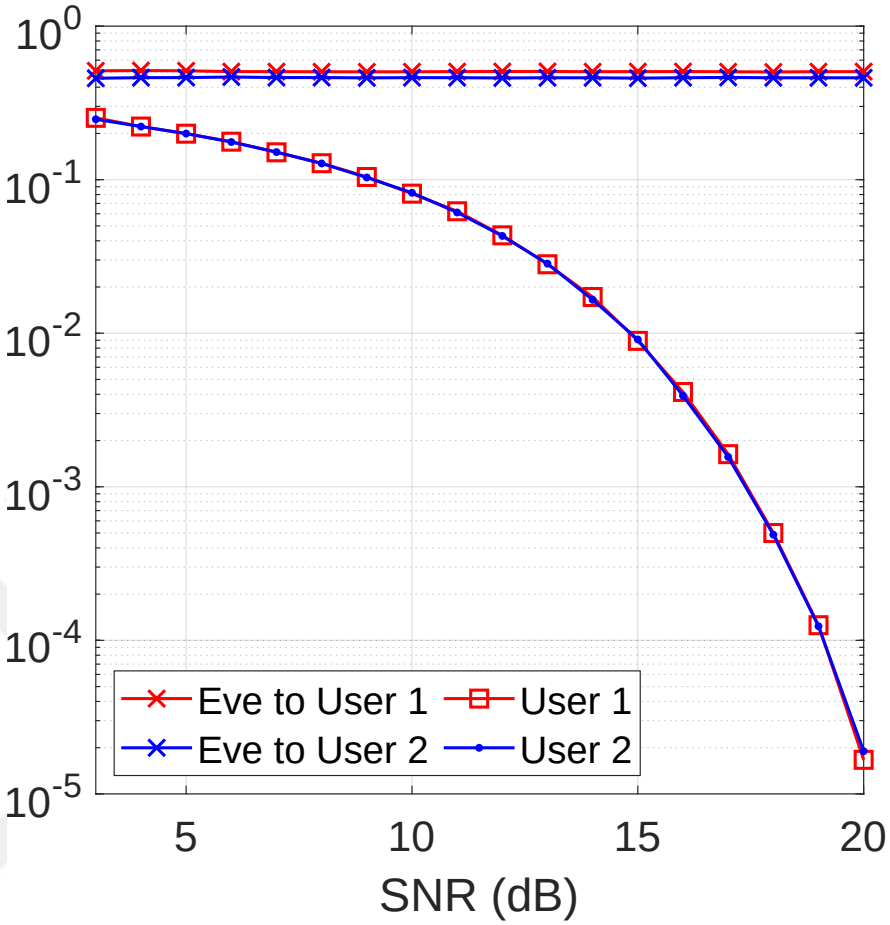

Figure 4.7. BER vs. SNR for Scenario 1. Eve is located at [1, -1, 0.85].

The BER performances under Scenario 2 and Scenario 3 are presented in Figures 4.8 - 4.13 for various locations of Eve. In Scenario 2, the legitimate users are placed parallel to the $x-$axis, whereas in Scenario 3, they are deliberately chosen very close to each other. The simulation results show that, for all featured user configurations, the BER performance of the MU-GSSK-SCD is almost identical. The results suggest that the proposed solution provides significantly lower BERs to legitimate users than to the eavesdropper regardless of legitimate users' and Eve's locations. Meanwhile, Eve's BER performance is greatly reduced by our design.

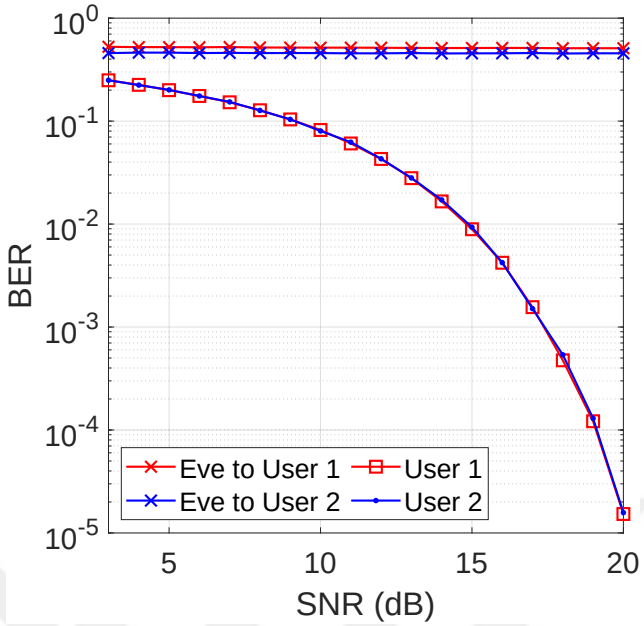

Figure 4.8. BER vs. SNR for Scenario 2. Eve is located at [-1.5, -0.375, 0.85].

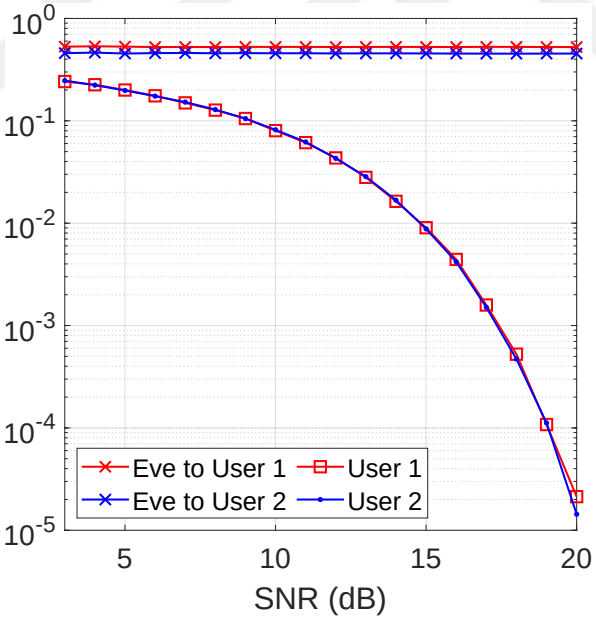

Figure 4.9. BER vs. SNR for Scenario 2. Eve is located at [-0.5, -0.25, 0.85].

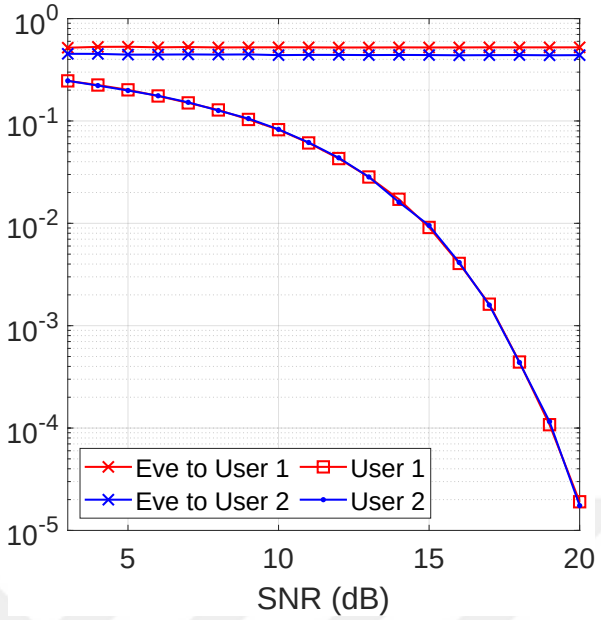

Figure 4.10. BER vs. SNR for Scenario 2. Eve is located at [0.5, -0.125, 0.85].

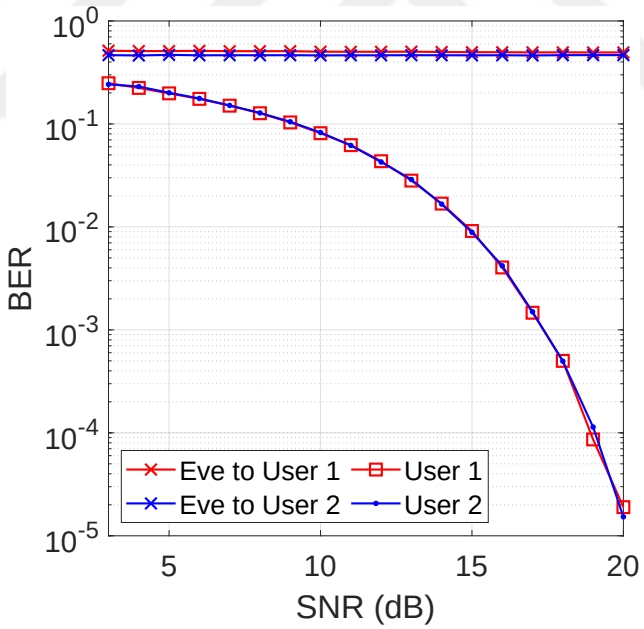

Figure 4.11. BER vs. SNR for Scenario 3. Eve is located at [1.125, -1, 0.85].

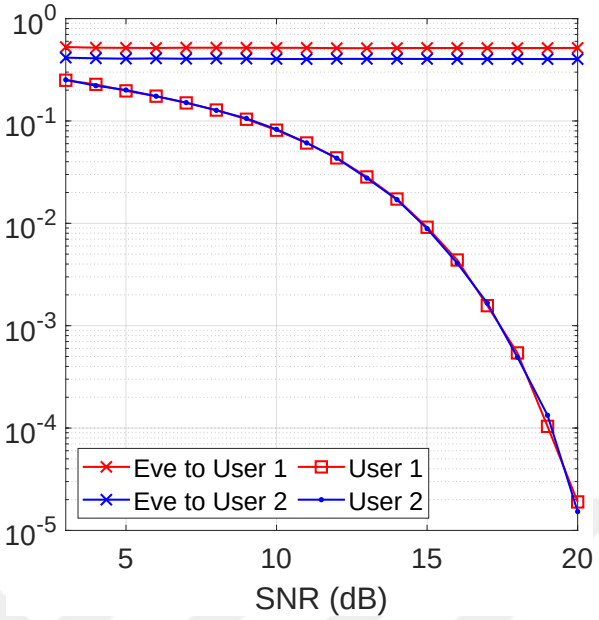

Figure 4.12. BER vs. SNR for Scenario 3. Eve is located at [1.25, -1, 0.85].

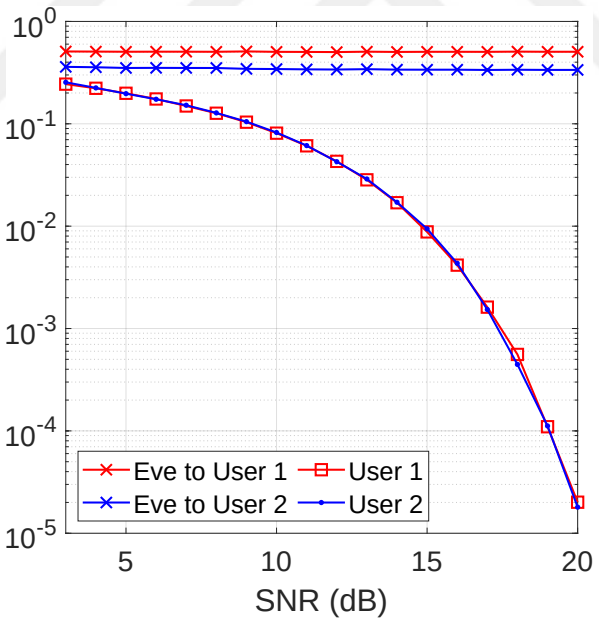

Figure 4.13. BER vs. SNR for Scenario 3. Eve is located at [1.375, -1, 0.85].

4.5.2. Practical System Design Considerations

To demonstrate insight into the system design, in the following, we vary several parameters such as the number of transmitting and receiving antennas, the user, and eavesdropper configurations within the indoor environment to investigate how secrecy capacity, as well as BER, affect the system design.

First, in Figure 4.14, we present the secrecy rate regions obtained by MU-GSSK-SCD with varying number of PDs ($N_r \in \{1, 2, 4\}$) at the users and Eve. In this case, $N_t = 16$ and $N_a = 8$ are assumed, and 6 bits are transmitted to each user at every signaling interval. It is observed that when the users are equipped with a single PD, the maximum secrecy rate barely exceeds 3 bpcu per user, even at 27 dB SNR, which is considered to be a high SNR value. By installing an extra PD to each user ($N_r = 2$), it is possible to increase the maximum secrecy rate very close to the upper bound, which is 6 bpcu, even at low SNR values, such as 0 dB. Furthermore, it is shown that when the users communicate with 4 PDs, the secrecy rate region reaches the 6 bpcu upper bound at 0 dB SNR. These results indicate that the number of PDs at the receiver circuits play a significant role in terms of PLS.

Secondly, we investigate the effect and dependence of different user's configuration as well as Eve's location on the BER performance obtained by Eve. To illustrate this, the simulation results in Figures 4.15-4.18 are obtained, where the BER of Eve is measured by Monte Carlo simulations as it moves within the indoor environment. Figures 4.15 and 4.16 represent the BER performance of Eve, listening to User 1 and User 2 respectively. Note that, in these figures, both users are denoted by red squares, and located relatively far from each other. The BER level of Eve is denoted by color, and the BER-to-color mapping is shown next to the plots. It is observed that Eve's BER is greater than or equal to 0.3 on almost every point in the environment, however, it improves to the 0.1 level as Eve gets closer to the user she is listening to.

When the users are located close to each other, refer to Figures 4.17 and 4.18, it is observed that the BER performance of Eve is around 0.5 levels in a very wide region of the environment. Additionally, in this case, Eve obtains reduced BERs in a much smaller region, compared to the former case. These results indicate that the proposed MU-GSSK-SCD strategy ensures poor BER performance for Eve almost everywhere, especially when the users are closely located to each other.

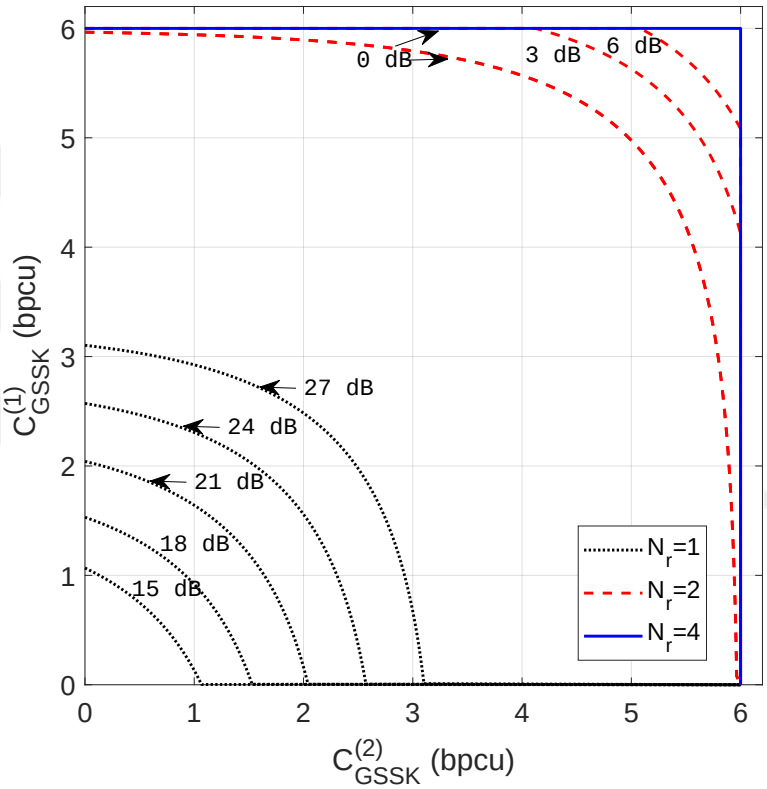

Figure 4.14. Secrecy rate regions obtained by MU-GSSK-SCD with $N_t = 16$, $N_a = 8$ and varying N_r.

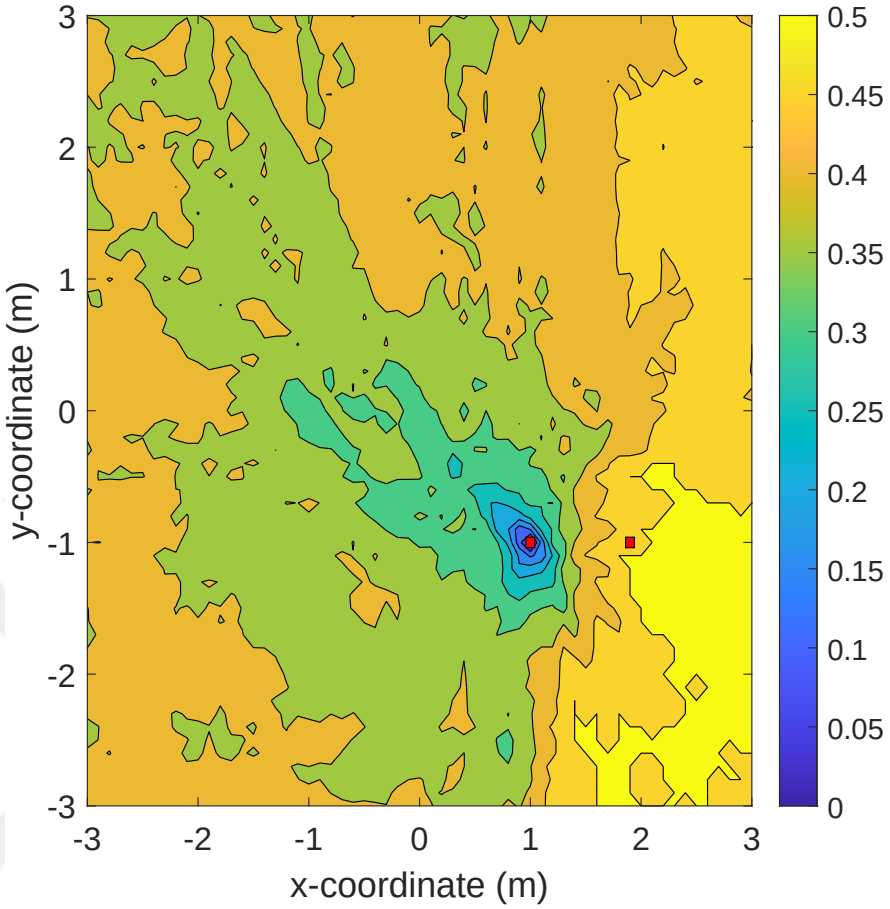

Figure 4.15. BER performance of Eve as Eve moves within the indoor environment, and intercepts User 1's communication. User 1 is located at [1, -1], and User 2 is located at [1.9, -1]. All units are in meters.

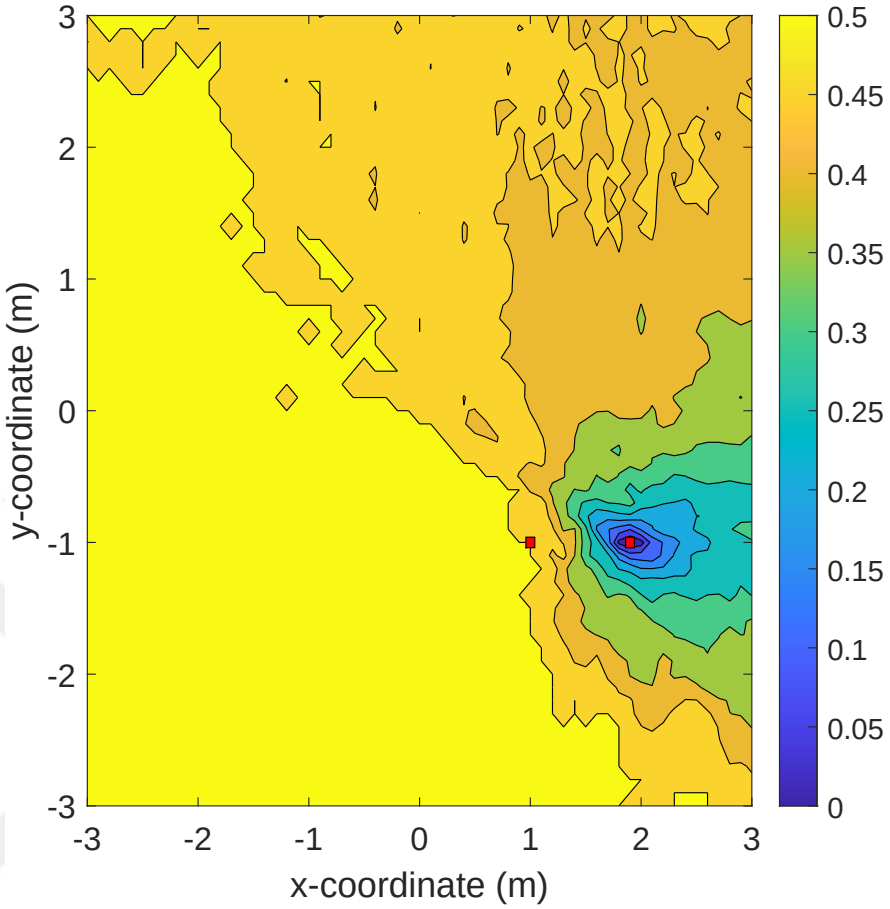

Figure 4.16. BER performance of Eve as Eve moves within the indoor environment, and intercepts User 2's communication. User 1 is located at $[1, \quad -1]$, and User 2 is located at $[1.9, \quad -1]$. All units are in meters.

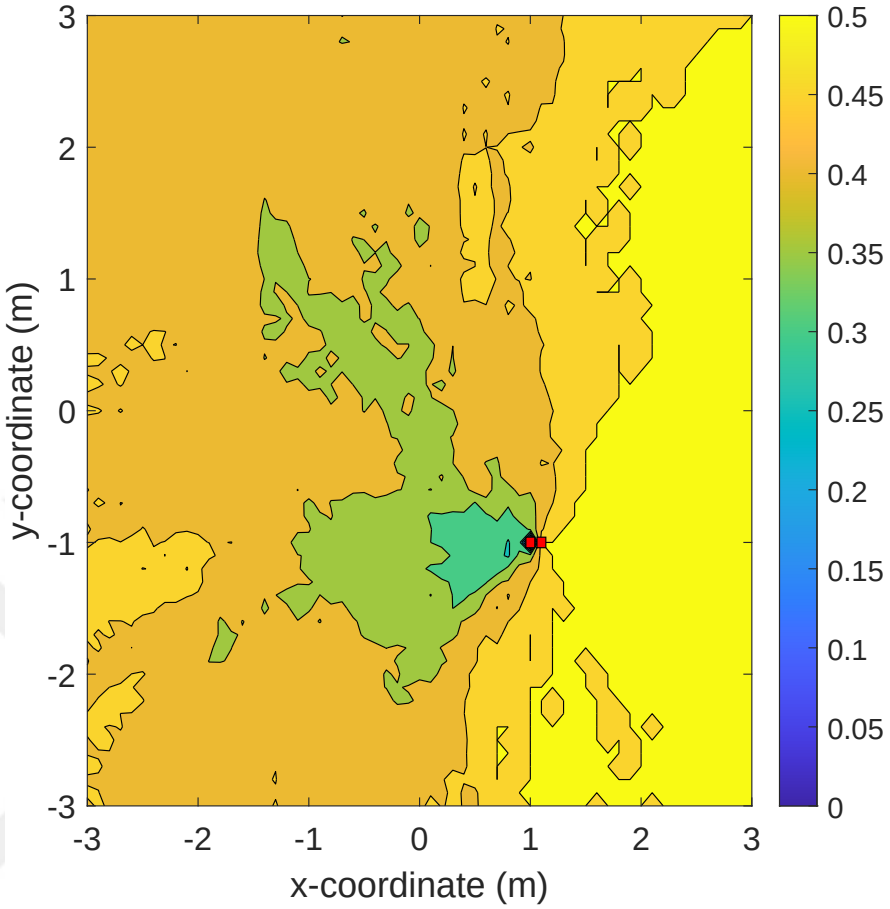

Figure 4.17. BER performance of Eve as Eve moves within the indoor environment, and intercepts User 1's communication. User 1 is located at [1, -1], and User 2 is located at [1.1, -1]. All units are in meters.

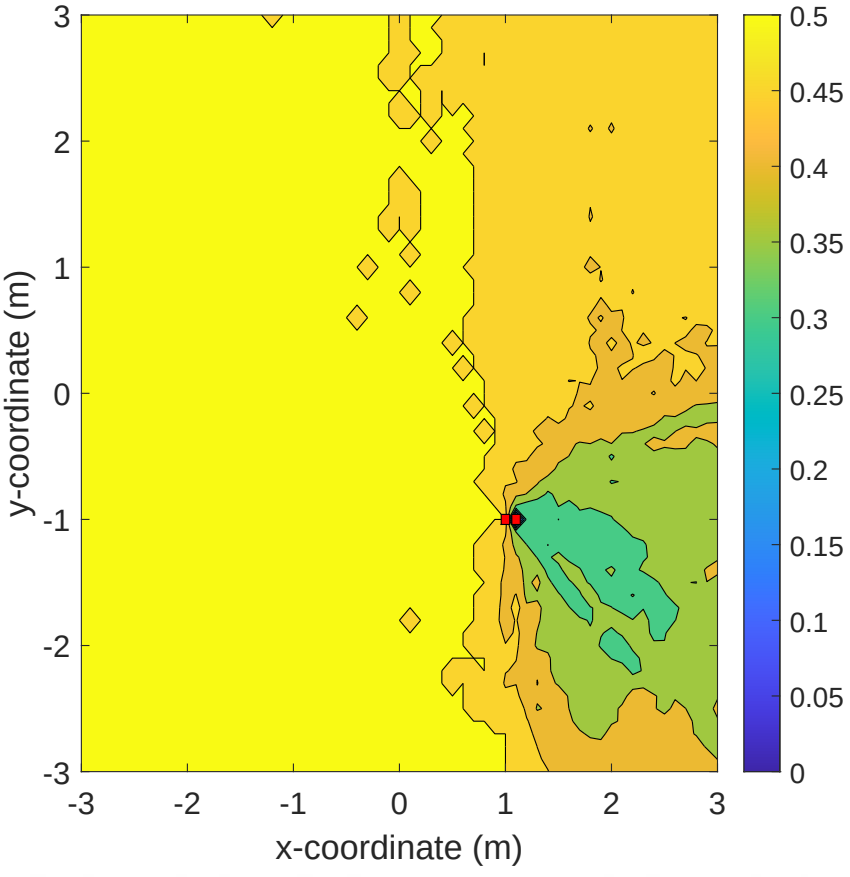

Figure 4.18. BER performance of Eve as Eve moves within the indoor environment, and intercepts User 2's communication. User 1 is located at [1, -1], and User 2 is located at [1.1, -1]. All units are in meters.

4.5.3. BER Performance of MU-GSSK-SCD with Imperfect CSI

In the previous subsection, it is shown that MU-GSSK-SCD provides very good BER performance for the GSSK based VLC system when perfect CSI is available at all terminals. However, since the CSI may not always be fully known in real applications, it is very important to analyze the sensitivity of the proposed security solution to channel estimation errors. Following (4.14) with the optimum LED power vector in (4.21), the received signals by the legitimate users can be expressed as

$$\mathbf{y}_k = \rho \mathbf{G} \mathbf{v}_{k,i_k} + \mathbf{n}_k, \quad k = 1, 2, \ldots, K, \tag{4.42}$$

where $\mathbf{G} \in \mathcal{R}^{KN_r \times KN_r}$ is defined as $\mathbf{G} = \tilde{\mathbf{H}} \left(\tilde{\mathbf{H}}^T \tilde{\mathbf{H}} \right)^{-1} \tilde{\mathbf{H}}^T$. As explained in Section 4.3.1, the parameter ρ is related with the channel coefficients in a nonlinear fashion and requires the knowledge of CSI perfectly both at the receivers and the transmitter. Also, under the perfect CSI at the transmitter, it is shown in Section 4.3 that $\mathbf{G}$ is a unit diagonal matrix. We now show that even if the CSI is not perfectly known at receiver, the optimal data detection is not affected by this imperfection.

Assume that the channel coefficient matrix $\mathbf{H}$ is known at the receiver with an error $\mathbf{E}$. Then, the estimated channel matrix $\widehat{\mathbf{H}}$ can be expressed in terms of the error-free channel matrix $\mathbf{H}$ as

$$\mathbf{H} = \widehat{\mathbf{H}} + \mathbf{E}.$$

Substituting this into the expression of $\mathbf{G}$ above, we have

$$\widehat{\mathbf{G}} = (\widehat{\mathbf{H}} + \mathbf{E}) \left((\widehat{\mathbf{H}} + \mathbf{E})^T (\widehat{\mathbf{H}} + \mathbf{E}) \right)^{-1} (\widehat{\mathbf{H}} + \mathbf{E})^T = \mathbf{I}_{2N_r}. \tag{4.43}$$

Consequently, the transmitted signal $\mathbf{v}_{\mathbf{k},\mathbf{i_k}}$ can be recovered optimally by the ML detection using the received signal $\mathbf{y}_k = \rho \mathbf{v}_{k,i} + \mathbf{n}_k$.

However, true value of ρ is not known at the kth user, hence needs to be estimated as accurate as possible from the received signal $\mathbf{y}_k$, by means of some pilot GSSK symbols prior to data detection at receiver. In the following, we explain the estimation of ρ based on the ML criterion.

4.5.3.1. ML Estimation of ρ. The power normalization coefficient ρ can be estimated at the kth user by transmitting pilot symbols $\mathbf{s}_p = [\mathbf{s}_{p,1}^T, \mathbf{s}_{p,2}^T, \ldots, \mathbf{s}_{p,K}^T]^T$, which are chosen from the joint symbol alphabet $\mathcal{C}_{\mathcal{S}}$. For independent and identically distributed pilot symbols, the likelihood function for ρ is defined as

$$\hat{\ell}(\rho; \mathbf{y}_k) = \frac{1}{N_p} \sum_{\ell=1}^{N_p} \ln f(\mathbf{y}_{k,\ell}|\rho), \tag{4.44}$$

where $\mathbf{y}_{k,\ell}$ is the ℓth received pilot symbol at the kth user. The conditional probability density function (pdf) of $\mathbf{y}_k$ given ρ, $f(\mathbf{y}_{\mathbf{k},\ell}|\rho)$, is found for the ℓth pilot symbol $\mathbf{s}_{p,\ell}$ using the observation equation in (4.20) as

$$\ln f(\mathbf{y}_{k,\ell}|\rho) = \ln \left(\frac{(2\pi)^{N_r/2}}{|\mathbb{C}_{\mathbf{n}_k}|^{1/2}} \right) - \frac{||\mathbf{y}_{k,\ell} - \rho \mathbf{s}_p||^2}{2},$$

for $\ell = 1, 2, \cdots, N_p$. Maximizing (4.44) with respect to ρ, the ML estimate of ρ is found as

$$\widehat{\rho} = \arg\max_{\rho} \{\hat{\ell}(\rho; \mathbf{y}_k)\} = \frac{1}{N_p} \sum_{\ell=1}^{N_p} \frac{\mathbf{y}_{k,\ell}^T \mathbf{s}_{p,\ell}}{\mathbf{s}_{p,\ell}^T \mathbf{s}_{p,\ell}}. \tag{4.45}$$

The estimation accuracy can be measured in terms of the root mean square of the error $\rho - \hat{\rho}$, which is defined by

$$\text{RMSE}(\hat{\rho}) = \frac{1}{N_p} \sum_{\ell=1}^{N_p} ||\rho - \hat{\rho}||^2. \tag{4.46}$$

Next, the MU-GSSK-SCD system is simulated with imperfect CSI, when there are 2 users, located according to the Scenario 1 from Figure 4.2.

For each SNR point, $N_p = 1000$ pilot symbols are broadcasted to users, which then estimate the power normalization coefficient as found in (4.45). The obtained RMSE values for $\hat{\rho}$ are normalized and presented in Figure 4.19. It is observed that the ML estimation resulted in an RMSE of 0.95ρ for 3 dB SNR. The RMSE is reduced exponentially down to 0.12ρ at 20 dB SNR. The BER performance of the proposed system with the estimated ρ values is presented in Figure 4.20. In this figure, the dashed curves represent the case where the users have full CSI, therefore ρ can be perfectly calculated at the users and RMSE becomes zero. It is observed that due to the estimation errors at the users, there is a loss of 2 to 3 dB SNR. However, the BER is obtained around 10^{-3} level at the high SNR band, which is an acceptable range for indoor VLC applications. Thus, the proposed MU-GSSK-SCD system provides excellent BER performance with negligible sensitivity to receiver CSI.

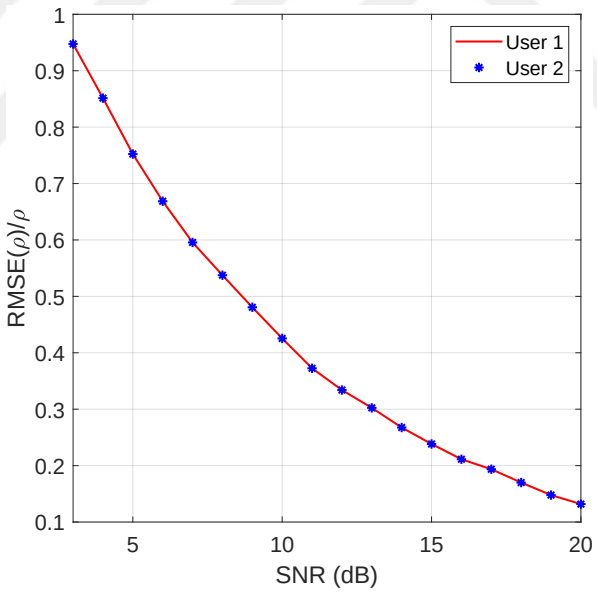

Figure 4.19. Root mean square of the estimation error $||\rho - \hat{\rho}||$ for Scenario 1 with the imperfect CSI at the users.

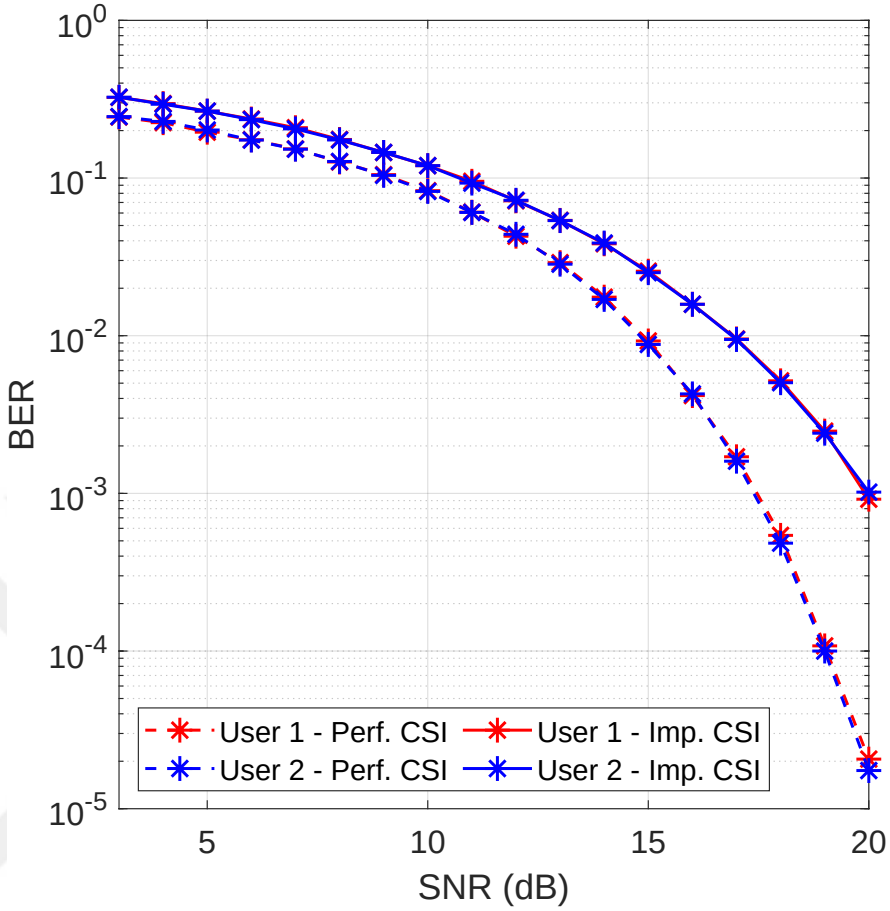

Figure 4.20. BER vs. SNR plots for Scenario 1 with the imperfect CSI at the users.

4.5.4. Comparison of Results with Existing Ones

Regarding comparing the results with existing ones, we considered the most appropriate ones in the existing literature, which are based on PLS techniques aided by friendly jamming with a DC-biased 8-level pulse amplitude modulation (8-PAM) scheme transmitted via single LED. At the receiver, the DC-bias is removed and data is recovered by the classical ML detection. The jammer was equipped with multiple LEDs without access to the transmitted information. Assuming that accurate CSI of the eavesdropper is known by the source, an optimal jamming beamformer was designed that degrades the eavesdropper's reception of the secured information sent to the legitimate users. We set the transmit powers of each system to unity for a fair comparison. For the 8-PAM-PLS system based on generating a friendly jamming signal, we reduced the average power of the transmitted data in the amount of the power of the jamming signal to keep equal transmitted power for both PLS systems.

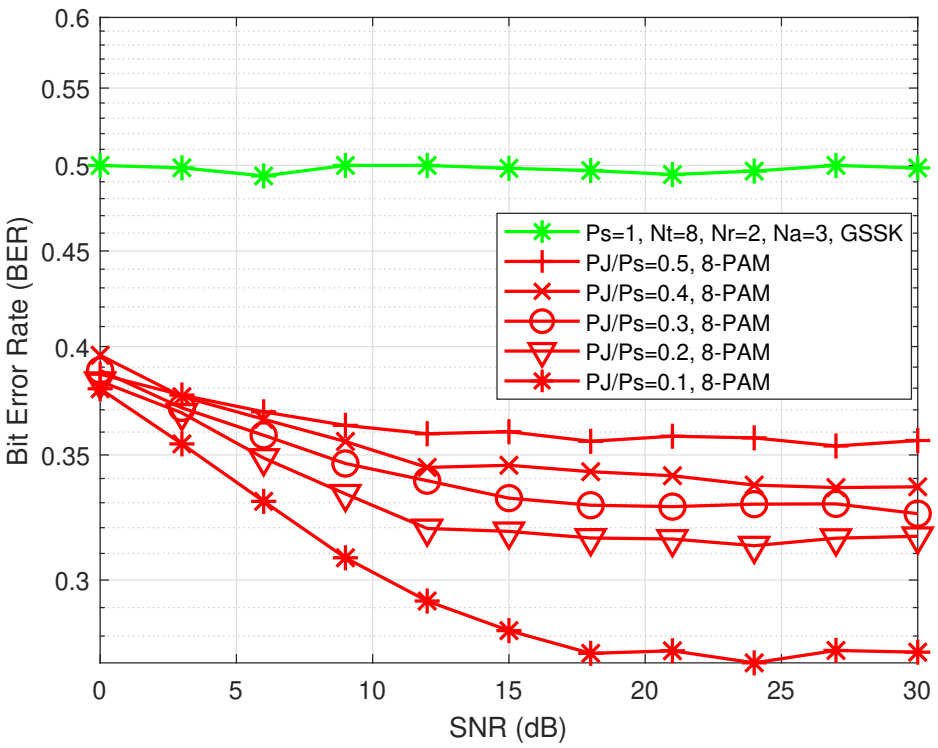

Figure 4.21. Eve's BER vs. SNR curves for 8-PAM and GSSK with 3 bits/sec/Hz per user.

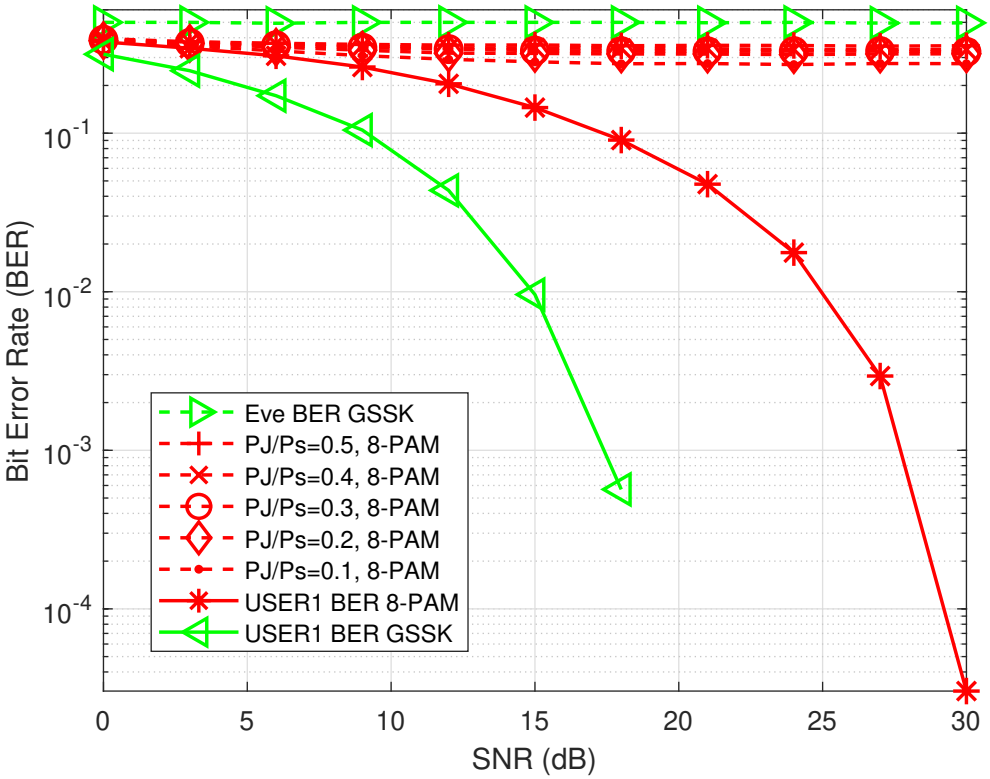

Figure 4.22. Bob's and Eve's BER vs. SNR curves for 8-PAM and GSSK with 3 bits/sec/Hz per user.

In Figure 4.21, we compare the BER performance of this technique, with the PLS-GSSK system having the same system parameters. Specifically, both VLC systems have $N_t = 8$ LEDs at the transmitter side designed with 3 bits/sec/Hz spectral efficiency each. We set the transmit powers of each system to unity for a fair comparison. Each BER curve of the PAM-PLS system in Figure 4.21 corresponds to the case where a certain percentage of the total transmit power is used for generating jamming signal, which is transmitted towards the eavesdropper. As can be seen from these curves, the BER performance of the PAM-PLS system is uniformly worse than that of the PLS-GSSK system. Figure 4.22 compares the BER performances of the legitimate users employing one of the PLS techniques mentioned above. The figure shows clear superiority of the proposed PLS scheme, since, for example, the obtained gain in SNR is more than 15 dB at a BER of 10^{-3}.

In addition to the degraded BER performances of the PAM-PLS systems, the assumption that the eavesdropper's CSI should be accurately known to the source is not a realistic one and hence, the performance curves provided in Figure 4.21 can only be an upper bound in the real applications.

4.5.5. Secrecy Performance

In this subsection, the secrecy rate regions defined in (4.38) and (4.39) are found for the proposed MU-GSSK-SCD strategy. First, both users are placed 30 cm apart at $[1, -1, 0.85]$ and $[1.3, -1, 0.85]$ and Eve is located in the middle of the two. The secrecy rate regions for this specific configuration is presented in Figure 4.23. It is observed that, around $0 - 3$ dB SNR, the secrecy rates of the users are around $2 - 2.5$ bpcu and increase approximately with 0.16 bpcu/dB in SNR. At around 6 dB SNR, the secrecy rate of both users get very close to 3 bpcu, which is the maximum for 8-QAM communication. In another configuration, the users are located at $[1, -1, 0.85]$ and $[1.9, -1, 0.85]$ and Eve is located closer to one of the users at $[1.15, -1, 0.85]$. The secrecy rate regions for this configuration are presented in Figure 4.24, which indicates that even at 0 dB SNR level, users can communicate with almost full secrecy. These results show that the PLS obtained with MU-GSSK-SCD improves as the users move away from each other. In Figure 4.25, the secrecy performance of MU-GSSK-SCD is presented for 0 dB SNR in the same user configuration from Figure 4.24, while Eve is moving straight away from User 1 to User 2. In this setting, the minimal separation of Eve to any user is $\min\{x, 90 - x\}$ cm, where x is the distance of Eve to User 1 as indicated in the legend. Note that, similar rate regions are obtained at identical minimal separations. It is observed that the achievable secrecy rate region enlarges as the minimal separation of Eve to any user increases. In fact, when the distance of Eve to any user is larger than 25 cm, the achievable secrecy rate region reaches its maximum size. These results indicate that PLS provided by MU-GSSK-SCD depends on Eve's location for a fixed user configuration. Also, MU-GSSK-SCD can provide maximal secrecy rates with 2 users positioned at a 90 cm separation from each other, hence PLS is ensured.

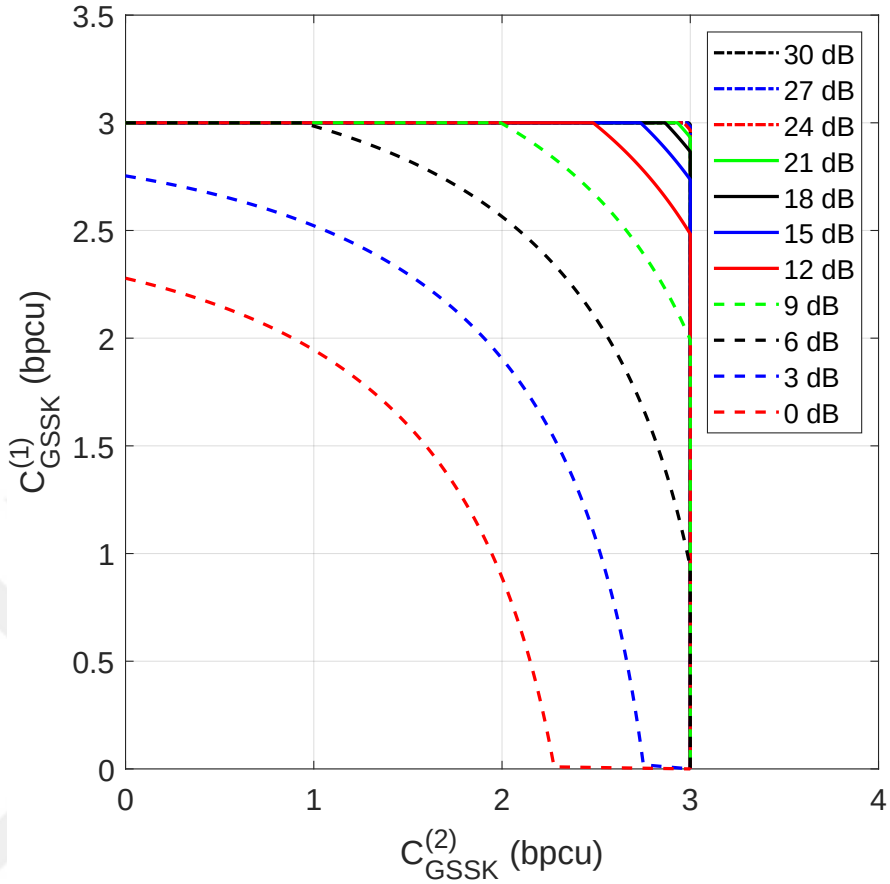

Figure 4.23. Secrecy rate regions when the users are 30 cms apart.

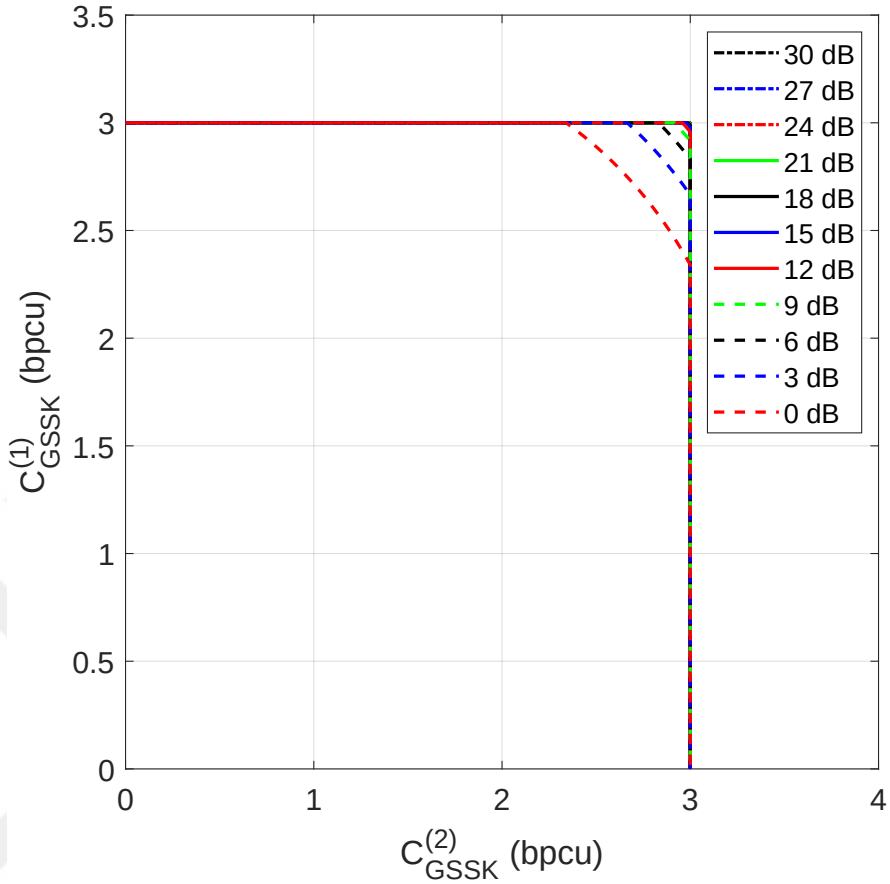

Figure 4.24. Secrecy rate regions when the users are 90 cms apart.

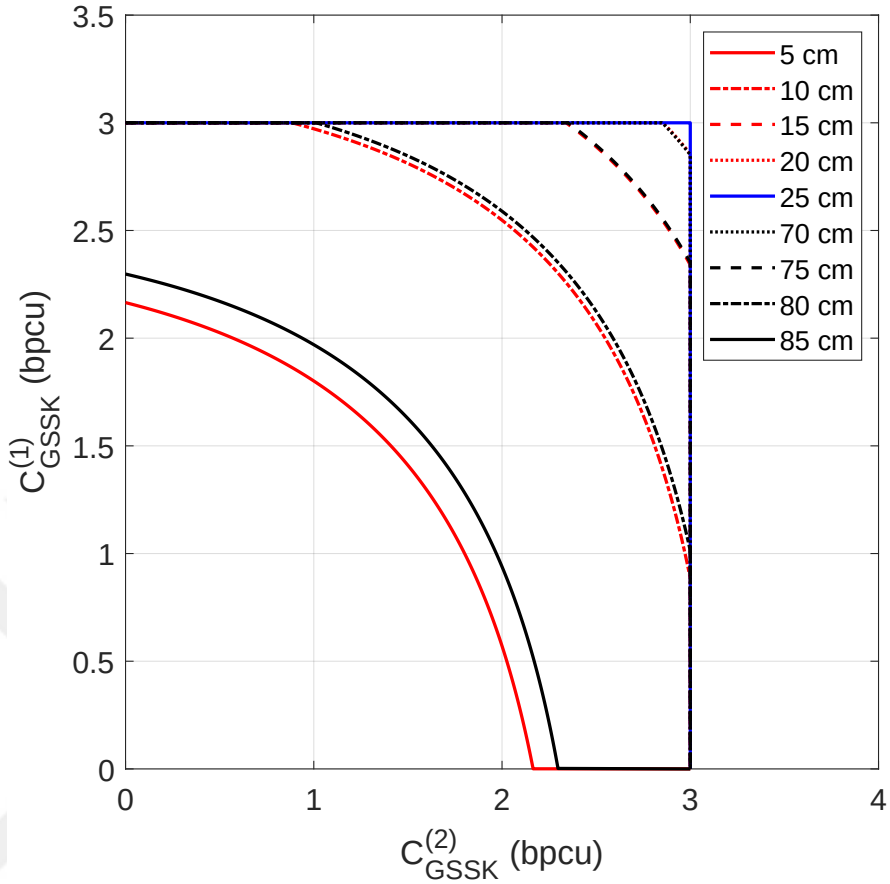

Figure 4.25. Secrecy rate regions for SNR of 0 dB while Eve moving away from User 1 to User 2. The separation values between the User 1 and Eve are indicated in the legend.

4.5.6. Computational Complexity Analysis

Computational issue arises in the proposed multi user PLS system, during precoding at the transmitter and data detection at the receiver. The source transmits data to the users via suitably designed linear regularized zero-forcing precoder, that can be computed according to (4.25) as

$$\mathbf{P}_k = \rho\tilde{\mathbf{H}}_k \left(\tilde{\mathbf{H}}^T\tilde{\mathbf{H}} + \epsilon\mathbf{I}_{N_a}\right)^{-1} \tilde{\mathbf{H}}^T\mathbf{v}_{\mathcal{S},s}, \tag{4.47}$$

where, $\tilde{\mathbf{H}} \in R^{N_r \times N_a}$ denotes the channel matrix between the source and the kth user, ρ is the power normalization factor and ϵ is the regularization parameter. In the above, matrix multiplication needs roughly $\mathcal{O}(N_r N_a^2)$ operations, and matrix inversion requires approximately $\mathcal{O}(N_a^3)$ operations.On the other end, when the transmitter precoding is capable of perfectly separating K users, low-complexity single stream detection is facilitated at the receiver. According to the received signal at the kth user

$$\mathbf{y}_k = \mathbf{s}_k + \mathbf{n}_k, \quad k = 1, 2, \cdots, K, \tag{4.48}$$

where $\mathbf{s}_k$ is the observed transmitted signal by the kth user and given by (4.25), the detection complexity increases linearly with K. Hence, the total complexity of the detection of signals at users is $\mathcal{O}(KM_kN_a)$ where M_k is the constellation size of the kth user's received signal. Hence, in summary, the MU-GSSK based PLS scheme proposed in this chapter has approximately complexity of $\mathcal{O}(N_rN_a^2 + N_a^3 + KM_kN_a)$.

4.6. Conclusion

In this chapter, we have presented a PLS technique to enhance the security of multiuser VLC systems in the presence of an eavesdropper. A novel design of spatial constellations has been proposed for the MIMO-GSSK based scheme to maximize the minimum Euclidean distance of the transmit symbol set with the aid of CSI of the legitimate users.

A zero-forcing precoder was also constructed at the transmitter by optimally reshaping the GSSK signal with the legitimate users' CSI to minimize their BERs. The signal shaping with precoding approach also acts as that of a friendly jammer that degrades the Eve's communication and SNR severely so as to prevent any meaningful confidential message leakage to Eve. In addition, the legitimate users' secrecy region was derived and shown by computer simulations that the proposed PLS technique effectively sends secure information to the multiple legitimate users and prohibits the reception of the same information by eavesdropper successfully in terms of the BER performance. It was also shown that the BER performances of the legitimate users were not very sensitive to parameter estimation errors under imperfect receiver CSI. Furthermore, it has been observed that for the same SNR level, the secrecy region was enlarged as the legitimate user separation increases, and full secrecy could be achieved at 0 dB SNR, when the user separation was 90 cm.

4.7. Spatial Constellation Design Based Generalized Space Shift Keying For Physical Layer Security of Multi User MIMO Communication Systems

4.7.1. Introduction

Wireless communication networks have been used for a large range of applications and services spanning business, government, military and personal interactions. However they are also open to a variety of malicious attacks, including eavesdropping, due to the broadcast nature of the networks. In this context, information security against these attacks can be enhanced on the physical link via physical layer security (PLS), by utilizing the channel characteristics of legitimate users and eavesdroppers (Eves), [138].

One of the fundamental tools for PLS provision is exploiting the randomness in wireless channels to deteriorate Eves' reception. In this regard, space shift keying (SSK) and generalized SSK (GSSK) have been among the effective modulation techniques for multiple-input multiple-output (MIMO) wireless systems with PLS benefits as reported in [139] and [140]. As shown in [141], it is possible to design secrecy capacity maximizing precoding systems for SSK for wireless multipath channels with an Eve even though this approach is computationally too complex to be applicable in practical communication systems. For this reason, other lower complexity transmission strategies exploiting the diversity provided by MIMO-GSSK to improve PLS have also been proposed. For instance, an optimal transmitter selection algorithm is proposed in [122] for a MIMO-GSSK broadcast system that enhances the achievable secrecy rate over a visible light communication channel. Another solution for PLS of MIMO-GSSK systems is proposed in [123], where the source transmits the confidential signal with a friendly jamming signal, which degrades the capacity of only Eve's channel, and thereby improving secrecy. Additionally, channel-inversion or zero-forcing (ZF) precoding is considered to be a practical transmission strategy to suppress the inter-user interference substantially and to improve the PLS of wireless communication systems as presented in [142].

The secrecy improvements in the aforementioned works are obtained in exchange for either *i)* increased computational complexity from extensive optimization, or *ii)* reduction in the available power for information-bearing signal transmission due to artificial noise addition. In this section, we propose a low-complexity spatial constellation design (SCD) technique combined with GSSK (GSSK-SCD) for multi-user (MU) MIMO communication systems, which does not rely on artificial noise but provides increased security. Prior to this work, the GSSK-SCD strategy has been shown to increase the secrecy capacity of visible light communication systems in [68, 69]. In the proposed GSSK-SCD, the legitimate users' CSI is exploited, which can be estimated at the receivers and fed back to the transmitter, as done similarly in e.g. [141, 142]. We do not utilize Eve's CSI, unlike some other works in the PLS literature, since its acquisition by the transmitter remains an open challenge as reported in [138].

The proposed GSSK-SCD improves the communication secrecy via *i)* random mapping between the transmitted symbols and activated antenna combinations, *ii)* emission power adjustment according to the legitimate users' CSI, and *iii)* optimized received spatial constellation for minimized bit error rates (BERs) at the legitimate users. Notice that antenna selection could be an alternative to GSSK, but the proposed technique is preferable for PLS for the two main reasons as follows: *i)* The random antenna and channel switching feature of GSSK makes it more difficult for the eavesdroppers to "guess" the intended user channels and therefore improves the PLS, *ii)* GSSK BER performance of the legitimate users can be shown to be generally superior to those obtained by the antenna selection methods. We show that through GSSK-SCD signaling, the BER performance of legitimate users is maximized, while Eve receives a jammed signal, reducing its BER performance significantly. The degradation in BER is shown to be effective even at high signal-to-noise ratios (SNRs). Furthermore, it is shown that the jamming is produced by only the GSSK-SCD signal modelling, and hence artifical noise transmission is not required.

4.7.2. System Description

We consider the PLS for a wireless communication system based on the MIMO-GSSK modulation technique, as illustrated in Figure 4.26. In this system, only a certain number of antennas are activated for transmission at each symbol instant and the selected antenna indices implicitly convey information [143]. The absence of information symbol transmission in GSSK significantly simplifies the radio-frequency (RF) detection complexity compared to spatial modulation (SM) while achieving similar performance gains.

In the considered MU-MIMO-GSSK system, K users, each equipped with N_r receiving antennas, are connected to a single wireless communications attocell with N_t transmitting antennas, $(N_r < N_t)$. We employ GSSK, with $N_a > 1$ activated antennas per transmission, where there is a total of $\binom{N_t}{N_a}$ distinct antenna combinations.

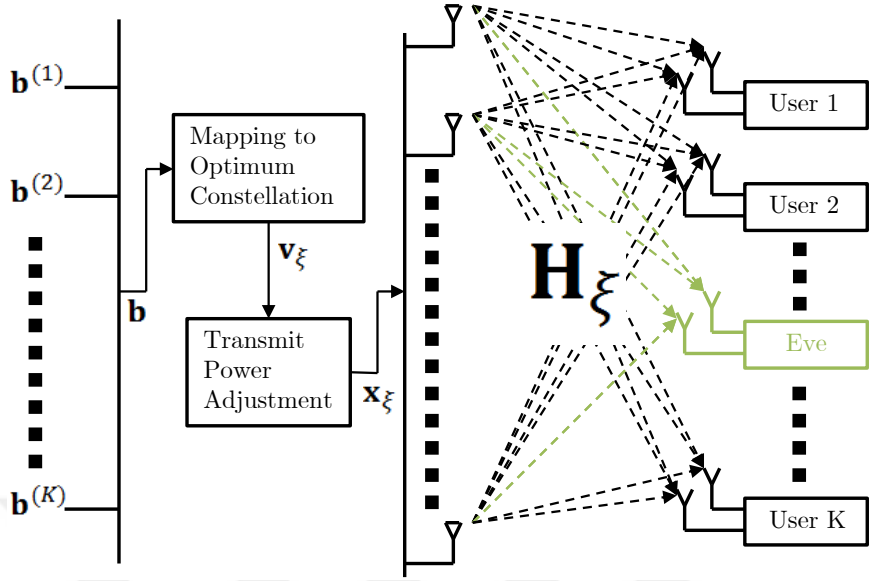

Figure 4.26. System architecture for GSSK-SCD for the multi-user MIMO communication system.

In contrast to generalized SM systems, where the antenna transmission amplitude is modulated with information, in the proposed regime only the indices of the selected antennas are used as spatial constellation points, and convey information to the receivers. However, the number of combinations that can be considered for activation must be a power of two. Therefore, only $M_a = 2^m$ combinations are randomly selected to activate antennas, where $m = \lfloor \log_2 \binom{N_t}{N_a} \rfloor$ and $\lfloor \cdot \rfloor$ is the floor operation. Consequently, random and independent binary data bits $\mathbf{b}^{(u)} = (b_1^{(u)}, b_2^{(u)}, \cdots, b_{m^{(u)}}^{(u)})$ enter a GSSK mapper for each user $u \in \{1, 2, \cdots, K\}$, where $m^{(u)} = \log_2(M_a^{(u)})$ is the spectral efficiency of the user u in terms of bits per channel use (bpcu). The GSSK mapper concatenates the groups of $m^{(u)}$ bits from all users, then $m = \sum_{u=1}^{K} m^{(u)}$ bits are mapped to a constellation point vector $\mathbf{x} = [x_1, x_2, \cdots, x_{N_t}]^T$. Since N_a antennas are active, only N_a elements in $\mathbf{x}$ are nonzero. We denote the constellation point of the user u with $\xi^{(u)} = 1, 2, \cdots, M_a^{(u)}$, which corresponds to the $m^{(u)}$ bits generated by that user.

The GSSK constellation point, which corresponds to the total m bits, is defined as $\xi = \xi^{(1)} \times \xi^{(2)} \times \cdots \times \xi^{(K)} = \left(q^{(1)}, q^{(2)}, \cdots, q^{(K)}\right)$, where $q^{(u)} \in \{1, 2, \cdots, M_a^{(u)}\}$ and $\xi = 1, 2, \cdots, M_a$. Now we define

$$\mathbf{x}_{I_\xi} = \begin{bmatrix} 0 & P_1 & \dots & 0 & \dots & P_2 & \dots & 0 & \dots & P_{N_a} & \dots \\ & \uparrow & & & & \uparrow & & & & \uparrow & \\ & x_{i_1} & & & & x_{i_2} & & & & x_{i_{N_a}} & \end{bmatrix}^T, \tag{4.49}$$

where $I_\xi = (i_1, i_2, \cdots, i_{N_a})$ stores the selected antenna indices for the GSSK constellation point ξ, and $\mathbf{x}_{I_\xi}$ is the GSSK transmit vector for ξ. Also, $\mathbf{P} = [P_1, P_2, \cdots, P_{N_a}]^T$ represents the radiation amplitudes of the selected antennas. The elements in $\mathbf{P}$ are found via precoding by exploiting the legitimate users' CSI at the transmitter as described in the next section. The pre-processed weight vector $\mathbf{P}$ is then transmitted by $\mathbf{x}_{I_\xi}$ over the user's respective channels $\mathbf{H}^{(u)} = [\mathbf{h}_1^{(u)}, \mathbf{h}_2^{(u)}, \ldots, \mathbf{h}_{N_t}^{(u)}] \in \mathbb{C}^{N_r \times N_t}$ where, $\mathbf{h}_k^{(u)} = [h_{1,k}^{(u)}, h_{2,k}^{(u)}, \ldots, h_{N_r,k}^{(u)}]^T$. The Rayleigh fading coefficients of each user's channel, $h_{n,k}^{(u)}$, are assumed to be complex Gaussian random variable with zero mean and unit variance. An N_r-dimensional additive, complex-valued white Gaussian noise (AWGN) vector, $\mathbf{w}^{(u)}$, with double sided power spectral density σ^2 is added to the received signal. Hence, the received signal by the uth user is given by

$$\mathbf{y}^{(u)} = \mathbf{H}^{(u)}\mathbf{x}_{I_\xi} + \mathbf{w}^{(u)} = \beta \mathbf{h}_{I_\xi,\text{eff}}^{(u)} + \mathbf{w}^{(u)} \tag{4.50}$$

where $\mathbf{h}_{I_\xi,\text{eff}}^{(u)} = \sum_{k=1}^{N_a} \mathbf{h}_{i_k}^{(u)} P_k$. Note that $\mathbf{h}_{I_\xi,\text{eff}}^{(u)}$ is called an "effective column vector" for $\xi^{(u)}$, representing the weighted-sum of the N_a distinct columns of $\mathbf{H}^{(u)}$ and β is a normalizing constant to be estimated.

At each user's side, detection of antenna indices is done by the optimal maximum likelihood (ML) rule given by

$$I_{\widehat{\xi}}^{(u)} = \arg\max_{\xi} p(\mathbf{y}^{(u)}|\mathbf{x}_{I_\xi}, \mathbf{H}^{(u)}) = \arg\min_{\xi} \parallel \mathbf{y}^{(u)} - \beta \mathbf{H}_{I_\xi}^{(u)} \mathbf{P} \parallel_F^2, \tag{4.51}$$

where $I_{\widehat{\xi}}^{(u)} = (\hat{i}_1, \hat{i}_2, \ldots, \hat{i}_{N_a})$ denotes the estimated antenna indices and $\mathbf{H}_{I_\xi}^{(u)}$ is obtained from $\mathbf{H}^{(u)}$ as

$$\mathbf{H}_{I_\xi}^{(u)} = \begin{bmatrix} h_{1,i_1}^{(u)} & h_{1,i_2}^{(u)} & \cdots & h_{1,i_{N_a}}^{(u)} \\ h_{2,i_1}^{(u)} & h_{2,i_2}^{(u)} & \cdots & h_{2,i_{N_a}}^{(u)} \\ \vdots & \ddots & \ddots & \\ h_{N_r,i_1}^{(u)} & h_{N_r,i_2}^{(u)} & \cdots & h_{N_r,i_{N_a}}^{(u)} \end{bmatrix} \in \mathcal{C}^{N_r \times N_a}. \tag{4.52}$$

The main problem with the detection rule in (4.51) is that the information detected by each user contains its own message along with those of other users. This would endanger the confidentiality of the information sent by the source to each user and make it difficult to establish secure transmission in the physical layer. Hence, we propose a novel precoding scheme for downlink MU-GSSK systems with two main advantages: (i) The precoder is capable of eliminating the MU interference completely so that the users can only receive their respective information sent by the source. (ii) The precoder is designed in such a way that effective channel vectors at the receiver are contained in a square QAM constellation in N_r-dim Euclidean space resulting in an improved BER performance while degrading Eve's BER performance profoundly.

4.7.3. SCD-based PLS Improvement Technique

In this section, we describe the proposed GSSK-SCD technique. We refer to the source and the multiple legitimate users, as 'Alice' and 'Bobs', respectively. The data sent by Alice is received by Bobs and Eve via their respective channels. In the proposed technique, a suitable precoder is designed without Eve's CSI, which is different from most of the PLS methods in the literature.

Our precoder design forces the effective channel column vectors received by Bobs to be equally-spaced in N_r dimensions. Consequently, it is ensured that Bobs receive the transmitted information with very high BER performance while Eve does not receive any reliable information at all. The precoder is presented in the following subsection.

4.7.3.1. Precoder Design. The proposed precoder shapes original channel's effective column vectors of all users, $\mathbf{H}_{\text{eff}}^{(u)} = [\mathbf{h}_{1,\text{eff}}^{(u)}, \ldots, \mathbf{h}_{M_a^{(u)},\text{eff}}^{(u)}] \in \mathcal{R}^{N_r \times M_a^{(u)}}$, scattered in N_r-dim Euclidean space so that they are maximally separated from each other. They are chosen from the set of vectors $\mathcal{V}_{M^{(u)}-\text{GQAM}}^{(u)} = \{\mathbf{v}_1^{(u)}, \mathbf{v}_2^{(u)}, \ldots, \mathbf{v}_{M^{(u)}}^{(u)}\}$, in an N_r-dim Euclidean space, forming a $M^{(u)}$-ary generalized quadrature-amplitude modulated ($M^{(u)}$-GQAM) signal constellation ($M^{(u)} \geq M_a^{(u)}$), where

$$\mathbf{v}_k^{(u)} = [v_k^{(u)}(1), v_k^{(u)}(2), \ldots, v_k^{(u)}(N_r)]^T \in \mathcal{R}^{N_r}, \tag{4.53}$$

$$v_k^{(u)}(\ell) \in \{\pm A, \pm 3A, \ldots, \pm(L^{(u)} - 1)A\}, \tag{4.54}$$

for $k = 1, 2, \ldots, M^{(u)}$, and $u = 1, 2, \ldots, K$. Here, $L^{(u)} = \left(M^{(u)}\right)^{1/N_r}$ for $L^{(u)} = 2, 4, 6, \ldots$. It can be shown that, for a given $M_a^{(u)}$ and N_r, the size of the GQAM constellation, $M^{(u)}$, can be determined as

$$M^{(u)} = \left\{ \begin{array}{cc} M_a^{(u)}; & \text{if } N_r = 1 \\ \left(2\left\lceil \frac{1}{2}\left(M_a^{(u)}\right)^{1/N_r} \right\rceil\right)^{N_r}; & \text{if } N_r > 1 \end{array} \right\}, \tag{4.55}$$

where $\lceil \cdot \rceil$ denotes ceiling operation. $A > 0$ is a real normalizing constant, whose value is determined by equating the average power of the signal constellation $\mathcal{V}_{M^{(u)}-\text{GQAM}}$ to that of the original effective channel vectors, that is

$$P_{av}(\mathbf{v}) = \mathbb{E}(\mathbf{v}^{(u)\dagger}\mathbf{v}^{(u)}) = P_{av}(\mathbf{h}_{I,\text{eff}}^{(u)}) \equiv 1, \tag{4.56}$$

where $(\cdot)^\dagger$ denotes the Hermitian operation.

The sequence of information bits transmitted to the respective users is mapped to the GSSK transmit vector $\mathbf{x}$, which specifies the activated antennas. Each combination $I \Leftrightarrow \{i_1, i_2, \cdots, i_{N_a}\}$ has the form given in (4.49). The received signal vector at the user u is required to be proportional to $\beta \mathbf{v}_k^{(u)}$ so that multiuser interference (MUI) is suppressed. To satisfy this condition, we design a precoder at the transmit unit with inputs $\mathbf{H}_{I_{\xi^{(u)}}}^{(u)} \in \mathcal{C}^{N_r \times N_a}$, $\xi^{(u)} = 1, 2, \cdots, M_a^{(u)}$ and $\mathbf{P}$. Consequently, to ensure that each user u receives an energy leak-free signal, the optimal precoding vector, $\mathbf{P}_{\text{opt}}$ is determined as

$$\mathbf{H}_{I_{\xi^{(u)}}}^{(u)} \mathbf{P}_{\text{opt}} = \mathbf{v}_{\xi^{(u)}}^{(u)}, \quad u = 1, 2, \cdots, K. \tag{4.57}$$

Combining the outcomes for all users, the relationship in (4.57) can be written as

$$\mathbf{H}_{I_\xi} \mathbf{P}_{\text{opt}} = \mathbf{v}_{I_\xi}, \tag{4.58}$$

where $\mathbf{H}_{I_\xi} = [\mathbf{H}_{I_{\xi^{(1)}}}^{(1)T}, \mathbf{H}_{I_{\xi^{(2)}}}^{(2)T}, \cdots, \mathbf{H}_{I_{\xi^{(K)}}}^{(K)T}]^T \in \mathcal{C}^{KN_r \times N_a}$, $\mathbf{v}_{I_\xi} = [\mathbf{v}_{\xi^{(1)}}^{(1)T}, \mathbf{v}_{\xi^{(2)}}^{(2)T}, \cdots, \mathbf{v}_{\xi^{(K)}}^{(K)T}]^T \in \mathcal{C}^{KN_r}$. Given that the matrix $\mathbf{H}_{I_\xi}^\dagger \mathbf{H}_{I_\xi}$ is nonsingular, the optimal precoding vector can be found with the generalized inverse of $\mathbf{H}_{I_\xi}$, as

$$\mathbf{P}_{\text{opt}} = \left(\mathbf{H}_{I_\xi}^\dagger \mathbf{H}_{I_\xi}\right)^{-1} \mathbf{H}_{I_\xi}^\dagger \mathbf{v}_{I_\xi}, \tag{4.59}$$

which satisfies (4.58), if $\mathbf{U} \triangleq \mathbf{H}_{I_\xi} \left(\mathbf{H}_{I_\xi}^\dagger \mathbf{H}_{I_\xi}\right)^{-1} \mathbf{H}_{I_\xi}^\dagger = \mathbf{I}_{KN_r}$ holds, where $\mathbf{I}_{KN_r} \in \mathcal{C}^{KN_r \times KNr}$ is a unit matrix. Because $\mathbf{H}_{I_\xi}$ in (4.58) has more columns than rows ($N_a \geq KN_r$), the matrix $\mathbf{H}_{I_\xi}^\dagger \mathbf{H}_{I_\xi}$ in (4.59) is positive semi-definite and therefore (4.58) may not have a unique solution. Hence, we apply linear processing exploiting regularization as in [144] to all $\mathbf{v}_{I_\xi}$ vectors. Consequently, the optimal precoding vector becomes

$$\mathbf{P}_{\text{opt}} = \left(\mathbf{H}_{I_\xi}^\dagger \mathbf{H}_{I_\xi} + \epsilon \mathbf{I}_{N_a}\right)^{-1} \mathbf{H}_{I_\xi}^\dagger \mathbf{v}_{I_\xi}, \tag{4.60}$$

where the regularization parameter, $0 < \epsilon < \lambda_{\min}$ makes $\mathbf{H}_{I_\xi}^\dagger \mathbf{H}_{I_\xi}$ positive definite.

Here, $\lambda_{\min}$ is the smallest nonzero eigenvalue of the matrix $\mathbf{H}_{I_\xi}^\dagger \mathbf{H}_{I_\xi}$.

4.7.3.2. Transmit Power Normalization. The signal components of $\mathbf{P}_{\text{opt}}$ arriving at each transmit antenna have substantial power fluctuations in a wide dynamic range. To prevent these, the output power after precoding is normalized by the power-normalization factor β given by $\beta = N_r/\text{Tr}\left\{\left(\mathbf{H}_{I_\xi}\mathbf{H}_{I_\xi}^\dagger\right)^{-1}\right\}$, [144], where $\text{Tr}\{(\cdot)\}$ is the trace operation. An average power constraint can also be employed as done in [145], such that $\beta = N_r\mathbb{E}\left[1/\text{Tr}\left\{\left(\mathbf{H}_{I_\xi}\mathbf{H}_{I_\xi}^\dagger\right)^{-1}\right\}\right]$ which makes β become a constant, depending only on the channel statistics. It can then be computed at the transmitter and passed on to the users.

4.7.3.3. MU Receiver with an Eavesdropper. The legitimate users receive the broadcast as

$$\mathbf{y} = \beta\mathbf{H}_{I_\xi}\mathbf{P}_{\text{opt}} + \mathbf{w} = \beta\mathbf{v}_{I_\xi} + \mathbf{w}, \tag{4.61}$$

where $\mathbf{y} = [\mathbf{y}^{(1),T}, \mathbf{y}^{(2),T}, \cdots, \mathbf{y}^{(K),T}]^T$. With the proposed GSSK-SCD technique, the received signals at the legitimate users are shaped according to (4.57) and (4.58). Hence, the received signal at the uth legitimate user is obtained with zero MUI as

$$\mathbf{y}^{(u)} = \beta\mathbf{H}_{I_\xi}^{(u)}\left(\mathbf{H}_{I_\xi}^\dagger\mathbf{H}_{I_\xi} + \epsilon\mathbf{I}_{N_a}\right)^{-1}\mathbf{H}_{I_\xi}^\dagger\mathbf{v}_{I_\xi} + \mathbf{w}^{(u)} \tag{4.62}$$

$$= \mathbf{s}^{(u)} + \mathbf{w}^{(u)}, \quad u = 1, 2, \ldots, K, \tag{4.63}$$

where $\mathbf{s}^{(u)} \triangleq \beta\mathbf{v}_{I_\xi}^{(u)}$ is the observed transmitted signal by the uth user. Eve receives the broadcast as

$$\mathbf{y}^{(E)} = \mathbf{s}^{(E)} + \mathbf{w}^{(E)}, \tag{4.64}$$

where $\mathbf{s}^{(E)} \triangleq \beta\mathbf{H}_{I_\xi}^{(E)}\left(\mathbf{H}_{I_\xi}^\dagger\mathbf{H}_{I_\xi} + \epsilon\mathbf{I}_{N_a}\right)^{-1}\mathbf{H}_{I_\xi}^\dagger\mathbf{v}_{I_\xi}$ is Eve's received signal.

The equation in (4.64) indicates that GSSK-SCD introduces a *friendly* jamming signal for Eve, mainly due to the random switching phenomenon in GSSK. Hence, $\mathbf{v}^{(u)}$ for any u, cannot be perfectly recovered by Eve. The jamming signal, $\mathbf{J}^{(u)}$ observed in GSSK-SCD when Eve wiretaps the uth user, can be expressed by rewriting Eve's signal in (4.64) as

$$\mathbf{y}^{(u,E)} = \mathbf{s}^{(u)} + \mathbf{J}^{(u)} + \mathbf{w}^{(E)}, \tag{4.65}$$

where $\mathbf{J}^{(u)}$ is the jamming signal at Eve, wiretapping the uth user, which is expressed as

$$\mathbf{J}^{(u)} = \beta \left(\mathbf{H}_I^{(E)} - \mathbf{H}_I^{(u)} \right) \mathbf{P}_{\text{opt}}. \tag{4.66}$$

Note that the term $\mathbf{J}^{(\text{u})}$ in (4.66) represents an effective jamming signal generated purely by channel differences between the legitimate users and Eve, as opposed to being generated separately by the multiple transmitting antennas. It is approximately an AWGN vector with zero mean and covariance $\mathbb{C}_{\mathbf{J}^{(\text{u})}}$. As will shortly be seen from the computer simulations, the jamming signal $\mathbf{J}^{(\text{u})}$ is very effective in increasing the interference experienced by Eve and degrades her BER substantially. From (4.65), we define $\mathbf{n} \triangleq \mathbf{J}^{(\text{u})} + \mathbf{w}^{\text{E}}$, which is a colored zero-mean Gaussian vector with the covariance matrix

$$\mathbb{C}_{\mathbf{n}} = \mathbb{E}\{\mathbf{n}\mathbf{n}^{\dagger}\} = \mathbb{C}_{\mathbf{J}^{(\text{u})}} + \sigma_{\text{E}}^2 \mathbb{I}_{N_r}. \tag{4.67}$$

The receivers extract the spatial information, I, from the observed signals at (4.62) and (4.64) by the ML criterion as

$$\widehat{I}_{\hat{\xi}}^{(u)} = \arg\max_{\xi} \{ \parallel \mathbf{y}^{(u)} - \mathbf{s}^{(u)} \parallel^2 \}, \tag{4.68}$$

$$\widehat{I}_{\hat{\xi}}^{(E)} = \arg\max_{\xi} \{ \parallel \mathbf{y}^{(E)} - \mathbf{s}^{(u)} \parallel^2 \}. \tag{4.69}$$

Notice that the transmitter has to compute $\mathbf{P}_{\text{opt}}$ as given in (4.59), so that secure GSSK-SCD signals are realized at each legitimate user. Therefore, there is a computational cost at the transmitter. On the other hand, the computational complexity at the receivers is small since they do not need to perform any post-processing for PLS, and can extract secure information with simple maximum likelihood detection.

4.7.3.4. Achievable Secrecy Sum Rates. We now consider the secrecy rates for the proposed system in the presence of a single Eve that can easily be extended to the multiple Eve case. In the proposed technique, the interference among users is cancelled completely as given in (4.62). For the proposed system, the achievable secrecy sum-rate R_s is found as the sum of the achievable secrecy rates of all users, $R_s^{(u)}$, in the presence of one Eve, as shown in

$$R_s = \sum_{u=1}^{K} R_s^{(u)}. \tag{4.70}$$

Assuming that the messages transmitted to each user u belong to the standard Gaussian distribution, $R_s^{(u)}$ can be written as

$$R_s^{(u)} = \left[\log_2(1 + \text{SNR}^{(u)}) - \log_2(1 + \text{SNR}^{(E)}) \right]^+, \tag{4.71}$$

where $[a]^+ = a$, if $a \geq 0$, $[a]^+ = 0$, if $a < 0$. Exact closed-form expressions for mutual information and achievable secrecy rates for GSSK cannot be obtained analytically, since the message input distribution $P(\mathbf{x}_{I_\xi}) = 1/N_t$ does not maximize the secrecy capacity of the MU-GSSK system with one Eve. However, in [146], secrecy rates were computed through numerical evaluations for SSK.

Similarly, a lower bound for the secrecy sum-rate achievable by the proposed system can be obtained from (4.68), (4.70) and (4.71) as

$$R_s \geq \sum_{u=1}^{K} \left[\log_2 \left(1 + \log_2 \left(\frac{\beta^2}{N_r \sigma_w^2} \right) \right) - \log_2 \left(1 + \log_2 \left(\frac{\beta^2}{\mathrm{Tr}(\mathbb{C}_{\mathbf{J}^{(u)}} + \sigma_w^2 \mathbf{I}) N_r} \right) \right) \right]^+. \tag{4.72}$$

4.7.4. Simulation Results

In this section, we present the security performance of the proposed GSSK-SCD system in terms of BER and achievable secrecy regions. The channel gains of all users and Eve are drawn independently from the standard complex Gaussian distribution. We assume that only legitimate user CSI is available at the access point and each user is aware of only own CSI. For benchmark comparisons, both conventional GSSK and GSSK with artificial noise have been considered. Consider the conventional GSSK signal model

$$\mathbf{y}^{(u)} = \mathbf{H}^{(u)} \mathbf{x}_{\mathrm{GSSK}} + \mathbf{w}^{(u)}, \tag{4.73}$$

where $\mathbf{x}_{\mathrm{GSSK}}$ is the GSSK transmit vector. The signal model in (4.73) is not useful for PLS purposes, since any third party can decode $\mathbf{x}_{\mathrm{GSSK}}$ by a simple zero-forcing equalizer. In order to increase the resilience against Eves, a popular approach is to transmit an *artificial noise*, $\mathbf{n}_{\mathrm{art}}$, which is superposed on the transmitted information signal, such that

$$\mathbf{y}^{(u)} = \mathbf{H}^{(u)} \left(\mathbf{x}_{\mathrm{GSSK}} + \sqrt{\rho\beta} \mathbf{n}_{\mathrm{art}} \right) + \mathbf{w}^{(u)}, \tag{4.74}$$

where $\mathbf{n}_{\mathrm{art}}$ has unit energy, and $0 \leq \rho \leq 1$ is the power ratio of the artificial noise and $\mathbf{x}_{\mathrm{GSSK}}$.

The artificial noise vector must be selected from the nullspace of $\mathbf{H} = [\mathbf{H}^{(1)T}, \mathbf{H}^{(2)T}, \cdots, \mathbf{H}^{(K)T}]^T \in \mathcal{C}^{KN_r \times N_t}$, so that none of the legitimate users are affected. Then, Eve's signal becomes

$$\mathbf{y}^{(E)} = \mathbf{H}^{(E)}\mathbf{x}_{\text{GSSK}} + \tilde{\mathbf{n}} + \mathbf{w}^{(E)}, \tag{4.75}$$

where $\tilde{\mathbf{n}} = \mathbf{H}^{(E)}\sqrt{\rho\beta}\mathbf{n}_{\text{art}}$. Here, the signal received by legitimate users is still given by (4.73).

For BER performance evaluations, we have assumed that there are $K = 2$ legitimate users and one Eve; and $N_t = 8$, $N_r = 2$ and $N_a = 4$. In this case, $m = \lfloor \log_2 \binom{N_t}{N_a} \rfloor = 6$ bpcu are transmitted, and $M^{(1)} = M^{(2)} = 2^{m/2} = 8$ since m is divided evenly among the legitimate users. Since $N_r = 2$ and $M = 8$, $\mathcal{V}^{(1)}$ and $\mathcal{V}^{(2)}$ are optimally chosen to be $8-$QAM symbol constellations. The BER performance results for this system are presented comparatively in Figure 4.27. These results indicate that GSSK-SCD provides minimized BERs to both legitimate users, due to the optimal precoding in (4.59). GSSK-SCD outperforms the conventional GSSK in terms of the legitimate user BERs whereas Eve's BER is degraded significantly to the 0.5-level.

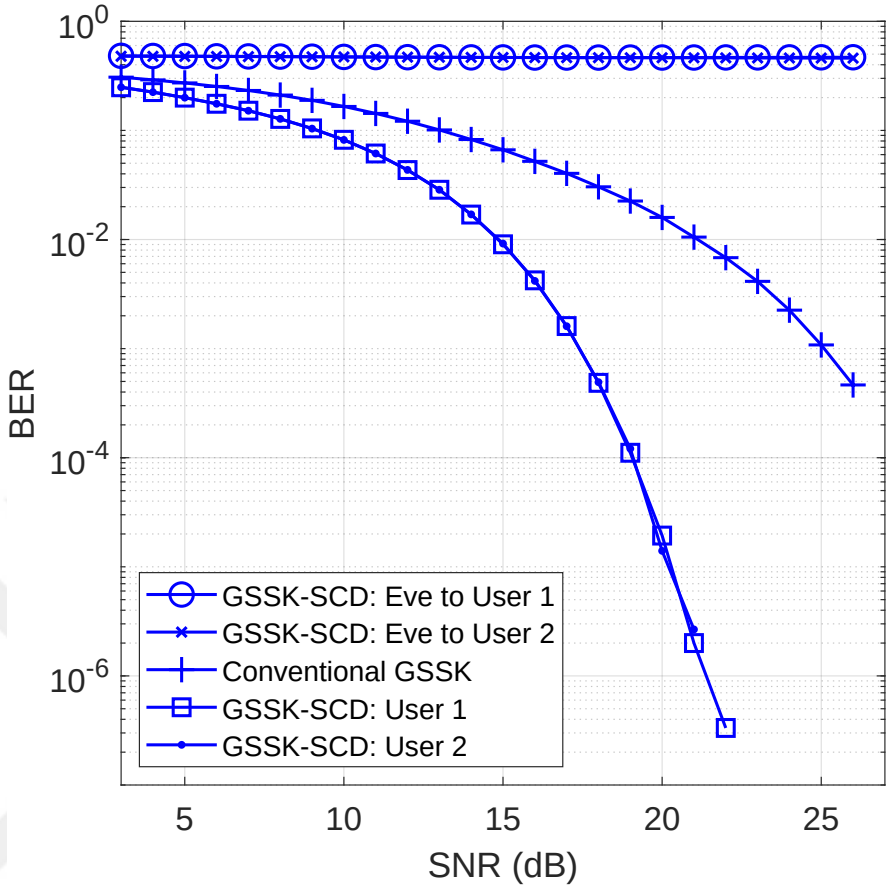

Figure 4.27. BER performance curves obtained by GSSK-SCD of 2 legitimate users and single Eve.

Next in Figure 4.28, we apply GSSK-SCD on the considered system in Figure 4.27, but the number of Eves are increased to 5. Here, the channel coefficients of Eve i ($i = 1, \ldots, 4$) are chosen as functions of the CSI of User 1, as $\mathbf{H}^{(E_i)} = \mathbf{H}^{(1)} + \kappa_i \mathbf{I}$, with $\kappa_i = \{0.1, 0.5, 1, 2\}$. The channel of Eve 5 is independent of other parties. According to the results in Figure 4.28, Eve's BER improves as its channel coefficients resemble more the legitimate user's CSI. This makes sense, since the energy of the GSSK-SCD jamming signal is small if the channel resemblance of Eve and the User is high, which is deduced from (4.66). Still, for larger κ values, Eve's communication is corrupted with large BERs. Thus, GSSK-SCD results in degraded BER performance at Eve for $\kappa > 0.5$. The results in Figures 4.27 and 4.28 suggest that the proposed GSSK-SCD system provides secure communication, unless Eves' channel is almost identical to that of any legitimate user's.

In Figure 4.29, the proposed GSSK-SCD is compared with the GSSK system with artificial noise, in terms of Eve's BER performance. In this case, $N_t = 12$ and $N_a = 6$ are assumed, so $N_a > KN_r$ holds and (4.74) can be applied since the nullity of $\mathbf{H}_{I_\xi}$ is positive. The system is simulated for the artificial noise power ratios of $\rho = \{0.1, 0.2, 0.3\}$. The results indicate that the conventional GSSK system with artificial noise results in degraded BER performance at Eve, for all considered ρ values. However, the proposed system ensures Eve to operate close to the 0.5 BER level, which is still larger than the benchmark strategy. Notice that the benchmark strategy dissipates a significant amount of power for artificial noise transmission. On the other hand, this is not needed in GSSK-SCD as it provides friendly jamming by the optimal spatial constellation design and uses all available power for only information broadcast. Therefore, the GSSK-SCD system is a low-cost PLS strategy, offering reduced interceptibility of the transmitted information.

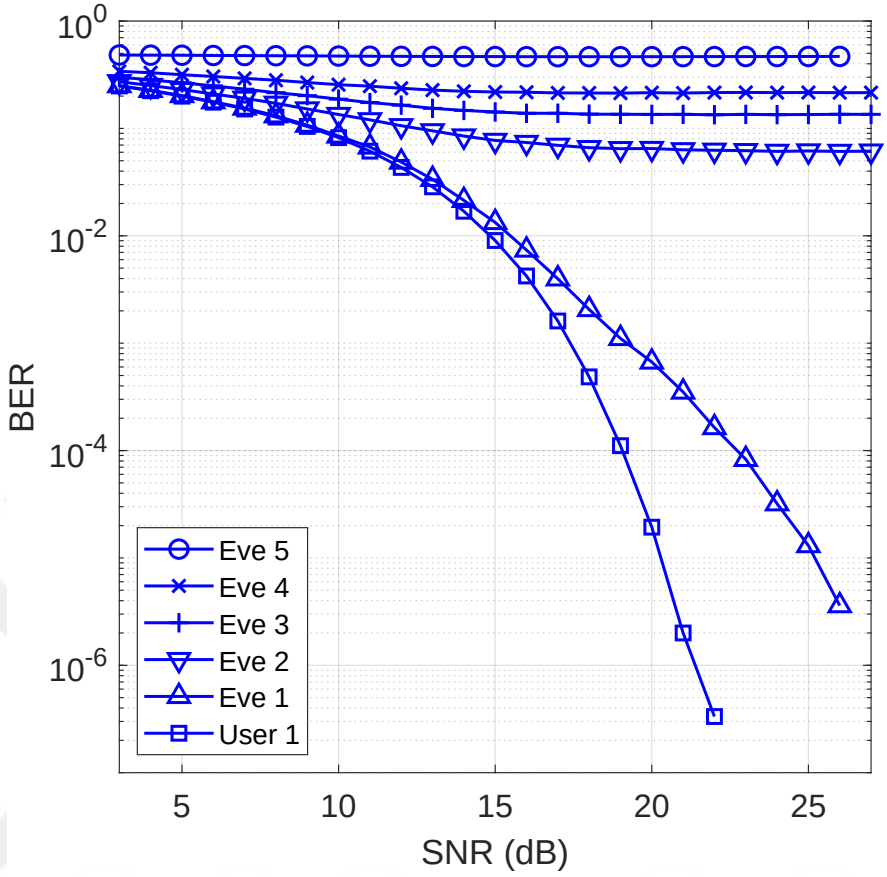

Figure 4.28. BER performance curves obtained by GSSK-SCD of 2 legitimate users and multiple Eves.

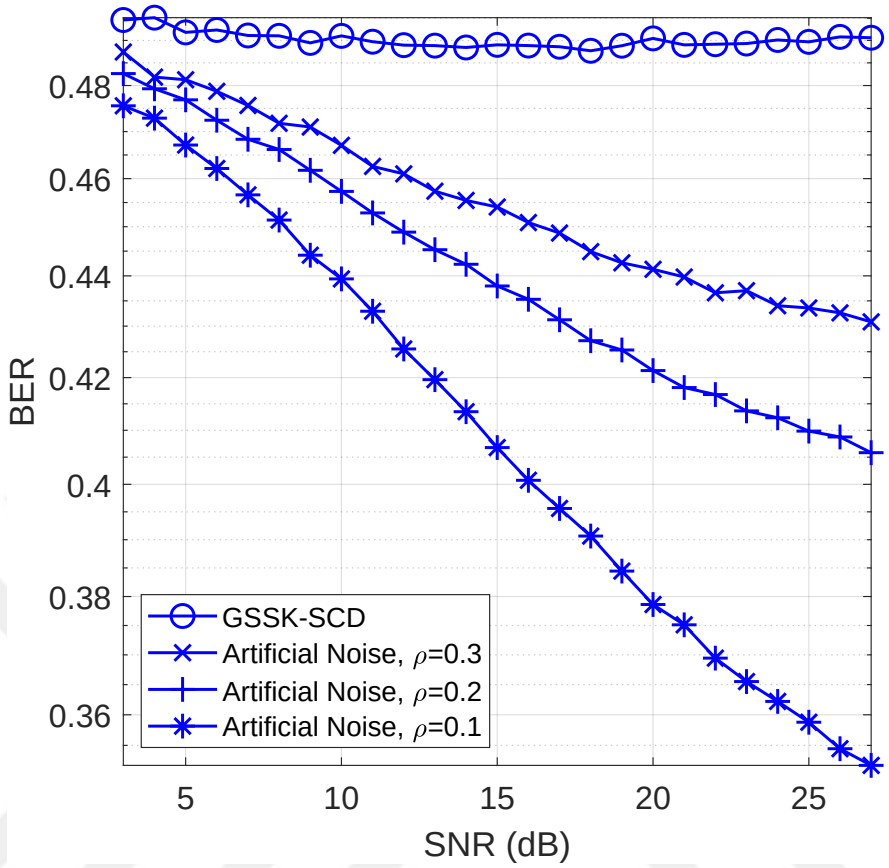

Figure 4.29. BER performance comparison of GSSK-SCD and GSSK with artificial noise.

Finally, we present the secrecy rate regions of 2 users employing GSSK-SCD for different SNR levels in Figure 4.30. These curves are obtained for $N_t = 8$, $N_a = 4$ and $m^{(1)} = m^{(2)} = 3$ bpcu which is the maximum achievable secrecy rate per user. It can be seen that at low SNR levels (0-12 dB), both users cannot be provided with the maximum achievable secrecy at the same time. For instance, at 0 dB SNR, if one user's secrecy rate is more than 2 bpcu, then the other user's secrecy rate cannot be maximized. On the other hand, GSSK-SCD ensures a secrecy rate of 2.5 bpcu to both users at 0 dB SNR. As expected the secrecy rates provided to both users increases with SNR and for the SNR $>$ 12 dB, both users are provided with maximum achievable secrecy rate.

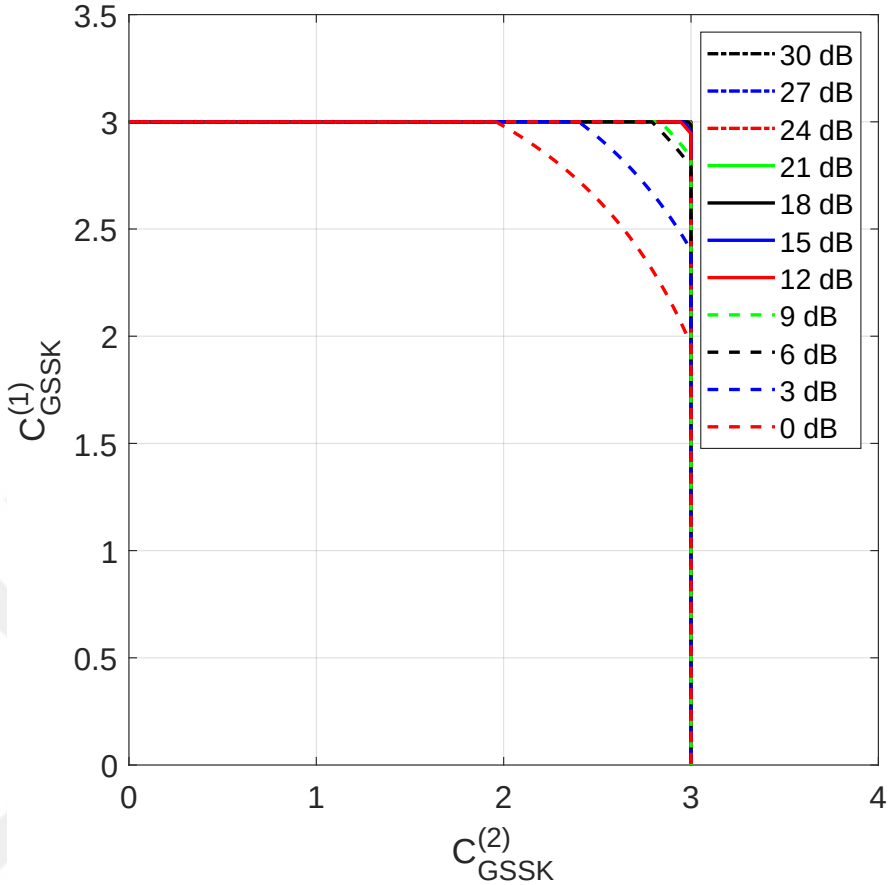

Figure 4.30. Secrecy rate regions of the 2−user GSSK-SCD.

4.7.5. Conclusion

In this section, we have presented GSSK-SCD, a novel SCD strategy based on GSSK, for PLS improvements in MU-MIMO communication systems with one or more Eves. In the proposed strategy, the GSSK signal is optimally reshaped with legitimate users' CSI to minimize their BERs. GSSK-SCD signaling simultaneously produces jamming in Eve's received signal, causing significant degradation in Eve's BER performance. The performance is evaluated for the 2−user setting via Monte Carlo simulations which indicate significant improvements compared to conventional GSSK and artificial noise aided GSSK strategies. The provided secrecy is quantified with analytical expressions for both users, through which we conclude that both users can be provided with maximum achievable secrecy rate for SNR levels greater than 12 dB.

5. TRANSMIT PRECODING FOR PHYSICAL LAYER SECURITY OF MIMO-NOMA BASED VISIBLE LIGHT COMMUNICATIONS

5.1. Introduction

Visible light communication (VLC) is an emerging technology with great potential to complement radio frequency (RF)-based wireless communication systems, especially for indoor environments such as workplaces, exhibition/conference halls etc, as reported in [7,9]. By accommodating light-emitting diodes (LEDs) with fast switching capabilities to wireless data transfer, VLC can provide simultaneous illumination and high-speed communication [92]. In addition, VLC is a cost-efficient technology in terms of installation and operations, as the existing LED infrastructure can be incorporated for VLC, which uses license-free spectrum [147]. The growing demand for wireless data transmission now expanding to machine-type communications requires emerging technologies to serve multiple users with secure and reliable communication. In this context, non-orthogonal multiple access (NOMA) offers increased spectral efficiency by enabling transmission using the same block of resources (time, frequency, code etc.) to multiple users [4]. NOMA principles can also be conveniently applied to VLC systems to improve the network connectivity as reported in [148, 149]. For instance in [150] and [151], NOMA is shown to provide improved bit error ratio (BER) and throughput performance for VLC systems compared with orthogonal frequency division multiple access (OFDMA). In [152], optimum power allocation policies are formulated for NOMA to maximize transmission rate under quality-of-service constraints for VLC. Similarly, optimum power allocation policies are determined in [37] to maximize achievable sumrates for a NOMA-VLC system with 2×2 multiple-input-multiple-output (MIMO) structure. NOMA, applied with an LED selection algorithm, is compared is to OFDMA in the presented MIMO-VLC system in [153], and is shown to support improved data rates with nonorthogonal multiple access.

As NOMA is shown to be a viable option for multiple access for multi-user VLC systems, communication security becomes an important challenge [67, 69]. Although VLC is inherently more secure compared with RF-based systems as the coverage of LEDs is much smaller due to the local confinement of light, physical layer security (PLS) is still threatened by the existence of eavesdroppers (Eves), through various types of attacks [154]. In this context, confidentiality can be ensured by PLS techniques which rely on shaping the transmitted signals with the knowledge of receivers' channel state information (CSI), to disrupt Eve's interception. The works in [84], [68] are examples of PLS applications in MIMO-VLC systems, where a precoding-based received signal optimization approach is shown to ensure security for the single user and the multiple user case, respectively. In [155], the secrecy capacity is analyzed with imperfect knowledge of Eve's CSI in a light-fidelity (LiFi) network, in which downlink and uplink communication utilize visible light and infrared light sources, respectively. The security problem has recently gained significant consideration in NOMA enabled MIMO-VLC systems as well. The secrecy rates are formulated for multiuser NOMA-VLC systems in [80], where increasing the number of LEDs is shown to improve the signal-to-noise ratio (SNR) along with enhanced PLS. For NOMA-VLC systems with mobile users, optimum power allocations for maximum secrecy are found in [81], by solving the formulated nonconvex optimization problem using an iterative algorithm. The security problem of NOMA-VLC systems threatened by collusive Eves is considered in [82], where a secrecy capacity maximizing precoding scheme is proposed whose solution is found by a concave-convex iterative algorithm. In [83], the problem of maximizing the minimum secrecy rate problem is considered for NOMA-VLC systems, and is solved with nonconvex beamforming approach.

In this chapter, we propose a novel transmit precoding strategy for PLS provisioning in MIMO-NOMA-VLC systems. Different from the line of work in the NOMA-VLC literature given above, our design does not involve computationally complex procedures such as solving nonconvex optimization problems to ensure PLS.

Instead, we develop a novel precoder, which ensures that the transmitted NOMA symbols are received by the legitimate users (Bobs) without any inter-user interference, while the eavesdropper obtains a significantly corrupted signal. The precoder shapes the information-carrying LED intensity with only Bobs' CSI and the transmitted information. In addition to that, we utilize a constellation coding matrix to further conceal the transmitted messages from the eavesdropper, which is not required for decoding at Bobs. The proposed precoder design is simulated for various user configurations in a practical indoor VLC environment. For both the similar and asymmetrical channel conditions, it is observed that Eve's BER performance is significantly worsened, while Bobs can successfully decode their confidential information, showing that the communication security is ensured by the proposed PLS precoding technique. The simulation results also suggest that the BER performance of Bobs can be improved by increasing the number of PDs, while maintaining high BERs at the eavesdropper.

5.2. MIMO-NOMA-VLC System Model

We consider an indoor MIMO-NOMA-VLC system where the access point (Alice) communicates with a cluster of 2 immobile Bobs. At each transmission instant, a NOMA information symbol is generated at Alice, which is the superposition of the information symbols intended for Bobs. The NOMA symbol is then transmitted by the LED array to Bobs, and Eve intercepts. With the objective of preventing Eve to successfully decode the transmitted NOMA symbol, we design a novel PLS precoding scheme by exploiting Bobs' CSI.

Alice is equipped with an array of N_t LEDs as the transmit unit, whereas Bobs and Eve utilize arrays of N_r photodetectors (PDs) as receive units. Here, the direct current (DC)-biased intensity-modulation/direct detection (IM/DD) technique is employed, where the emitted light intensity is modulated with the transmitted information symbol. The PDs at the receive units convert the received light to electric current, which is used to perform decoding. As all users and Alice are fixed in this scenario, the indoor VLC channel can be considered time-invariant.

Furthermore, the small-scale fading effects in VLC systems are negligible unlike RF communication systems, since the area of each receive unit (PD) is very large compared to the wavelength of the visible light, the information carrying medium [15]. Also, the effects of the reflected lightwaves are minimal when the users are located far from the edges and walls, [126]. Therefore, the LoS component dominates the indoor VLC channel. As reported in [127], the channel gain between the tth LED at Alice and r^{th} PD at the kth legitimate user is described by

$$h_k^{r,t} = \frac{(\eta+1)A_{\text{PD}}}{2\pi(d_k^{r,t})^2}\cos^{\eta}(\phi_k^{r,t})\cos(\theta_k^{r,t})\mathbb{1}_{\Psi_{1/2}}(\theta_k^{r,t}), \tag{5.1}$$

where A_{PD} denotes the effective area of the PD. $\eta = -1/\log_2(\cos(\Phi_{1/2}))$ is the Lambertian emission order of the LED with its semi-angle of the half-power denoted by $\Phi_{1/2}$. The parameter $d_k^{r,t}$ stands for the distance, and $\phi_k^{r,t}$ and $\theta_k^{r,t}$ indicate the angles of emergence and incidence between the tth LED and the rth receiver of the kth user, respectively. The parameter $\Psi_{1/2}$ is the half-angle of the field-of-view (FOV) of the PD. The binary indicator function $\mathbb{1}_{\Psi_{1/2}}(\cdot)$ results 1 if the incidence angle is within the FOV of the PD, i.e. $||\theta_k^{r,t}|| \leq \Psi_{1/2}$, and 0 otherwise. Using the formula in (5.1), the channel matrix between Alice and the kth user can be constructed as

$$\mathbf{H}_k = \begin{bmatrix} h_k^{1,1} & h_k^{1,2} & \dots & h_k^{1,N_t} \\ h_k^{2,1} & h_k^{2,2} & \dots & h_k^{2,N_t} \\ \vdots & \vdots & \ddots & \vdots \\ h_k^{N_r,1} & h_k^{N_r,2} & \dots & h_k^{N_r,N_t} \end{bmatrix}_{N_r \times N_t}. \tag{5.2}$$

Denoting the LED intensity vector with $\mathbf{x} \in \Re^{N_t \times 1}$, the received light intensity at the kth user is described by

$$\mathbf{y}_k = \mathbf{H}_k(\mathbf{x} + \mathbf{B}_{\text{DC}}) + \mathbf{n}_k, \tag{5.3}$$

where $\mathbf{n}_k \in \Re^{N_r \times 1}$ is the zero-mean additive white Gaussian noise (AWGN) vector, modelling the distortion due to the thermal noise at the PDs.

The covariance matrix of $\mathbf{n}_k$ is $(\sigma_n^2/N_r)\mathbf{I}_{N_r}$, where $\mathbf{I}_{N_r}$ is the identity matrix. The pre-determined DC bias $\mathbf{B}_{\text{DC}} \in \Re^{N_t \times 1}$ ensures that the resulting vector is non-negative so that the transmitted signal is not clipped due to the LED operation characteristics. The vector $\mathbf{x}$ is constructed as the superposition of the information symbols intended for the legitimate users, and given by

$$\mathbf{x} = \gamma(\sqrt{\alpha}\mathbf{s}_1 + \sqrt{(1-\alpha)}\mathbf{s}_2), \tag{5.4}$$

where $\mathbf{s}_k$ denotes the information symbol for the kth user, with average energy of 1. The parameters γ and α denote the signal amplitude and the NOMA power ratio, which is the fraction of Bob 1's signal power in the total signal power. The parameter γ is designed such that the emitted light intensity is in the limited dynamic range of the LEDs. The transmitted NOMA symbol can be received by Bobs according to (5.3). Conventionally, the weak user is assigned a lower fraction in signal power, and performs successive interference cancellation (SIC), followed by maximum likelihood (ML) detection, while the strong user can extract their information without SIC.

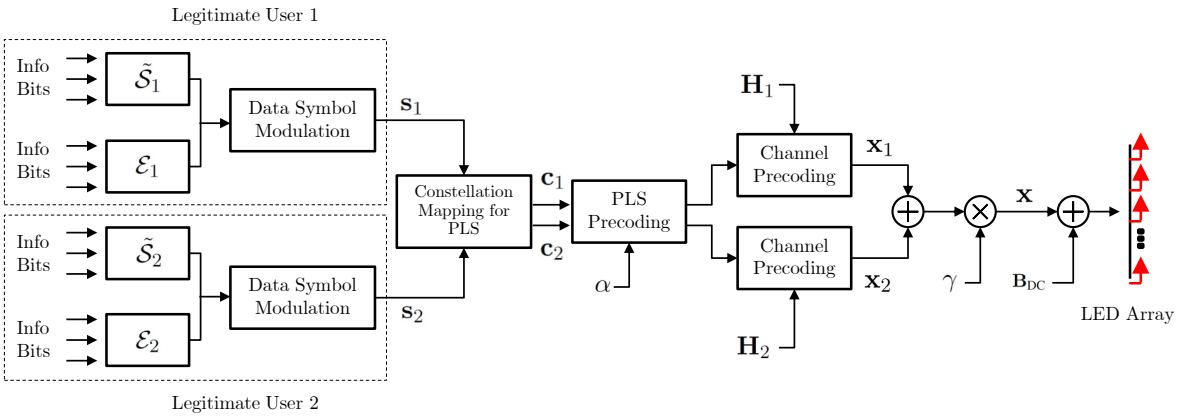

Figure 5.1. The transmitter design for the proposed PLS precoding scheme.

The NOMA-VLC signal in (5.4) is open to passive eavesdropping attacks, when a third party obtains the parameters, $\gamma, \alpha, \mathbf{B}_{\text{DC}}$, which are passed on to the users from Alice. In order to counteract this threat, we design a PLS precoder, as visualized in Figure 5.1, reinforced with random constellation mapping.

The proposed precoder is designed such that the transmitted signal activates only one selected PD at the target user. As will be evident shortly, the PD selection strategy renders the transmission of extra information possible. For PD selection, we define the M-ary symbol constellation and the spatial symbol constellation for user k as

$$\tilde{\mathcal{S}}_k = \{s_k^1, s_k^2, \ldots, s_k^M\}, \tag{5.5}$$

$$\mathcal{E}_k = \{\mathbf{e}_1, \mathbf{e}_2, \ldots, \mathbf{e}_{N_r}\}, \quad k = 1, 2, \tag{5.6}$$

respectively. The target PD of user k is determined by $\mathcal{E}_k$, where the vector $\mathbf{e}_j$ for $j = 1, \ldots, N_r$ is the jth column of the $\{N_r \times N_r\}$ identity matrix. We construct the received signal constellation by the multiplication of s_k^i and $\mathbf{e}_j$ as

$$\mathcal{S}_k = \{s_k^1\mathbf{e}_1, s_k^2\mathbf{e}_1, \ldots, s_k^i\mathbf{e}_j, \ldots, s_k^M\mathbf{e}_{N_r}\}. \tag{5.7}$$

Here, $s_k^i\mathbf{e}_j$ is a vector of length N_r, whose j^{th} element is s_k^i. For simplicity, we will denote the selected symbol from $\mathcal{S}_k$ with $\mathbf{s}_k$, which carries $m^{(k)} = \log_2(MN_r)$ bits of information.

Notice that by employing the spatial symbol constellation $\mathcal{E}_k$, $\tilde{\mathcal{S}}_k$ is expanded to a larger constellation $\mathcal{S}_k$, thereby increasing the rate of transmission per symbol. In the proposed scheme, PLS is ensured by two components. The first component is the random constellation matrix $\mathbf{C} \in \mathbb{R}^{N_r \times N_r}$, which is generated at Alice. The symbol $\mathbf{s}_k$ is multiplied with $\mathbf{C}$ to produce

$$\mathbf{c}_k = \mathbf{C}\mathbf{s}_k. \tag{5.8}$$

The second component is the user-specific precoder matrix $\mathbf{Q}_k$, which is constructed diagonally as

$$\mathbf{Q}_k = \begin{bmatrix} q_k(1) & 0 & \dots & 0 \\ 0 & q_k(2) & \dots & 0 \\ \vdots & \vdots & \ddots & \vdots \\ 0 & 0 & \dots & q_k(N_r) \end{bmatrix}_{(N_r \times N_r)} . \tag{5.9}$$

The design of $\mathbf{Q}_k$ is explained in detail in the subsequent section. The information signal for user k is formed as

$$\mathbf{x}_k = \beta_k \mathbf{P}_k \mathbf{Q}_k \mathbf{C} \mathbf{s}_k, \tag{5.10}$$

where $\mathbf{P}_k \in \mathbb{R}^{N_t \times N_r}$ is the channel inversion matrix, to compensate for the channel effects at Bobs and is defined as

$$\mathbf{P}_k = (\mathbf{H}_k^T \mathbf{H}_k)^{-1} \mathbf{H}_k^T. \tag{5.11}$$

The coefficient β_k in (5.10) is related to the channel conditions of the user k and is calculated by

$$\beta_k = \sqrt{N_r / \mathrm{tr}(\mathbf{H}_k^T \mathbf{H}_k)}, \tag{5.12}$$

where $\mathrm{tr}(\cdot)$ denotes the trace operation. Then, Alice generates the NOMA symbol by superposing $\mathbf{x}_1$ and $\mathbf{x}_2$, and obtains

$$\mathbf{x} = \gamma(\mathbf{x}_1 + \mathbf{x}_2). \tag{5.13}$$

The NOMA power ratio is related to β_k via $\alpha = \beta_1^2/(\beta_1^2 + \beta_2^2)$. Here, the user with greater channel gains is assigned with lower power in (5.13), due to the design of β_k in (5.12).

The NOMA symbol is transmitted following the DC bias addition and received by the user k as

$$\mathbf{y}_k = \mathbf{H}_k(\mathbf{x} + \mathbf{B}_{\mathrm{DC}}) + \mathbf{n}_k, \quad k = 1, 2. \tag{5.14}$$

5.3. PLS Ensuring NOMA Precoder Design

The received NOMA symbols in (5.14) can be rewritten as

$$\mathbf{y}_1 = \beta_1 \mathbf{H}_1 \mathbf{P}_1 \mathbf{Q}_1 \mathbf{c}_1 + \beta_2 \mathbf{H}_1 \mathbf{P}_2 \mathbf{Q}_2 \mathbf{c}_2 + \mathbf{n}_1, \tag{5.15}$$

$$\mathbf{y}_2 = \beta_1 \mathbf{H}_2 \mathbf{P}_1 \mathbf{Q}_1 \mathbf{c}_1 + \beta_2 \mathbf{H}_2 \mathbf{P}_2 \mathbf{Q}_2 \mathbf{c}_2 + \mathbf{n}_2. \tag{5.16}$$

Since the channel inversion matrix is selected as given in (5.11),

$$\mathbf{H}_k(\mathbf{H}_k^T \mathbf{H}_k)^{-1} \mathbf{H}_k^T = \mathbf{I}_{N_r}, \tag{5.17}$$

so that the channel effects on the information symbol of the respective users are cancelled out. Additionally, the precoder matrix $\mathbf{Q}_k$ is designed to be diagonal, therefore

$$\mathbf{Q}_k \mathbf{c}_k = \mathrm{diag}(\mathbf{c}_k)\mathbf{q}_k, \tag{5.18}$$

where the diag$(\cdot)$ produces an $N \times N$ diagonal matrix with the elements of the argument vector of size $N \times 1$ on the main diagonal. Similarly, $\mathbf{q}_k \in \mathbb{R}^{N_r \times 1}$ is the vector with elements on the main diagonal of $\mathbf{Q}_k$, defined as

$$\mathbf{q}_k = \mathrm{diag}(\mathbf{Q_k}) = [q_k(1), q_k(2), \ldots, q_k(N_r)]^T. \tag{5.19}$$

The received signals in (5.15) can be rewritten as a matrix-vector product by using (5.17), (5.18) and (5.19) as

$$\begin{bmatrix} \mathbf{y}_1 \\ \mathbf{y}_2 \end{bmatrix} = \mathbf{V}\mathbf{q} + \begin{bmatrix} \mathbf{n}_1 \\ \mathbf{n}_2 \end{bmatrix}, \tag{5.20}$$

where

$$\mathbf{V} = \begin{bmatrix} \beta_1 \mathrm{diag}(\mathbf{c}_1) & \beta_2 \mathbf{H}_1 \mathbf{P}_2 \mathrm{diag}(\mathbf{c}_2) \\ \beta_1 \mathbf{H}_2 \mathbf{P}_1 \mathrm{diag}(\mathbf{c}_1) & \beta_2 \mathrm{diag}(\mathbf{c}_2) \end{bmatrix}, \mathbf{q} = \begin{bmatrix} \mathbf{q}_1 \\ \mathbf{q}_2 \end{bmatrix}. \tag{5.21}$$

As shown in (5.21), the received signals in (5.20) consist of both user information and inter-user interference. At this point, we aim to both remove the interference in $\mathbf{y}_k$ and degenerate the received signal at Eve. Therefore, $\mathbf{q}_k$ is designed as

$$\mathbf{q} = \begin{bmatrix} \mathbf{q}_1 \\ \mathbf{q}_2 \end{bmatrix} = \mathbf{V}^{-1} \begin{bmatrix} \sqrt{\alpha}\mathbf{s}_1 \\ \sqrt{(1-\alpha)}\mathbf{s}_2 \end{bmatrix}, \tag{5.22}$$

where the NOMA signal power is shared between users by

$$\alpha = \beta_1^2/(\beta_1^2 + \beta_2^2). \tag{5.23}$$

The precoding matrices can be formulated by

$$\mathbf{Q}_k = \mathrm{diag}(\mathbf{q}_k), \tag{5.24}$$

Now, $\mathbf{x}_k$ can be found by (5.10).

5.3.1. The Design of the DC Bias and γ

For successful transmission of the NOMA symbol $\mathbf{x}$ in (5.13), the LEDs must always operate in their dynamic range. Otherwise, the VLC signals may be clipped at the LED front-end. LEDs may also overheat and their electro-optical efficiency may reduce if their driving current is over the maximum threshold [133].

Therefore, the elements in $\mathbf{x}$ must obey

$$I_{\min} < \mathbf{x}^{(t)} < I_{\max}, \quad t = 1, \ldots, N_t, \tag{5.25}$$

where $\mathbf{x}^{(t)}$ denotes the tth element of $\mathbf{x}$. The average of the current limits must also maintain a constant level during communication for eye safety concerns, [134]. Hence, we bias the LEDs at $\mathbf{B}_{\text{DC}} = (I_{\min} + I_{\max})/2$, which is determined by the illumination requirements of the indoor environment. As an example, assume that the illumination preferences require $B_{\text{DC}} = 75$ mA. Since off-the-shelf LEDs usually work below $I_{\max} = 100$ mA in average, [133], $I_{\min}$ is set to 50 mA. Then, γ is calculated by $\gamma = (I_{\max} - I_{\min})/\max\{||\mathbf{x}_1 + \mathbf{x}_2||\}$, where $\max\{||\mathbf{x}_1 + \mathbf{x}_2||\}$ is the maximum norm of the LED driving vector for any $\mathbf{c}_1$ and $\mathbf{c}_2$. An upper bound for $\max\{||\mathbf{x}_1 + \mathbf{x}_2||\}$ can found by

$$\max\{||\mathbf{x}_1 + \mathbf{x}_2||\} \prec \sum_{\forall k} \beta_k \mathbf{P}_k \max\{||\mathbf{Q}_k||\} \max\{||\mathbf{c}_k||\}.$$

Consequently, the LED driving vector becomes

$$\mathbf{x} = \gamma(\beta_1 \mathbf{P}_1 \mathbf{Q}_1 \mathbf{c}_1 + \beta_2 \mathbf{P}_2 \mathbf{Q}_2 \mathbf{c}_2) + \mathbf{B}_{\text{DC}}. \tag{5.26}$$

Bobs receive the transmitted signal in (5.26) in accordance with (5.14). The DC bias is removed and the received signals become

$$\begin{bmatrix} \mathbf{y}_1 \\ \mathbf{y}_2 \end{bmatrix} = \gamma \begin{bmatrix} \sqrt{\alpha}\mathbf{s}_1 \\ \sqrt{(1-\alpha)}\mathbf{s}_2 \end{bmatrix} + \begin{bmatrix} \mathbf{n}_1 \\ \mathbf{n}_2 \end{bmatrix}, \tag{5.27}$$

since the precoder $\mathbf{Q}$ is designed to satisfy (5.22). The user k extracts own information with ML detection as shown in Figures 5.2 and 5.3.

The detected symbols by ML detection are found by

$$\hat{\mathbf{s}}_1 = \arg \min_{\mathbf{s}_1 \in \mathcal{S}_1} \{||\mathbf{y}'_1 - \sqrt{\alpha}\mathbf{s}_1||\}, \tag{5.28}$$

$$\hat{\mathbf{s}}_2 = \arg \min_{\mathbf{s}_2 \in \mathcal{S}_2} \{||\mathbf{y}'_2 - \sqrt{(1-\alpha)}\mathbf{s}_2||\}, \tag{5.29}$$

where $\mathbf{y}'_k = \mathbf{y}_k/\gamma$ and $\mathbf{n}'_k = \mathbf{n}_k/\gamma$. As a result of the PLS precoder, Bobs obtain own information with a known coefficient γ. On the other hand, since $\mathbf{H}_e$ is an unauthorized channel, Eve's received signal, $\mathbf{y}_e$, is highly distorted as shown in

$$\mathbf{y}_e = \gamma\sqrt{\alpha}\mathbf{s}_1 + \mathbf{J}_1 + \mathbf{n}_e, \tag{5.30}$$

$$= \gamma\sqrt{(1-\alpha)}\mathbf{s}_2 + \mathbf{J}_2 + \mathbf{n}_e. \tag{5.31}$$

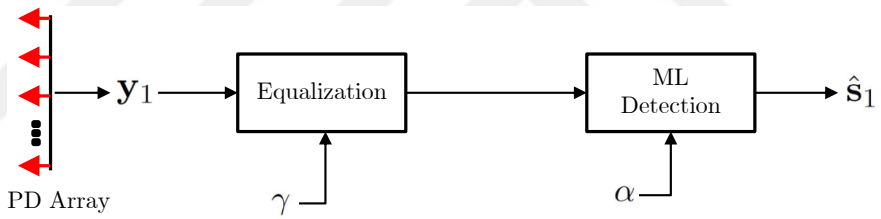

Figure 5.2. The receiver design of User 1 for the proposed PLS precoding scheme.

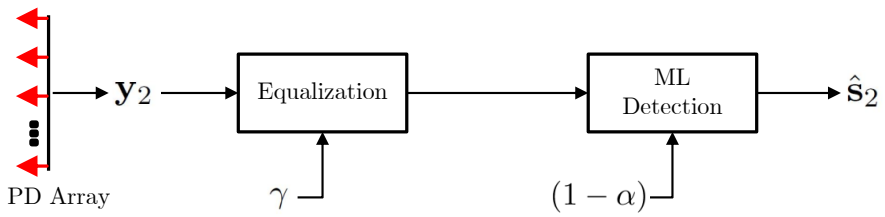

Figure 5.3. The receiver design of User 2 for the proposed PLS precoding scheme.

In (5.30), the term $\mathbf{J}_k$ denotes the precoding-based jamming signal affecting Eve, when the user k is intercepted, and it is found by

$$\mathbf{J}_k = (\mathbf{H}_e - \mathbf{H}_k)\mathbf{x}. \tag{5.32}$$

Eve can attempt to decode $\mathbf{s}_k$ with ML detection as

$$\hat{\mathbf{s}}_e^{(1)} = \arg \min_{\mathbf{s}_1 \in \mathcal{S}_1} \{||\mathbf{y}_e - \gamma\sqrt{\alpha}\mathbf{s}_1||\}, \tag{5.33}$$

$$\hat{\mathbf{s}}_e^{(2)} = \arg \min_{\mathbf{s}_2 \in \mathcal{S}_2} \{||\mathbf{y}_e - \gamma\sqrt{(1-\alpha)}\mathbf{s}_2||\}, \tag{5.34}$$

assuming that γ and α are known by the eavesdropper.

5.4. Simulation Results

In this section, we present the computer simulation results for the proposed PLS precoding scheme, whose effectiveness is measured in terms of BERs at Bobs and Eve. For this purpose, we assume that VLC takes place in an indoor environment with the dimensions of 6 m $\times$ 6 m $\times$ 3 m. The transmit unit of Alice consists of $N_t = 8$ LEDs and is located on the ceiling. The LED coordinates are

$$\mathrm{LED}_{\mathrm{coord}}(x,y,z) = \begin{bmatrix} -2.25, & -0.75, & 0.75, & 2.25, & -2.25, & -0.75, & 0.75, & 2.25 \\ 1.5, & 1.5, & 1.5, & 1.5, & -1.5, & -1.5, & -1.5, & -1.5 \\ 3, & 3, & 3, & 3, & 3, & 3, & 3, & 3 \end{bmatrix}^T \text{ m}, \tag{5.35}$$

where x and y denote the horizontal axes and z the vertical axis. The legitimate users are located according to three different scenarios, as shown in Table 5.1. The receive units of all users, including Eve, are equipped with $N_r = 4$ PDs, which are situated 3 centimeters apart from each other. The half-power and half-angle of the LEDs and the areas of the PDs are assumed to be

$$\Phi_{1/2} = 60^\circ, \quad \Psi_{1/2} = 70^\circ, \quad A_{\mathrm{PD}} = 1 \text{ cm}^2. \tag{5.36}$$

The rest of the channel parameters are found using the positions and orientations of the PDs and LEDs. Then, the VLC channel coefficients between all the LEDs and PDs are found in accordance with (5.1), and the ratio α is found for each user configuration according to (5.23).

Table 5.1. User configurations.

	User 1	User 2	Eve	α
Scenario 1	[-1, 1, 0.85]	[1, -1, 0.85]	[0, 0, 0.85]	0.49
Scenario 2	[-1.5, 1, 0.85]	[0, 1, 0.85]	[1, -1, 0.85]	0.51
Scenario 3	[0, 0, 2]	[3.1, 3.1, 0.3]	[1.55, 1.55, 1.15]	0.21

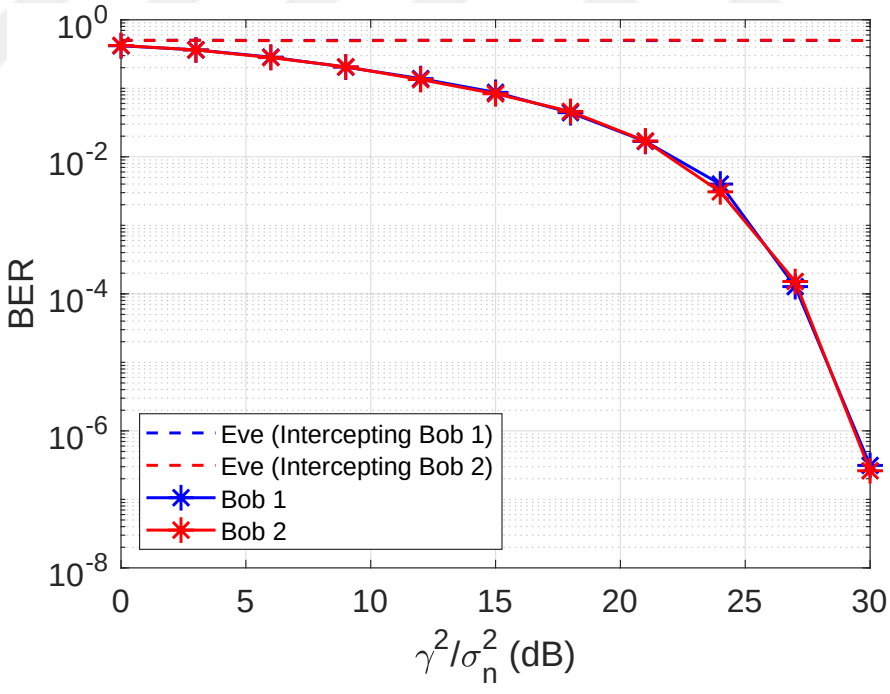

Figure 5.4. BER performance results obtained by the proposed PLS precoding scheme. Users are located according to Scenario 1.

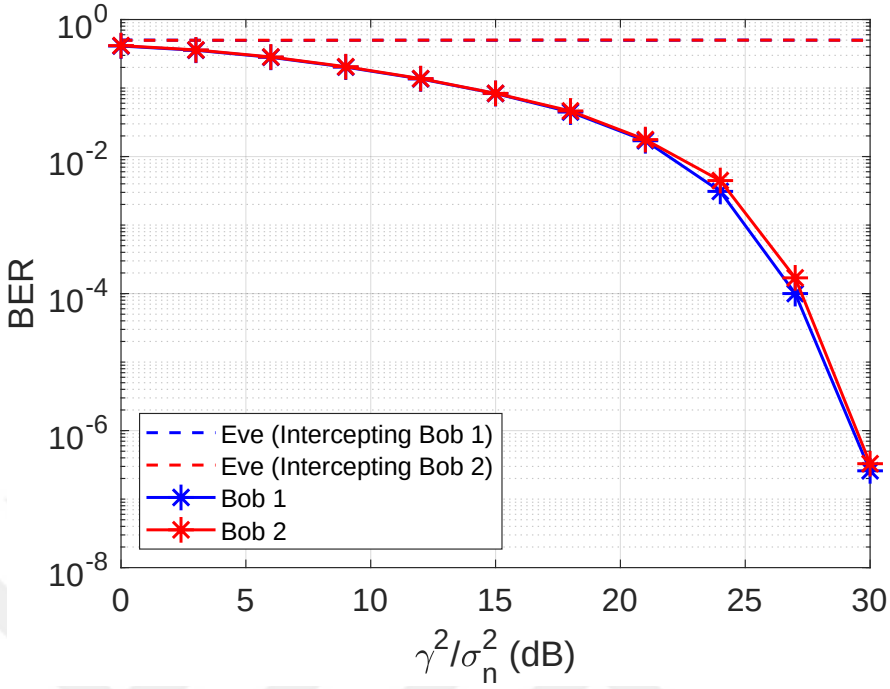

Figure 5.5. BER performance results obtained by the proposed PLS precoding scheme. Users are located according to Scenario 2.

We have simulated the MIMO-NOMA-VLC system with the proposed PLS scheme according to the given specifications. Additionally, we employ $8-$PAM signal constellations for $\tilde{\mathcal{S}}_1$ and $\tilde{\mathcal{S}}_2$. The BER performance results for Scenarios 1 and 2 are presented in Figures 5.4 and 5.5, respectively. Note that in these two scenarios, the legitimate users are positioned with similar distances and angles to Alice, making their average channel gains similar. Therefore, the coefficients β_1 and β_2 are also similar according to (5.12), and hence $\alpha \approx 0.5$ as shown in Table 5.1. According to the presented results, the BER obtained at Eve is significantly large for all SNR levels, while the legitimate users can reach a BER level of 10^{-5} in the $20-25$ dB SNR band. The BER performance of Eve is observed to be independent of which user being eavesdropped. The detected information at Eve's side cannot be intelligible, since the BER is at 0.5 level, on all SNR values. The BER performance results are similar for both scenarios, indicating that the natural jamming caused by the proposed scheme, (5.30), effectively ensures PLS.

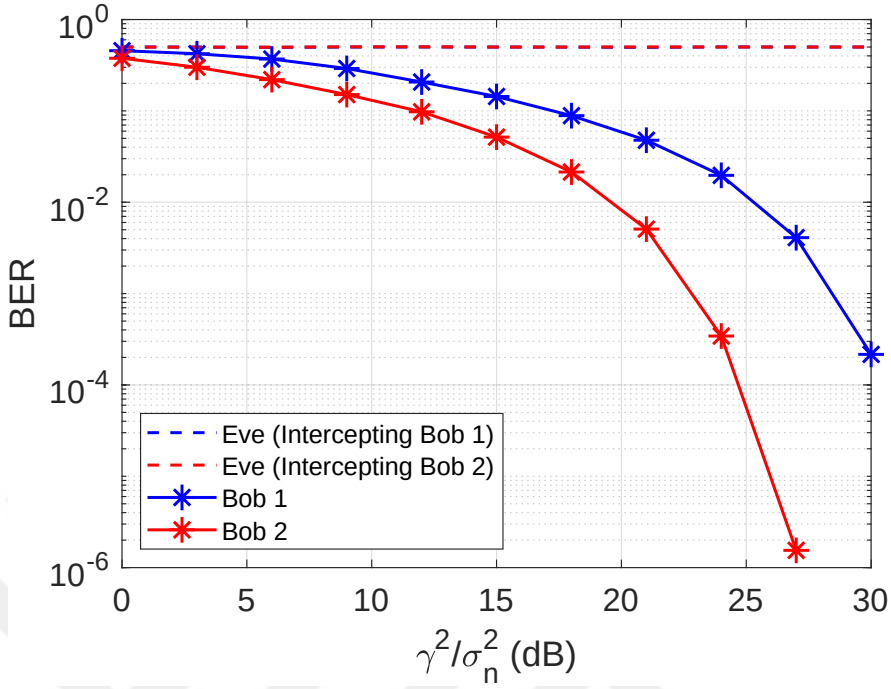

Figure 5.6. The BER performance obtained by the proposed PLS precoding scheme for Scenario 3.

Next, the BER performance for Scenario 3 are presented in Figure 5.6. Notice that in Scenario 3, Bob 1 is much closer to Alice compared with Bob 2, therefore average VLC channel gains of Bob 1 is larger than that of Bob 2, leading to $\alpha < 0.5$. Hence, Bob 1 is allocated a smaller portion of the signal power according to (5.27). Assigned a smaller SNR, Bob 1 experiences higher BERs compared with Bob 2, as indicated in Figure 5.6. Still, Bob 1 performs at 10^{-4} level of BER at 30 dB. It is observed that, Eve's communication suffers from high BERs in this scenario as well. These results, combined with the results in Figures 5.4 and 5.5, show that the proposed PLS precoding scheme ensures secure communication when Bobs are situated either in similar or asymmetrical positions with respect to Alice.

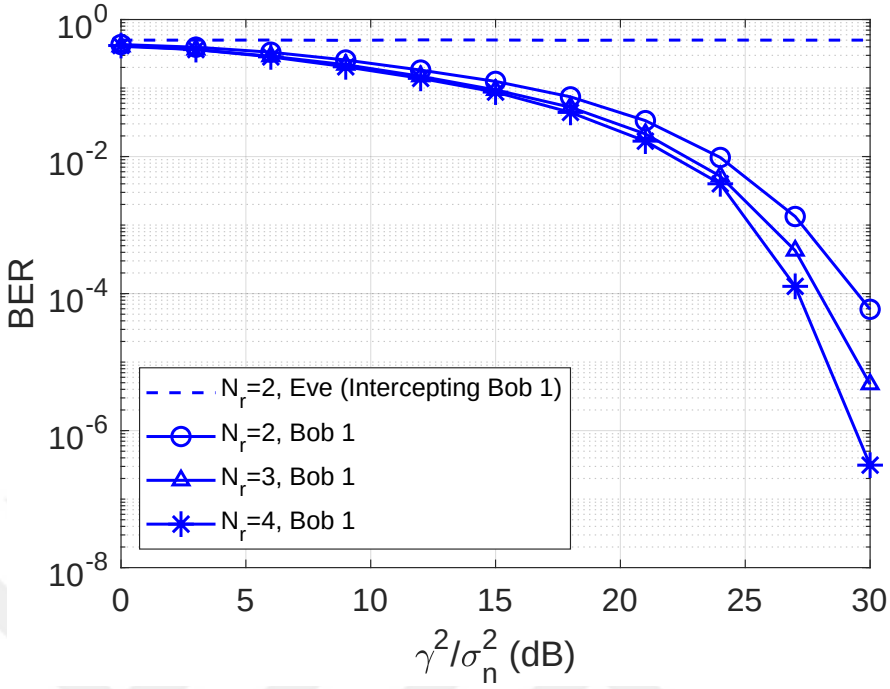

Figure 5.7. The BER performance obtained by the proposed PLS precoding scheme for Scenario 1, with increasing N_r.

We present the effect of number of PDs on the BER performance in Figure 5.7. These BER curves are obtained in Scenario 1 for Bob 1, where the communication performance of both users is shown to be similar in Figure 5.4. These results suggest that increasing the number of PDs improves the BERs of MIMO-NOMA-VLC, which is expected due to increased diversity gain. In Figure 5.7, the BER performance of Eve is also included for $N_r = 2$, which is significantly degraded. These results show that the proposed PLS precoding scheme ensures PLS, while maintaining decent BER levels for legitimate users, even when the PD number is low.

5.5. Conclusion

We have developed a novel transmit precoding technique for PLS provision in MIMO-NOMA enabled VLC systems. The proposed precoder is designed such that the eavesdropper obtains a significantly corrupted signal, while the legitimate users get interference-free signals and can successfully perform decoding. The PLS performance of the proposed system is measured in terms of BERs at both Eve and the legitimate users. The proposed strategy is shown to ensure PLS in various user configurations and PD numbers, for which Eve's BER performance is at 0.5−level at all SNR values.

6. CONCLUSION

In this thesis, VLC transmission techniques are sought for improved cooperation efficiency and physical layer security. First, an efficient cooperative communication strategy is proposed for two-hop DCO-OFDM VLC systems, such that the end-to-end transmission rates are maximized for AF and DF relaying. For this purpose, the received SNR expressions are derived for both relaying schemes considering the LED signal clipping at all transmitting terminals. The transmission rates are found as functions of received SNRs, and maximized by optimizing the subcarrier power allocation, constraint to the illumination preferences dictated by the VLC environment. The optimization problem is nonconvex due to the nonlinear relationship between the clipping noise parameters and the statistical properties of the transmitted signal. Via computer simulations, it is observed that compared to HD relaying, FD relaying with optimized power allocation can improve the transmission rates and BERs for environments requiring high illumination.

Next, the secrecy problem is challenged for multi-user MIMO-VLC systems, and novel precoding-aided PLS techniques are proposed to ensure information security in the presence of eavesdroppers. First, MU-GSSK-SCD, a novel GSSK-based precoding strategy, is introduced, in which the emittances of the activated LEDs are adjusted such that optimum reception at the legitimate users is guaranteed. For optimum reception, the BERs of all legitimate users are minimized by multi-dimensional spatial constellation design. Secondly, a NOMA enabled MIMO-VLC system is considered to support low-complexity superposition for multi-user communication. For that system, an RSM based PLS precoding strategy is proposed utilizing random constellation coding and secret parameter exchange. Both precoding frameworks exploit the CSI of only the legitimate users to guarantee successful decoding at the legitimate users, while significantly corrupting the reception of the eavesdroppers, thereby ensuring PLS. The information secrecy rates, bounds and regions are derived for both frameworks, given the locations of the legitimate users and their CSI.

The PLS provision is illustrated for various user and eavesdropper configurations. The obtained secrecy rates and BER performances indicate that the proposed strategies effectively improve PLS compared to other frameworks based on artificial noise broadcast.

REFERENCES

1. Agiwal, M., A. Roy and N. Saxena, "Next Generation 5G Wireless Networks: A Comprehensive Survey", *IEEE Communications Surveys Tutorials*, Vol. 18, No. 3, pp. 1617–1655, 2016.

2. Al-Fuqaha, A., M. Guizani, M. Mohammadi, M. Aledhari and M. Ayyash, "Internet of Things: A Survey on Enabling Technologies, Protocols, and Applications", *IEEE Communications Surveys Tutorials*, Vol. 17, No. 4, pp. 2347–2376, 2015.

3. Gupta, A. and R. K. Jha, "A Survey of 5G Network: Architecture and Emerging Technologies", *IEEE Access*, Vol. 3, pp. 1206–1232, 2015.

4. Ding, Z., X. Lei, G. K. Karagiannidis, R. Schober, J. Yuan and V. K. Bhargava, "A Survey on Non-Orthogonal Multiple Access for 5G Networks: Research Challenges and Future Trends", *IEEE Journal on Selected Areas in Communications*, Vol. 35, No. 10, pp. 2181–2195, 2017.

5. Wollschlaeger, M., T. Sauter and J. Jasperneite, "The Future of Industrial Communication: Automation Networks in the Era of the Internet of Things and Industry 4.0", *IEEE Industrial Electronics Magazine*, Vol. 11, No. 1, pp. 17–27, 2017.

6. Yang, F. and J. Gao, "Dimming Control Scheme with High Power and Spectrum Efficiency for Visible Light Communications", *IEEE Photonics Journal*, Vol. 9, No. 1, pp. 1–12, 2017.

7. Pathak, P. H., X. Feng, P. Hu and P. Mohapatra, "Visible Light Communication, Networking, and Sensing: A Survey, Potential and Challenges", *IEEE Communications Surveys Tutorials*, Vol. 17, No. 4, pp. 2047–2077, 2015.

8. Dimitrov, S. and H. Haas, *Principles of LED Light Communications: Towards Networked Li-Fi*, Cambridge Univ. Press, Cambridge, U.K., March 2015.

9. Karunatilaka, D., F. Zafar, V. Kalavally and R. Parthiban, "LED Based Indoor Visible Light Communications: State of the Art", *IEEE Communications Surveys Tutorials*, Vol. 17, No. 3, pp. 1649–1678, 2015.

10. Tsonev, D., S. Videv and H. Haas, "Towards a 100 Gb/s Visible Light Wireless Access Network", *Optics Express*, Vol. 23, No. 2, pp. 1627–1637, January 2015.

11. Mufutau, A. O., F. P. Guiomar, M. A. Fernandes, A. Oliveira and P. P. Monteiro, "On the Suitability of VLC Enabled Fronthaul for Future Mobile Network", *Proceedings of Telecoms Conference (ConfTELE)*, pp. 1–4, 2021.

12. Ghassemlooy, Z., P. Luo and S. Zvanovec, "Optical Camera Communications", *Optical Wireless Communications*, pp. 547–568, Springer, Berlin/Heidelberg, Germany, August 2016.

13. Takai, I., T. Harada, M. Andoh, K. Yasutomi, K. Kagawa and S. Kawahito, "Optical Vehicle-to-Vehicle Communication System Using LED Transmitter and Camera Receiver", *IEEE Photonics Journal*, Vol. 6, No. 5, pp. 1–14, 2014.

14. Liu, H., H. Darabi, P. Banerjee and J. Liu, "Survey of Wireless Indoor Positioning Techniques and Systems", *IEEE Transactions on Systems, Man, and Cybernetics, Part C (Applications and Reviews)*, Vol. 37, No. 6, pp. 1067–1080, 2007.

15. Chen, C., D. A. Basnayaka and H. Haas, "Downlink Performance of Optical Attocell Networks", *Journal of Lightwave Technology*, Vol. 34, No. 1, pp. 137–156, 2016.

16. Rea, M. and I. E. S. of North America, *The IESNA Lighting Handbook: Reference & Application*, Illuminating Engineering Society of North America, 2000.

17. Berman, S., D. Greenhouse, I. Bailey, R. Clear and T. Raasch, "Human Electroretinogram Responses to Video Displays, Fluorescent Lighting, and Other High Frequency Sources", *Optometry and vision science: Official Publication of the American Academy of Optometry*, Vol. 68, No. 8, p. 645—662, August 1991.

18. "IEEE Standard for Local and Metropolitan Area Networks–Part 15.7: Short-Range Wireless Optical Communication Using Visible Light", *IEEE Std 802.15.7-2011*, pp. 1–309, 2011.

19. Mejia, C. E., C. N. Georghiades, M. M. Abdallah and Y. H. Al-Badarneh, "Code Design for Flicker Mitigation in Visible Light Communications Using Finite State Machines", *IEEE Transactions on Communications*, Vol. 65, No. 5, pp. 2091–2100, 2017.

20. Park, S., D. Jung, H. Shin, D. Shin, Y. Hyun, K. Lee, Y. Oh, B. Park, H. Shin and K. Lee, "Information Broadcasting System Based on Visible Light Signboard", *Wireless and Optical Communications Conference Proceedings*, pp. 311–313, 2007.

21. Muthu, S. and J. Gaines, "Red, Green and Blue LED-based White Light Source: Implementation Challenges and Control Design", *Proceedings of 38th IAS Annual Meeting on Conference Record of the Industry Applications Conference*, Vol. 1, pp. 515–522 vol.1, 2003.

22. Kaur, S., W. Liu and D. Castor, "VLC Dimming Support - IEEE P802.15 Working Group for Wireless Personal Area Networks (WPANs)", `https://mentor.ieee.org/802.15/dcn/09/15-09-0641-00-0007-vlc-dimming-proposal.pdf`, 2009, accessed in November 2021.

23. Ntogari, G., T. Kamalakis, J. Walewski and T. Sphicopoulos, "Combining Illumination Dimming Based on Pulse-Width Modulation with Visible-Light Communications Based on Discrete Multitone", *IEEE/OSA Journal of Optical Communications and Networking*, Vol. 3, No. 1, pp. 56–65, 2011.

24. Noshad, M. and M. Brandt-Pearce, "Multilevel Pulse-Position Modulation Based on Balanced Incomplete Block Designs", *Proceedings of IEEE Global Communications Conference (GLOBECOM)*, pp. 2930–2935, 2012.

25. Sugiyama, H., S. Haruyama and M. Nakagawa, "Brightness Control Methods for Illumination and Visible-Light Communication Systems", *Proceedings of International Conference on Wireless and Mobile Communications (ICWMC)*, pp. 78–78, 2007.

26. Afgani, M., H. Haas, H. Elgala and D. Knipp, "Visible Light Communication using OFDM", *Proceedings of International Conference on Testbeds and Research Infrastructures for the Development of Networks and Communities (TRIDENTCOM)*, pp. 6–11, 2006.

27. Armstrong, J. and A. Lowery, "Power Efficient Optical OFDM", *Electronics Letters*, Vol. 42, pp. 370 – 372, April 2006.

28. Carruthers, J. and J. Kahn, "Multiple-Subcarrier Modulation for Nondirected Wireless Infrared Communication", *IEEE Journal on Selected Areas in Communications*, Vol. 14, No. 3, pp. 538–546, 1996.

29. Armstrong, J. and B. J. Schmidt, "Comparison of Asymmetrically Clipped Optical OFDM and DC-Biased Optical OFDM in AWGN", *IEEE Communications Letters*, Vol. 12, No. 5, pp. 343–345, 2008.

30. Zeng, L., D. C. O'Brien, H. L. Minh, G. E. Faulkner, K. Lee, D. Jung, Y. Oh and E. T. Won, "High Data-Rate Multiple Input Multiple Output (MIMO) Optical Wireless Communications using White LED Lighting", *IEEE Journal on Selected Areas in Communications*, Vol. 27, No. 9, pp. 1654–1662, December 2009.

31. Bykhovsky, D. and S. Arnon, "Multiple Access Resource Allocation in Visible Light Communication Systems", *Journal of Lightwave Technology*, Vol. 32, No. 8, pp. 1594–1600, 2014.

32. Feng, L., R. Q. Hu, J. Wang, P. Xu and Y. Qian, "Applying VLC in 5G Networks: Architectures and Key Technologies", *IEEE Network*, Vol. 30, No. 6, pp. 77–83, 2016.

33. Li, Z. and C. Zhang, "An Improved FD-DFE Structure for Downlink VLC Systems Based on SC-FDMA", *IEEE Communications Letters*, Vol. 22, No. 4, pp. 736–739, 2018.

34. Shoreh, M. H., A. Fallahpour and J. A. Salehi, "Design Concepts and Performance Analysis of Multicarrier CDMA for Indoor Visible Light Communications", *Journal of Optical Communications and Networking*, Vol. 7, No. 6, pp. 554–562, 2015.

35. Abdelhady, A. M., O. Amin, A. Chaaban, B. Shihada and M.-S. Alouini, "Downlink Resource Allocation for Dynamic TDMA-Based VLC Systems", *IEEE Transactions on Wireless Communications*, Vol. 18, No. 1, pp. 108–120, 2019.

36. Chen, Z. and H. Haas, "Space Division Multiple Access in Visible Light Communications", *Proceedings of IEEE International Conference on Communications (ICC)*, pp. 5115–5119, 2015.

37. Chen, C., W.-D. Zhong, H. Yang and P. Du, "On the Performance of MIMO-NOMA-Based Visible Light Communication Systems", *IEEE Photonics Technology Letters*, Vol. 30, No. 4, pp. 307–310, 2018.

38. Ding, Z., Z. Yang, P. Fan and H. V. Poor, "On the Performance of Non-Orthogonal Multiple Access in 5G Systems with Randomly Deployed Users", *IEEE Signal Processing Letters*, Vol. 21, No. 12, pp. 1501–1505, 2014.

39. Zhang, X., Q. Gao, C. Gong and Z. Xu, "User Grouping and Power Allocation for NOMA Visible Light Communication Multi-Cell Networks", *IEEE Communications Letters*, Vol. 21, No. 4, pp. 777–780, 2017.

40. Guan, X., Q. Yang, Y. Hong and C. C.-K. Chan, "Non-Orthogonal Multiple Access with Phase Pre-distortion in Visible Light Communication", *Optics Express*, Vol. 24, No. 22, pp. 25816–25823, October 2016.

41. Yin, L., W. O. Popoola, X. Wu and H. Haas, "Performance Evaluation of Non-Orthogonal Multiple Access in Visible Light Communication", *IEEE Transactions on Communications*, Vol. 64, No. 12, pp. 5162–5175, 2016.

42. Marshoud, H., V. M. Kapinas, G. K. Karagiannidis and S. Muhaidat, "Non-Orthogonal Multiple Access for Visible Light Communications", *IEEE Photonics Technology Letters*, Vol. 28, No. 1, pp. 51–54, 2016.

43. Chowdhury, H. and M. Katz, "Cooperative Multihop Connectivity Performance in Visible Light Communications", *IFIP Wireless Days (WD)*, pp. 1–4, 2013.

44. Prince, G. B. and T. D. C. Little, "On the Performance Gains of Cooperative Transmission Concepts in Intensity Modulated Direct Detection Visible Light Communication Networks", *Proceedings of 6th International Conference on Wireless and Mobile Communications*, pp. 297–302, September 2010.

45. Kizilirmak, R. C. and M. Uysal, "Relay-assisted OFDM Transmission for Indoor Visible Light Communication", *Proceedings of IEEE International Black Sea Conference on Communications and Networking (BlackSeaCom)*, pp. 11–15, May 2014.

46. Kizilirmak, R. C., O. Narmanlioglu and M. Uysal, "Relay-Assisted OFDM-Based Visible Light Communications", *IEEE Transactions on Communications*, Vol. 63, No. 10, pp. 3765–3778, October 2015.

47. Narmanlioglu, O., R. C. Kizilirmak and M. Uysal, "Relay-assisted OFDM-based Visible Light Communications over Multipath Channels", *Proceedings of 17th International Conference on Transparent Optical Networks (ICTON)*, pp. 1–4, July 2015.

48. Sun, Z. G., H. Yu and Y. J. Zhu, "A Superimposed Relaying Strategy and Power Allocation for Outdoor Visible Light Communications", *IEEE Access*, Vol. 5, pp. 9555–9561, May 2017.

49. Narmanlioglu, O., R. C. Kizilirmak, F. Miramirkhani and M. Uysal, "Cooperative Visible Light Communications with Full-Duplex Relaying", *IEEE Photonics Journal*, Vol. 9, No. 3, pp. 1–11, June 2017.

50. Wang, Z.-Y., H.-Y. Yu and D.-M. Wang, "Energy-Efficient Network Coding Scheme for Two-Way Relay Visible Light Communications", *Proceedings of IEEE 18th International Conference on Communication Technology (ICCT)*, pp. 310–315, 2018.

51. Yang, H. and A. Pandharipande, "Full-Duplex Relay VLC in LED Lighting Linear System Topology", *Proceedings of 39th Annual Conference of the IEEE Industrial Electronics Society (IECON)*, pp. 6075–6080, November 2013.

52. Yang, H. and A. Pandharipande, "Full-Duplex Relay VLC in LED Lighting Triangular System Topology", *Proceedings of 6th International Symposium on Communications, Control and Signal Processing (ISCCSP)*, pp. 85–88, May 2014.

53. Satō, H., *Information Transmission Through a Channel with Relay*, The Aloha System, Univ. Hawaii, Honolulu, Tech. Rep. B76-7, March 1976.

54. Cover, T. and A. Gamal, "Capacity Theorems for the Relay Channel", *IEEE Transactions on Information Theory*, Vol. 25, No. 5, pp. 572–584, 1979.

55. Vallimayil, A., K. M. K. Raghunath, V. R. S. Dhulipala and R. M. Chandrasekaran, "Role of Relay Node in Wireless Sensor Network: A survey", *Proceedings of 3rd International Conference on Electronics Computer Technology*, Vol. 5, pp. 160–167, 2011.

56. Hussein, A. T. and J. M. H. Elmirghani, "10 Gbps Mobile Visible Light Communication System Employing Angle Diversity, Imaging Receivers, and Relay Nodes", *IEEE/OSA Journal of Optical Communications and Networking*, Vol. 7, No. 8, pp. 718–735, August 2015.

57. Feng, L., R. Q. Hu, J. Wang and Y. Qian, "Deployment Issues and Performance Study in a Relay-Assisted Indoor Visible Light Communication System", *IEEE Systems Journal*, Vol. 13, No. 1, pp. 562–570, March 2019.

58. Shannon, C. E., "Communication Theory of Secrecy Systems", *Bell System Technical Journal*, Vol. 28, No. 4, pp. 656–715, October 1949.

59. Wyner, A. D., "The Wire-Tap Channel", *Bell System Technical Journal*, Vol. 54, No. 8, pp. 1355–1387, October 1975.

60. Mostafa, A. and L. Lampe, "Securing Visible Light Communications via Friendly Jamming", *Proceedings of IEEE Global Communications Conference (GLOBECOM) Workshops*, pp. 524–529, December 2014.

61. Arfaoui, M. A., Z. Rezki, A. Ghrayeb and M. S. Alouini, "On the Secrecy Capacity of MISO Visible Light Communication Channels", *Proceedings of IEEE Global Communications Conference (GLOBECOM)*, pp. 1–7, 2016.

62. Ma, S., Z. Dong, H. Li, Z. Lu and S. Li, "Optimal and Robust Secure Beamformer for Indoor MISO Visible Light Communication", *Journal of Lightwave Technology*, Vol. 34, No. 21, pp. 4988–4998, 2016.

63. Mukherjee, A., "Secret-Key Agreement for Security in Multi-Emitter Visible Light Communication Systems", *IEEE Communications Letters*, Vol. 20, No. 7, pp. 1361–1364, 2016.

64. Hassan, O., E. Panayirci, H. V. Poor and H. Haas, "Physical-Layer Security for Indoor Visible Light Communications with Space Shift Keying Modulation", *Proceedings of IEEE Global Communications Conference (GLOBECOM)*, pp. 1–6, 2018.

65. Arfaoui, M. A., H. Zaid, Z. Rezki, A. Ghrayeb, A. Chaaban and M. Alouini, "Artificial Noise-Based Beamforming for the MISO VLC Wiretap Channel", *IEEE Transactions on Communications*, Vol. 67, No. 4, pp. 2866–2879, 2019.

66. Arfaoui, M. A., A. Ghrayeb and C. M. Assi, "Secrecy Performance of the MIMO VLC Wiretap Channel with Randomly Located Eavesdropper", *IEEE Transactions on Wireless Communications*, Vol. 19, No. 1, pp. 265–278, 2020.

67. Arfaoui, M. A. *et al.*, "Physical Layer Security for Visible Light Communication Systems: A Survey", *IEEE Communications Surveys Tutorials*, Vol. 22, No. 3, pp. 1887–1908, 2020.

68. Panayirci, E., A. Yeşilkaya, T. Çoğalan, H. V. Poor and H. Haas, "Physical-Layer Security with Optical Generalized Space Shift Keying", *IEEE Transactions on Communications*, Vol. 68, No. 5, pp. 3042–3056, 2020.

69. Yesilkaya, A., T. Cogalan, S. Erkucuk, Y. Sadi, E. Panayirci, H. Haas and H. V. Poor, "Physical-Layer Security in Visible Light Communications", *Proceedings of 2nd 6G Wireless Summit (6G SUMMIT)*, pp. 1–5, 2020.

70. Mukherjee, A., S. A. A. Fakoorian, J. Huang and A. L. Swindlehurst, "Principles of Physical Layer Security in Multiuser Wireless Networks: A Survey", *IEEE Communications Surveys Tutorials*, Vol. 16, No. 3, pp. 1550–1573, 2014.

71. Fan, L., N. Yang, T. Q. Duong, M. Elkashlan and G. K. Karagiannidis, "Exploiting Direct Links for Physical Layer Security in Multiuser Multirelay Networks", *IEEE Transactions on Wireless Communications*, Vol. 15, No. 6, pp. 3856–3867, 2016.

72. Shu, F., X. Wu, J. Hu, J. Li, R. Chen and J. Wang, "Secure and Precise Wireless Transmission for Random-Subcarrier-Selection-Based Directional Modulation Transmit Antenna Array", *IEEE Journal on Selected Areas in Communications*, Vol. 36, No. 4, pp. 890–904, 2018.

73. Pham, T. V., T. Hayashi and A. T. Pham, "Artificial-Noise-Aided Precoding Design for Multi-User Visible Light Communication Channels", *IEEE Access*, Vol. 7, pp. 3767–3777, 2019.

74. Shen, T., S. Zhang, R. Chen, J. Wang, J. Hu, F. Shu and J. Wang, "Two Practical Random-Subcarrier-Selection Methods for Secure Precise Wireless Transmissions", *IEEE Transactions on Vehicular Technology*, Vol. 68, No. 9, pp. 9018–9028, 2019.

75. Choi, J., J. Joung and B. C. Jung, "Space–Time Line Code for Enhancing Physical Layer Security of Multiuser MIMO Uplink Transmission", *IEEE Systems Journal*, Vol. 15, No. 3, pp. 3336–3347, 2021.

76. Jeganathan, J., A. Ghrayeb and L. Szczecinski, "Generalized Space Shift Keying Modulation for MIMO Channels", *Proceedings of IEEE International Symposium on Personal, Indoor and Mobile Radio Communications (PIMRC)*, pp. 1–5, 2008.

77. Popoola, W., E. Poves and H. Haas, "Generalised Space Shift Keying for Visible Light Communications", *Proceedings of 8th International Symposium on CSNDSP*, pp. 1–4, 2012.

78. Popoola, W. O., E. Poves and H. Haas, "Error Performance of Generalised Space Shift Keying for Indoor Visible Light Communications", *IEEE Transactions on Communications*, Vol. 61, No. 5, pp. 1968–1976, 2013.

79. Chau, Y. A. and Shi-Hong Yu, "Space Modulation on Wireless Fading Channels", *Proceedings of the IEEE 54th Vehicular Technology Conference*, Vol. 3, pp. 1668–1671 vol.3, 2001.

80. Zhao, X., H. Chen and J. Sun, "On Physical-Layer Security in Multiuser Visible Light Communication Systems with Non-Orthogonal Multiple Access", *IEEE Access*, Vol. 6, pp. 34004–34017, 2018.

81. Zhao, X. and J. Sun, "Physical-Layer Security for Mobile Users in NOMA-Enabled Visible Light Communication Networks", *IEEE Access*, Vol. 8, pp. 205411–205423, 2020.

82. Peng, H., Z. Wang, S. Han and Y. Jiang, "Physical Layer Security for MISO NOMA VLC System Under Eavesdropper Collusion", *IEEE Transactions on Vehicular Technology*, pp. 1–1, 2021.

83. Du, C. *et al.*, "Secure Transmission for Downlink NOMA Visible Light Communication Networks", *IEEE Access*, Vol. 7, pp. 65332–65341, 2019.

84. Su, N., E. Panayirci, M. Koca, A. Yesilkaya, H. V. Poor and H. Haas, "Physical Layer Security for Multi-User MIMO Visible Light Communication Systems with Generalized Space Shift Keying", *IEEE Transactions on Communications*, Vol. 69, No. 4, pp. 2585–2598, 2021.

85. Su, N., E. Panayirci, M. Koca and H. V. Poor, "Spatial Constellation Design-Based Generalized Space Shift Keying for Physical Layer Security of Multi-User MIMO Communication Systems", *IEEE Wireless Communications Letters*, Vol. 10, No. 8, pp. 1785–1789, 2021.

86. Su, N., E. Panayirci, M. Koca and H. Haas, "Transmit Precoding for Physical Layer Security of MIMO-NOMA-Based Visible Light Communications", *Proceedings of 17th International Symposium on Wireless Communication Systems (ISWCS)*, pp. 1–6, 2021.

87. Price, R., "A Useful Theorem for Nonlinear Devices having Gaussian Inputs", *IRE Transactions on Information Theory*, Vol. 4, No. 2, pp. 69–72, June 1958.

88. Burchardt, H., N. Serafimovski, D. Tsonev, S. Videv and H. Haas, "VLC: Beyond Point-to-Point Communication", *IEEE Communications Magazine*, Vol. 52, No. 7, pp. 98–105, 2014.

89. Hanzo, L., H. Haas, S. Imre, D. O'Brien, M. Rupp and L. Gyongyosi, "Wireless Myths, Realities, and Futures: From 3G/4G to Optical and Quantum Wireless", *Proceedings of the IEEE*, Vol. 100, No. Special Centennial Issue, pp. 1853–1888, May 2012.

90. DiLouie, C., *Advanced Lighting Controls: Energy Savings, Productivity, Technology and Applications*, CRC Press, 2006.

91. Stefan, I., H. Burchardt and H. Haas, "Area Spectral Efficiency Performance Comparison between VLC and RF Femtocell Networks", *Proceedings of IEEE International Conference on Communications (ICC)*, pp. 3825–3829, 2013.

92. Bian, R., I. Tavakkolnia and H. Haas, "15.73 Gb/s Visible Light Communication with Off-the-Shelf LEDs", *Journal of Lightwave Technology*, Vol. 37, No. 10, pp. 2418–2424, May 2019.

93. Uysal, M., F. Miramirkhani, O. Narmanlioglu, T. Baykas and E. Panayirci, "IEEE 802.15.7r1 Reference Channel Models for Visible Light Communications", *IEEE Communications Magazine*, Vol. 55, No. 1, pp. 212–217, January 2017.

94. Elamassie, M., F. Miramirkhani and M. Uysal, "Performance Characterization of Underwater Visible Light Communication", *IEEE Transactions on Communications*, Vol. 67, No. 1, pp. 543–552, January 2019.

95. Miramirkhani, F. and M. Uysal, "Channel Modeling and Characterization for Visible Light Communications", *IEEE Photonics Journal*, Vol. 7, No. 6, pp. 1–16, December 2015.

96. Komine, T. and M. Nakagawa, "Fundamental Analysis for Visible-Light Communication System using LED Lights", *IEEE Transactions on Consumer Electronics*, Vol. 50, No. 1, pp. 100–107, February 2004.

97. Armstrong, J., "OFDM for Optical Communications", *Journal of Lightwave Technology*, Vol. 27, No. 3, pp. 189–204, February 2009.

98. Elgala, H., R. Mesleh and H. Haas, "Indoor Optical Wireless Communication: Potential and State-of-the-Art", *IEEE Communications Magazine*, Vol. 49, No. 9, pp. 56–62, September 2011.

99. Cvijetic, N., "OFDM for Next-Generation Optical Access Networks", *Journal of Lightwave Technology*, Vol. 30, No. 4, pp. 384–398, February 2012.

100. Djengomemgoto, G., O. Narmanlioglu and M. Uysal, "Performance of eU-OFDM based Relay-assisted Visible Light Communications", *Proceedings of 10th International Symposium on Communication Systems, Networks and Digital Signal Processing (CSNDSP)*, pp. 1–5, July 2016.

101. Elgala, H., R. Mesleh and H. Haas, "Indoor Broadcasting via White LEDs and OFDM", *IEEE Transactions on Consumer Electronics*, Vol. 55, No. 3, pp. 1127–1134, August 2009.

102. Mossaad, M. S. A., S. Hranilovic and L. Lampe, "Visible Light Communications Using OFDM and Multiple LEDs", *IEEE Transactions on Communications*, Vol. 63, No. 11, pp. 4304–4313, November 2015.

103. Yesilkaya, A., E. Basar, F. Miramirkhani, E. Panayirci, M. Uysal and H. Haas, "Optical MIMO-OFDM with Generalized LED Index Modulation", *IEEE Transactions on Communications*, Vol. 65, No. 8, pp. 3429–3441, August 2017.

104. Chen, C., M. Ijaz, D. Tsonev and H. Haas, "Analysis of Downlink Transmission in DCO-OFDM-based Optical Attocell Networks", *Proceedings of IEEE Global Communications Conference (GLOBECOM)*, pp. 2072–2077, December 2014.

105. Ling, X., J. Wang, X. Liang, Z. Ding and C. Zhao, "Offset and Power Optimization for DCO-OFDM in Visible Light Communication Systems", *IEEE Transactions on Signal Processing*, Vol. 64, No. 2, pp. 349–363, January 2016.

106. Rodríguez, S. P., R. P. Jiménez, B. R. Mendoza, F. J. L. Hernández and A. J. A. Alfonso, "Simulation of Impulse Response for Indoor Visible light Communications using 3D CAD Models", *EURASIP Journal on Wireless Communications and Networking*, Vol. 2013, No. 1, p. 7, January 2013.

107. Dimitrov, S., S. Sinanovic and H. Haas, "Clipping Noise in OFDM-Based Optical Wireless Communication Systems", *IEEE Transactions on Communications*, Vol. 60, No. 4, pp. 1072–1081, April 2012.

108. Al-Kinani, A., C. Wang, H. Haas and Y. Yang, "Characterization and Modeling of Visible Light Communication Channels", *Proceedings of IEEE 83rd Vehicular Technology Conference (VTC Spring)*, pp. 1–5, May 2016.

109. Dongweon Yoon, Kyongkuk Cho and Jinsock Lee, "Bit Error Probability of M-ary Quadrature Amplitude Modulation", *Vehicular Technology Conference Fall 2000*, Vol. 5, pp. 2422–2427 vol.5, September 2000.

110. Zhang, T., L. Guo and Z. Liu, "Study on Modeling of Visible Light Communication in Indoor Furniture Scene", *2018 Cross Strait Quad-Regional Radio Science and Wireless Technology Conference (CSQRWC)*, pp. 1–3, July 2018.

111. Andrews, J. G., S. Buzzi, W. Choi, S. V. Hanly, A. Lozano, A. C. K. Soong and J. C. Zhang, "What Will 5G Be?", *IEEE Journal on Selected Areas in Communications*, Vol. 32, No. 6, pp. 1065–1082, 2014.

112. Mostafa, A. and L. Lampe, "Physical-Layer Security for Indoor Visible Light Communications", *Proceedings of IEEE International Conference on Communications (ICC)*, pp. 3342–3347, June 2014.

113. Telatar, E., "Capacity of Multi-Antenna Gaussian Channels: Capacity of Multi-antenna Gaussian Channels", *European Transactions on Telecommunications*, Vol. 10, No. 6, pp. 585–595, November 1999.

114. Oggier, F. and B. Hassibi, "The Secrecy Capacity of the MIMO Wiretap Channel", *IEEE Transactions on Information Theory*, Vol. 57, No. 8, pp. 4961–4972, 2011.

115. Wu, Y., A. Khisti, C. Xiao, G. Caire, K. Wong and X. Gao, "A Survey of Physical Layer Security Techniques for 5G Wireless Networks and Challenges Ahead", *IEEE Journal on Selected Areas in Communications*, Vol. 36, No. 4, pp. 679–695, 2018.

116. Mesleh, R. Y., H. Haas, S. Sinanovic, C. W. Ahn and S. Yun, "Spatial Modulation", *IEEE Transactions on Vehicular Technology*, Vol. 57, No. 4, pp. 2228–2241, 2008.

117. Mesleh, R., H. Elgala and H. Haas, "Optical Spatial Modulation", *IEEE Journal of Optical Communications and Networking*, Vol. 3, No. 3, pp. 234–244, 2011.

118. Haas, H., E. Costa and E. Schulz, "Increasing Spectral Efficiency by Data Multiplexing using Antenna Arrays", *Proceedings of IEEE International Symposium on Personal, Indoor and Mobile Radio Communications (PIMRC)*, Vol. 2, pp. 610–613 vol.2, 2002.

119. Yang, L., "Transmitter Preprocessing Aided Spatial Modulation for Multiple-Input Multiple-Output Systems", *Proceedings of IEEE Vehicular Technology Conference (VTC Spring)*, pp. 1–5, 2011.

120. Sinanovic, S., N. Serafimovski, M. Di Renzo and H. Haas, "Secrecy Capacity of Space Keying with Two Antennas", *Proceedings of IEEE Vehicular Technology Conference (VTC Fall)*, pp. 1–5, 2012.

121. Aghdam, S. R. and T. M. Duman, "Secure Space Shift Keying Transmission Using Dynamic Antenna Index Assignment", *Proceedings of IEEE Global Communications Conference (GLOBECOM)*, pp. 1–6, 2017.

122. Wang, F., C. Liu, Q. Wang, J. Zhang, R. Zhang, L. Yang and L. Hanzo, "Secrecy Analysis of Generalized Space-Shift Keying Aided Visible Light Communication", *IEEE Access*, Vol. 6, pp. 18310–18324, 2018.

123. Wang, F., C. Liu, Q. Wang, J. Zhang, R. Zhang, L. Yang and L. Hanzo, "Optical Jamming Enhances the Secrecy Performance of the Generalized Space-Shift-Keying-Aided Visible-Light Downlink", *IEEE Transactions on Communications*, Vol. 66, No. 9, pp. 4087–4102, 2018.

124. Chen, Y., L. Wang, Z. Zhao, M. Ma and B. Jiao, "Secure Multiuser MIMO Downlink Transmission via Precoding-Aided Spatial Modulation", *IEEE Communications Letters*, Vol. 20, No. 6, pp. 1116–1119, 2016.

125. Pham, T. V. and A. T. Pham, "On the Secrecy Sum-Rate of MU-VLC Broadcast Systems with Confidential Messages", *Proceedings of 10th Int. Symp. on Communication Systems, Networks and Digital Signal Processing (CSNDSP)*, pp. 1–6, 2016.

126. Al-Kinani, A., C. Wang, L. Zhou and W. Zhang, "Optical Wireless Communication Channel Measurements and Models", *IEEE Communications Surveys Tutorials*, Vol. 20, No. 3, pp. 1939–1962, 2018.

127. Kahn, J. M. and J. R. Barry, "Wireless Infrared Communications", *Proceedings of the IEEE*, Vol. 85, No. 2, pp. 265–298, 1997.

128. Shi, J., J. He, K. Wu and J. Ma, "Enhanced Performance of Asynchronous Multi-Cell VLC System Using OQAM/OFDM-NOMA", *Journal of Lightwave Technology*, Vol. 37, No. 20, pp. 5212–5220, October 2019.

129. Yang, H., C. Chen and W. Zhong, "Cognitive Multi-Cell Visible Light Communication with Hybrid Underlay/Overlay Resource Allocation", *IEEE Photonics Technology Letters*, Vol. 30, No. 12, pp. 1135–1138, June 2018.

130. Tran, C.-N., T.-M. Hoang and N.-H. Nguyen, "Coordinated Multi-Channel Transmission Scheme for Indoor Multiple Access Points VLC Networks", *Proceedings of 19th International Symposium on Communications and Information Technologies (ISCIT)*, pp. 611–615, 2019.

131. Yesilkaya, A., T. Cogalan, E. Panayirci, H. Haas and H. V. Poor, "Achieving Minimum Error in MISO Optical Spatial Modulation", *Proceedings of IEEE International Conference on Communications (ICC)*, pp. 1–6, 2018.

132. Purwita, A. A., A. Yesilkaya, I. Tavakkolnia, M. Safari and H. Haas, "Effects of Irregular Photodiode Configurations for Indoor MIMO VLC with Mobile Users", *Proceedings of IEEE International Symposium on Personal, Indoor and Mobile Radio Communications (PIMRC)*, pp. 1–7, 2019.

133. Khalid, A. M., G. Cossu, R. Corsini, P. Choudhury and E. Ciaramella, "1-Gb/s Transmission Over a Phosphorescent White LED by Using Rate-Adaptive Discrete Multitone Modulation", *IEEE Photonics Journal*, Vol. 4, No. 5, pp. 1465–1473, 2012.

134. Tsiatmas, A., C. P. M. J. Baggen, F. M. J. Willems, J. M. G. Linnartz and J. W. M. Bergmans, "An Illumination Perspective on Visible Light Communications", *IEEE Communications Magazine*, Vol. 52, No. 7, pp. 64–71, 2014.

135. Leung-Yan-Cheong, S. and M. Hellman, "The Gaussian Wire-tap Channel", *IEEE Transactions on Information Theory*, Vol. 24, No. 4, pp. 451–456, 1978.

136. Cover, T. M. and J. A. Thomas, *Elements of Information Theory (Wiley Series in Telecommunications and Signal Processing)*, Wiley-Interscience, USA, 2006.

137. Cheng, R., "Multirate Achievability in Memoryless Multiaccess Channel", *Proceedings of IEEE International Symposium on Information Theory (ISIT)*, p. 58, 1994.

138. Zou, Y., J. Zhu, X. Wang and L. Hanzo, "A Survey on Wireless Security: Technical Challenges, Recent Advances, and Future Trends", *Proceedings of the IEEE*, Vol. 104, No. 9, pp. 1727–1765, 2016.

139. Wen, M., B. Zheng, K. J. Kim, M. Di Renzo, T. A. Tsiftsis, K. Chen and N. Al-Dhahir, "A Survey on Spatial Modulation in Emerging Wireless Systems: Research Progresses and Applications", *IEEE Journal on Selected Areas in Communications*, Vol. 37, No. 9, pp. 1949–1972, 2019.

140. Wei, Y., L. Wang and T. Svensson, "Analysis of Secrecy Rate Against Eavesdroppers in MIMO Modulation Systems", *Proceedings of International Conference on Wireless Communications Signal Processing (WCSP)*, pp. 1–5, 2015.

141. Aghdam, S. R. and T. M. Duman, "Physical Layer Security for Space Shift Keying Transmission with Precoding", *IEEE Wireless Communications Letters*, Vol. 5, No. 2, pp. 180–183, 2016.

142. Wu, F., R. Zhang, L.-L. Yang and W. Wang, "Transmitter Precoding-Aided Spatial Modulation for Secrecy Communications", *IEEE Transactions on Vehicular Technology*, Vol. 65, No. 1, pp. 467–471, 2016.

143. Lv, P., W.-b. Yu and N.-s. Chen, "GSSK: A Generalization Step Safe Algorithm in Anonymizing Data", *Proceedings of International Conference on Communications and Mobile Computing*, Vol. 1, pp. 183–187, 2010.

144. Peel, C., B. Hochwald and A. Swindlehurst, "A Vector-Perturbation Technique for Near-Capacity Multiantenna Multiuser Communication-Part I: Channel Inversion and Regularization", *IEEE Transactions on Communications*, Vol. 53, No. 1, pp. 195–202, 2005.

145. Dytso, A., M. Goldenbaum, S. Shamai and H. V. Poor, "Upper and Lower Bounds on the Capacity of Amplitude-Constrained MIMO Channels", *Proceedings of IEEE Global Communications Conference (GLOBECOM)*, pp. 1–6, 2017.

146. Geraci, G., M. Egan, J. Yuan, A. Razi and I. B. Collings, "Secrecy Sum-Rates for Multi-User MIMO Regularized Channel Inversion Precoding", *IEEE Transactions on Communications*, Vol. 60, No. 11, pp. 3472–3482, 2012.

147. Haas, H., L. Yin, Y. Wang and C. Chen, "What is LiFi?", *Journal of Lightwave Technology*, Vol. 34, No. 6, pp. 1533–1544, 2016.

148. Marshoud, H., S. Muhaidat, P. C. Sofotasios, S. Hussain, M. A. Imran and B. S. Sharif, "Optical Non-Orthogonal Multiple Access for Visible Light Communication", *IEEE Wireless Communications*, Vol. 25, No. 2, pp. 82–88, 2018.

149. Obeed, M., A. M. Salhab, M.-S. Alouini and S. A. Zummo, "On Optimizing VLC Networks for Downlink Multi-User Transmission: A Survey", *IEEE Communications Surveys Tutorials*, Vol. 21, No. 3, pp. 2947–2976, 2019.

150. Lin, B. *et al.*, "A NOMA Scheme for Visible Light Communications using a Single Carrier Transmission", *Proceedings of 1st South American Colloquium on Visible Light Communications (SACVLC)*, pp. 1–4, 2017.

151. Kizilirmak, R. C., C. R. Rowell and M. Uysal, "Non-Orthogonal Multiple Access (NOMA) for Indoor Visible Light Communications", *Proceedings of 4th International Workshop on Optical Wireless Communications (IWOW)*, pp. 98–101, 2015.

152. Shen, H., Y. Wu, W. Xu and C. Zhao, "Optimal Power Allocation for Downlink Two-User Non-Orthogonal Multiple Access in Visible Light Communication", *Journal of Communications and Information Networks*, Vol. 2, No. 4, pp. 57–64, 2017.

153. Chen, C., Y. Yang, X. Deng, P. Du, H. Yang, Z. Chen and W.-D. Zhong, "NOMA for MIMO Visible Light Communications: A Spatial Domain Perspective", *Proceedings of IEEE Global Communications Conference (GLOBECOM)*, pp. 1–6, 2019.

154. Wang, N., P. Wang, A. Alipour-Fanid, L. Jiao and K. Zeng, "Physical-Layer Security of 5G Wireless Networks for IoT: Challenges and Opportunities", *IEEE Internet of Things Journal*, Vol. 6, No. 5, pp. 8169–8181, 2019.

155. Abumarshoud, H., M. D. Soltani, M. Safari and H. Haas, "Secrecy Capacity of LiFi Systems", *Emerging Imaging and Sensing Technologies for Security and Defence V; and Advanced Manufacturing Technologies for Micro- and Nanosystems in Security and Defence III*, Vol. 11540, pp. 127 – 137, International Society for Optics and Photonics, SPIE, 2020.